UNIVERSIDADE DE LISBOA
FACULDADE DE CIÊNCIAS
DEPARTAMENTO DE FÍSICA

Follow the water on Mars: Assessing the Mineralogy of Fluvial-Marine Environments

Eduardo Henrique de Ornelas Caetano

Mestrado em Física e Astrofísica

Dissertação orientada por:
Prof. Dr. Pedro Machado (FCUL, IA)
Prof.ª Dr.ª Zita Martins (IST, CQE)

2025

Resumo

A geologia e a biologia são ciências que, embora tradicionalmente tratadas como distintas, revelam uma profunda interligação quando se trata de compreender a história da vida no Universo. As rochas, frequentemente vistas apenas como matéria inorgânica e imóvel, funcionam na realidade como arquivos naturais que guardam informação preciosa sobre os ambientes primitivos do nosso sistema solar. Através da análise detalhada da sua composição, estrutura e contexto geológico, é possível inferir as condições ambientais do passado, nomeadamente aquelas que poderão, ou não, ter sido propícias ao surgimento e manutenção de formas de vida. Neste contexto, o estudo geológico de Marte ganha especial importância para a astrobiologia, uma vez que nos permite reconstruir possíveis cenários habitáveis e avaliar a sua persistência ao longo do tempo.

Marte, o quarto planeta do sistema solar, é um dos mundos mais estudados no âmbito das ciências planetárias, precisamente pela sua relevância para questões de habitabilidade. Apesar de hoje ser um planeta frio e árido, a sua superfície preserva múltiplas evidências de um passado radicalmente diferente, com rios, lagos e possivelmente oceanos que existiram há milhares de milhões de anos. A presença de minerais hidratados, como filossilicatos e sulfatos, observados por orbitadores e rovers, indica que a água esteve presente em quantidades significativas e em contextos geológicos diversos. Estes minerais, ao formarem-se em interação com a água, registam, nas suas estruturas cristalinas, as condições físicas e químicas desses ambientes primitivos, funcionando como testemunhos diretos do passado aquoso de Marte.

Um dos principais problemas que surgem, aquando do estudo da superfície marciana, é a grande discrepância entre o número de crateras de impacto entre o hemisfério norte e o hemisfério sul. Uma das teorias mais aceites é a de que Marte, enquanto jovem, era o lar de um oceano no hemisfério norte, o oceano Borealis. Esta teoria propõe uma resposta simples mas elegante à questão da falta de crateras de pequeno/médio porte na parte norte de Marte. Se de facto estivéssemos na presença de um oceano relativamente profundo, nenhum dos impactos de pequeno/médio porte deixaria vestígios de impacto no fundo oceânico.

Este trabalho de mestrado é dedicado à análise mineralógica e espectroscópica de depósitos marcianos ao longo da potencial linha costeira do antigo oceano Borealis, uma vasta bacia no hemisfério norte de Marte que poderá ter albergado um oceano primitivo. O objetivo principal é identificar assinaturas minerais que possam indicar ambientes de interação entre água e rocha, característicos de zonas costeiras ou ambientes flúvio-marinhos rasos. Para tal, recorre-se a dados espectrais obtidos pelas sondas orbitais Mars Express (especificamente através do instrumento OMEGA) e Mars Reconnaissance Orbiter (através do instrumento CRISM). A análise destes dados é complementada por espectros laboratoriais de análogos terrestres, permitindo uma comparação detalhada que ajude a interpretar os contextos geoquímicos marcianos. Este trabalho é desenvolvido em colaboração com investigadores do Instituto de Astrofísica e Ciências do Espaço, cuja experiência tem sido essencial no tratamento, calibração e análise de dados espectrais de alta resolução no âmbito da ciência planetária.

Os minerais hidratados são alguns dos compostos mais relevantes no estudo da história climática e potencial habitabilidade passada de Marte. Minerais como os filossilicatos (argilas), sulfatos e carbonatos são considerados indicadores diretos da interação prolongada entre rocha e água, um requisito essencial para a emergência de vida. Estes minerais apresentam bandas de absorção características no infravermelho próximo, sobretudo entre 1 μm e 2.5 μm, associadas a vibrações de ligações OH^-, H_2O e grupos funcionais como SO_4^{2-} e CO_3^{2-}. Por exemplo, os filossilicatos ricos em ferro apresentam uma banda de absorção marcada em torno dos 2.29 μm, enquanto que os sulfatos hidratados mostram feições nos $\sim$1.9 μm e $\sim$2.4 μm, relacionadas com a presença de água estruturada.

Para esta tarefa, os dois principais instrumentos utilizados na órbita de Marte são: O OMEGA (Observatoire pour la Minéralogie, l'Eau, les Glaces et l'Activité) que oferece uma resolução espectral de cerca de 14 nm e uma resolução espacial que pode atingir os 300 metros/pixel em modos de observação mais detalhados; e o CRISM (Compact Reconnaissance Imaging Spectrometer for Mars), com resolução espectral em torno dos 6.5 nm, que permite observar a superfície com resolução espacial até 18 metros/pixel no modo de alta resolução (targeted mode), tornando-se mais adequado para análises localizadas e detalhadas, por exemplo, de deltas, paleolagos ou afloramentos geológicos específicos.

Os espectros obtidos por instrumentos orbitais como o CRISM e OMEGA sofrem inevitavelmente da influência da atmosfera marciana, composta principalmente por dióxido de carbono (CO_2), bem como da presença de poeiras em suspensão e aerossóis que afetam a reflectância observada à superfície. Para que as bandas de absorção mineralógica sejam corretamente interpretadas, é fundamental aplicar correções atmosféricas rigorosas. Estas correções são geralmente baseadas em modelos radiativos que simulam a transmissão da radiação solar através da atmosfera marciana, permitindo isolar a componente espectral real da superfície. Um dos modelos mais comuns faz essa correção a partir da reflectância medida no monte Olimpo ($\sim$30 km de altitude) e remove essa camada de atmosfera, resultando numa aproximação boa, mas longe de perfeita.

Além disso, para se obterem espectros representativos e com robustez estatística, é essencial analisar um grande número de espectros individuais provenientes da mesma zona geológica. Após a remoção de artefactos e de ruído instrumental, faz-se uma média desses espectros, o que permite reduzir a variabilidade pontual e reforçar as assinaturas espectrais consistentes da região em estudo.

O interesse da comunidade científica em Marte tem vindo a intensificar-se nas últimas décadas, não só devido à sua proximidade e semelhanças geológicas com a Terra primitiva, mas também pela crescente evidência de um passado húmido e potencialmente habitável. Entre os diversos alvos de estudo à superfície marciana, as crateras de impacto assumem particular relevância científica. Quando um corpo impacta violentamente a crosta marciana, escava as camadas superiores e expõe material proveniente de profundidades que, de outro modo, permaneceriam inacessíveis aos instrumentos remotos. Este processo cria verdadeiras "janelas" estratigráficas, revelando depósitos antigos, frequentemente menos alterados pela oxidação e erosão moderna, e que podem conservar assinaturas geoquímicas e mineralógicas cruciais para a reconstrução das condições ambientais do Marte primitivo.

No hemisfério norte de Marte, dominado por vastas lowlands, os depósitos finos de poeira e sedimentos acumulam-se ao longo de milhares de milhões de anos, obscurecendo as camadas mais antigas da crosta. Nessas regiões, as crateras de impacto tornam-se praticamente a única via para aceder a materiais subsuperficiais preservados. Durante o meu trabalho de mestrado usei software criado para a leitura e correção de imagens hiperespectrais, CAT (CRISM analysis tool) para imagens CRISM, e OMEGAPY para a análise de imagens OMEGA. Foram também, criados por mim, vários scripts de python com o objetivo de normalizar e calcular a média dos espectros obtidos, de forma a estudar todas estas zonas de interesse anteriormente mencionadas.

Concluindo, estudar a superfície de Marte ao longo da potencial linha costeira do antigo oceano Borealis, através de espectroscopia orbital com os instrumentos OMEGA e CRISM, permite investigar zonas onde processos sedimentares e aquáticos podem ter ocorrido de forma prolongada. A análise mineralógica destas regiões, complementada pela exposição pontual de camadas subsuperficiais em crateras de impacto, oferece pistas cruciais sobre os ambientes primitivos do planeta. Este trabalho realça também a importância de abordar conjuntamente a geologia e a biologia, uma vez que a caracterização dos contextos geológicos é fundamental para avaliar a habitabilidade e o potencial de preservação de bioassinaturas. Ao reconstruir a história paleoambiental do hemisfério norte de Marte, este estudo contribui para a preparação de futuras missões in situ, essenciais para compreender a evolução geológica e astrobiológica do planeta vermelho.

Palavras chave: Mineralogia, Marte, Água, Refletância, Oceano primitivo

Abstract

The mineralogical record of Mars offers a compelling window into the planet's aqueous past, with decades of orbital and in situ exploration revealing widespread evidence for ancient liquid water. Spectroscopic data from instruments such as CRISM and OMEGA have identified hydrated minerals including phyllosilicates, sulfates, and carbonates, which are indicative of diverse water-rock interactions across multiple geologic epochs. In this work, we used both of these spectrometers to follow the lead of the Zhurong mission and successfully gathered evidence that could support the existence of an ancient Borealis Ocean in the northern hemisphere of Mars. Particular attention was given to the co-occurrence of opals and serpentines, minerals that reflect distinct aqueous environments. Opals were found in association with low-temperature, acidic conditions involving silica-rich fluids, while serpentines pointed to alkaline hydrothermal alteration of ultramafic rocks. Their simultaneous presence in key regions revealed that Mars experienced chemically diverse and long-lasting water activity, underscoring a complex hydrologic history and the potential for environments conducive to prebiotic chemistry or habitability. This study not only focused on promising sites along the proposed ancient coastline but also examined large impact craters, which appear to have excavated and exposed deeper, otherwise hidden sedimentary layers that further illuminate Mars' early oceanic and climatic evolution.

Keywords: Mineralogy, Mars, Water, Reflectance, Ancient ocean

Acknowledgements

I would like to, first of all, thank my family for all the love and unconditional support throughout my life and this journey. Ever since I started on this academic path they have motivated and accompanied me through every step of the way. They showed me, that, with hard work, anything can be achieved.

I would also like to thank my second family and dear friends, my martial arts family, that have shown me that respect and discipline are a way of life, and that no matter how big an obstacle is, there is always a way around it.

A big thank you to my supervisors, Dr. Pedro Machado and Dr.^{a} Zita Martins for guiding me through this master thesis work, and for all the opportunities created to meet and learn from other, also very accomplished and successful scientists in the area. They also gave me the opportunity to fulfill my childhood dream of studying the stars and the universe, and look for the potential of life outside our home world. I was also shown that the world of investigation is hard and demanding, but very enjoyable when surrounded by the right people. I also wish to thank all the IA's solar system team for all the invaluable help they have provided. I want to specially thank Francisco Brasil for all the time and effort he has surrendered in order to make sure I was on the right track.

At last I would also like to give a great thank you to my two dearest friends, Rúben Calvinho and Rodrigo Botelho, for the long sleepless nights looking at spectra and talking about minerals, just like any group of normal friends would. To them I started as an unofficial tutor, but they quickly grew into being the two people I cannot look at Mars without.

Index

List of Figures

List of Tables

Chapter 1

Introduction

1.1 Mars - A geologically inactive Earth?

Mars is one of our closest neighbors within Solar System, meaning it is a prime candidate to intense and recurring studies of the atmosphere as well as its surface. A planet whose features evoke a distant, yet strikingly familiar vision of what Earth might become. Although now geologically inactive and barren, Mars may once have shared many of the dynamic conditions that nurtured life on our own planet. This resemblance has drawn growing attention from planetary science and astrobiology in an attempt to understand the real impact that large flowing bodies of water as well as an active lithosphere had in the origin of life as we know it.

Mars is thought to have formed approximately 4.6 billion years ago through the rapid accretion of material in the inner solar system. Its relatively small mass, about 10% that of Earth, meant it cooled quickly, allowing a crust to solidify early and limiting the duration of its internal geologic activity. Geochemical evidence from Martian meteorites, specifically SNC (Shergottites, Nakhlites and Chassignites) meteorites, and surface data suggests the planet differentiated into a core, mantle, and crust within the first 50 million years of its history (Dauphas et al. 2011). The early Martian history is characterized by extensive fluvial activity, valley networks, and weathering signatures that suggest a more Earth-like climate, possibly sustained by episodic warming events or transient greenhouse atmospheres. Volcanic provinces such as Tharsis and Elysium began forming in this era and continued erupting, contributing to prolonged but spatially limited geologic activity (Dauphas et al. 2011) (Encrenaz et al. 2003). Unlike Earth, Mars lacks plate tectonics, so the volcanic and tectonic processes remained localized.

Mars stands apart from Earth not only in appearance but also in internal structure (see Figure 1.1). Its lower average density suggests a smaller overall iron content, estimated at about 25%, in contrast to Earth's 33%, though this is accompanied by a higher iron concentration in the outer layers, particularly the crust and mantle (Sánchez-Lavega 2011) (Encrenaz et al. 2003). Measurements of the planet's moment of inertia, especially those obtained by the Mars Pathfinder mission, have offered critical insights. A value of 0.366 (Encrenaz et al. 2003) indicates a significant central mass concentration, implying a dense core. From these findings, two main models have been proposed: one where Mars harbors a small, dense core composed predominantly of iron, making up 15% of the planet's mass with a radius of 1300 km; and another where the core is larger, reaching 2000 km in radius, composed of an iron-sulfur alloy, and representing roughly 25% of the planet's mass (Encrenaz et al. 2003).

Atmospheric models indicate that early Mars may have sustained pressures of 1–2 bar of CO_2 and water vapor from volcanic outgassing, potentially creating a greenhouse effect sufficient to raise global temperatures above freezing (Zurek et al. 2017). However, Mars' smaller gravity and lack of a sustained

1. INTRODUCTION

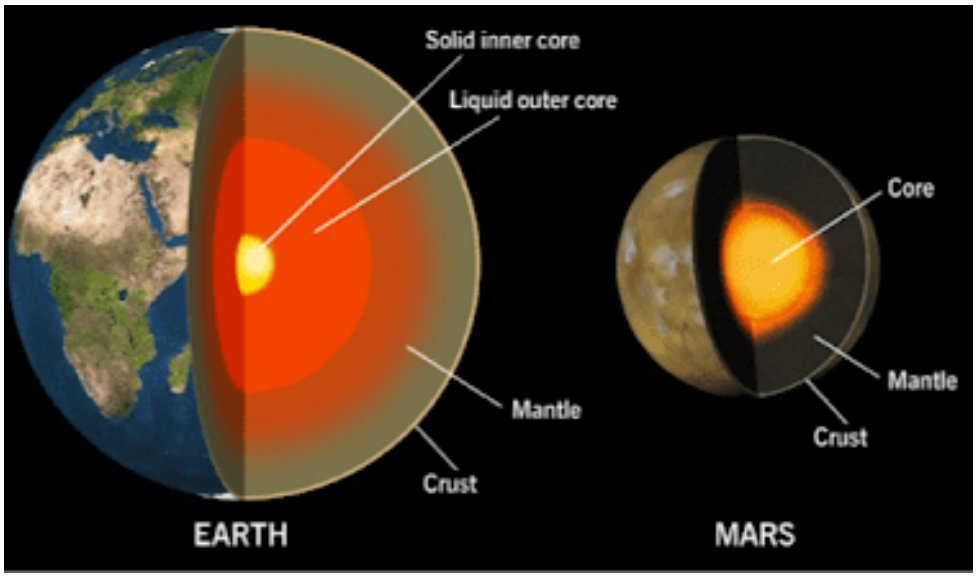

Figure 1.1: Schematic diagram of both Earth's and Mars' inner structure. A core-mantle-crust interior means that the planet went through a differentiation process. Credits:ZME Science

magnetic field led to the progressive loss of its atmosphere over the past 3.5 billion years (Sánchez-Lavega 2011). Isotopic enrichment in species such as ^{13}C, ^{18}O, and ^{38}Ar supports the interpretation of extensive atmospheric escape via hydrodynamic and nonthermal processes, including solar wind stripping (Sánchez-Lavega 2011) (Zurek et al. 2017). The residual atmosphere today is thin, primarily composed of CO_2, and subject to seasonal variations including CO_2 condensation at the poles (Figure 1.2).

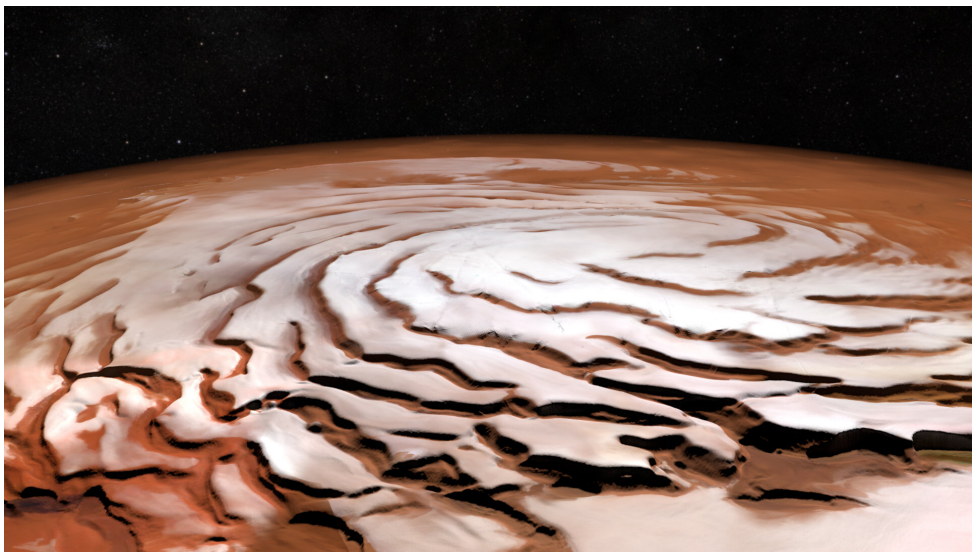

Figure 1.2: Image of Mars' north pole showcasing the vast amounts of water ice deposited in the planet's surface. Credits: ESA

Unlike Earth, Mars lacks a global intrinsic magnetic field (Langlais et al. 2004). However, strong crustal magnetism has been detected by the Mars Global Surveyor, especially across the ancient terrains of the southern hemisphere (Langlais et al. 2004). This may be a remnant of an early magnetic field generated by a once-active dynamo, suggesting Mars was more geologically alive in its early history. The mantle, composed mainly of silicates like olivine ($(Mg,Fe)SiO_4$) (Encrenaz et al. 2003), is estimated to range from 1500 to 2100 km in thickness(Encrenaz et al. 2003), depending on the core's properties. Geochemical analysis further reveals that Mars is generally richer in iron and poorer in aluminum compared to Earth

(Encrenaz et al. 2003). Its crust, with a lower density, varies widely in thickness between 30 and 150 km (Encrenaz et al. 2003) and appears to be primarily made up of hydrated silicates. Altogether, these characteristics portray a planet that, while now geologically quiet, once bore internal dynamics and compositions not entirely unlike those of the early Earth.

The Martian surface is marked by a stark and complex landscape composed primarily of volcanic rocks, basaltic in nature, interspersed with dust and sediments shaped by both internal and external forces (Barlow 2008)(Encrenaz et al. 2003). Much of the visible terrain is coated in fine-grained iron oxide particles, giving the planet its distinctive reddish hue (Barlow 2008), as seen in Figure 1.3. Remote sensing has revealed that olivine and pyroxene, two iron and magnesium-rich silicates (Mustard et al. 2005), are widespread, particularly across the southern highlands (Barlow 2008)(Mustard et al. 2005). These minerals are indicative of a volcanic origin (Mustard et al. 2005), supporting the notion of extensive lava flows in the planet's early history. In contrast, regions such as Syrtis Major and Noachian-aged plains contain phyllosilicates and sulfates, suggesting episodes of aqueous alteration that transformed the basaltic crust through interaction with water and atmospheric gases (Encrenaz et al. 2003).

Figure 1.3: Image of the martian surface taken by the Curiosity rover. Credits: NASA

Beyond mineral composition, the surface of Mars presents a variety of geomorphological units, each bearing witness to different eras of planetary evolution. The highlands are densely cratered and fractured, containing preserved impact features that date back over 4 billion years (Encrenaz et al. 2003) (Kreslavsky et al. 2000). These terrains are intercut by extensive graben (tectonic induced valleys/pits) systems and fault lines, revealing a history of tectonic deformation, likely driven by lithospheric stress and cooling (Encrenaz et al. 2003). In contrast, the northern plains exhibit fewer craters and smoother topography, hinting at resurfacing processes such as volcanism or sediment deposition (Kreslavsky et al. 2000). Wind-sculpted features like yardangs, dunes, and dust devil tracks (seen in 1.4) dominate these lowlands, shaped by persistent aeolian activity in the thin Martian atmosphere (Encrenaz et al. 2003).

Among the most striking surface features are the layered deposits found within crater basins, polar terrains, and sedimentary mounds like those in Gale Crater. These stratified formations contain alternating bands of clays, sulfates, and silicates (Xiao et al. 2023) (Encrenaz et al. 2003), offering a potential chronological archive of changing environmental conditions. The rhythmic nature of many of these

1. INTRODUCTION

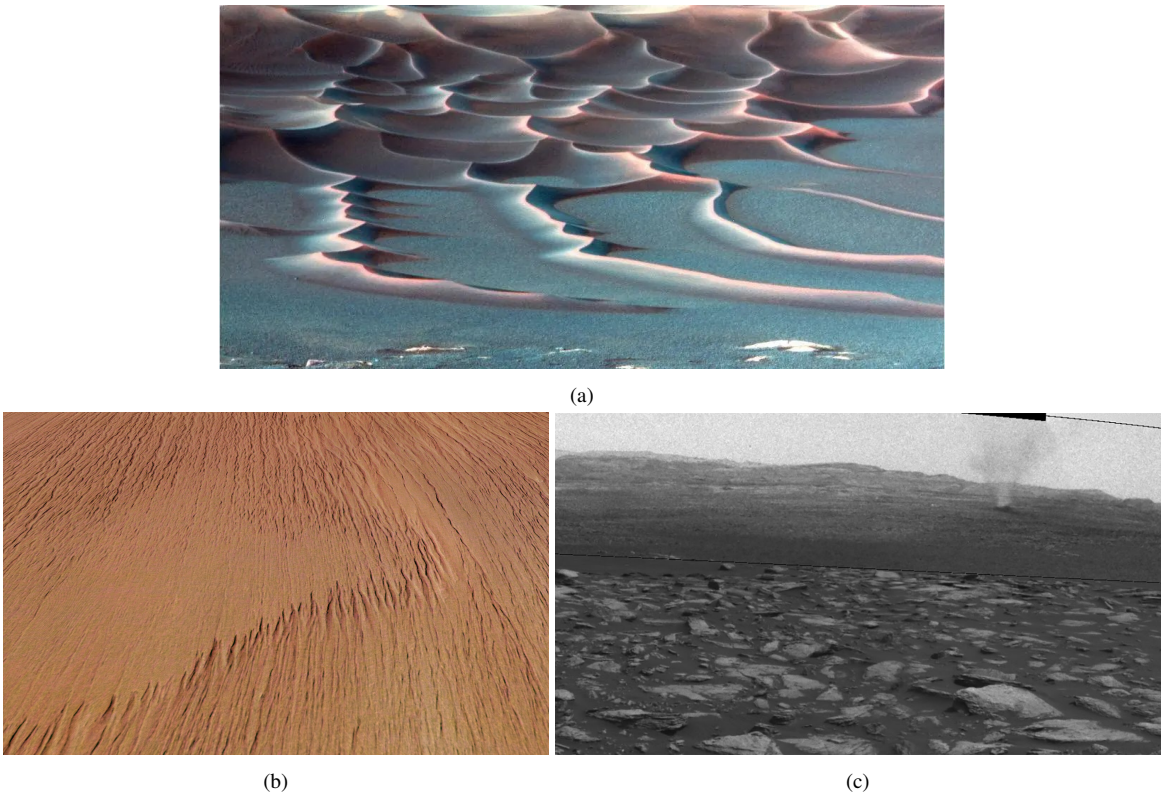

(a)

(b)

(c)

Figure 1.4: Dunes on Mars (a), Yardangs, phenomenon caused by aeolian erosion (b) and a dust devil caught on Curiosity rover's camera (c). Credits: NASA

layers suggests that they may have formed under cyclic processes, perhaps linked to variations in the planet's temperature, leading to constant the melting, condensation and freezing of the surface water, which in turn would result in torrential rains and violent floods that eroded the surface (Encrenaz et al. 2003).

The exploration of Mars began in earnest during the 1960s (Harvey 1996) (Perminov 1999), as American and Soviet missions alternated in their attempts to photograph the surface, study the atmosphere, and measure the planet's physical properties. Mariner 4 (Reiff 1966), in 1965, transmitted the first 21 images of Mars, revealing a heavily cratered, seemingly lifeless surface that evoked comparisons with the Moon. Subsequent missions, Mariner 6 and 7 (Collins 1971) (Stallkamp et al. 1971), reinforced this perception. It was not until the arrival of Mariner 9 in 1971 (McCauley et al. 1972) that this view began to shift. As the first spacecraft to orbit another planet, Mariner 9 delivered near-complete surface coverage in remarkable detail, capturing features such as immense volcanoes and vast canyon systems, none of which resembled the legendary "canals" early astronomers had once imagined (McCauley et al. 1972). This mission laid the groundwork for Mars' first geological maps and transformed our understanding of its surface evolution. The Viking program (Corliss 1974) followed in the mid-1970s, marking a turning point in planetary science. Each of the two Viking missions included both an orbiter and a lander, allowing for coordinated orbital observation and in situ analysis. Viking 1 (Mutch et al. 1976) landed on July 20, 1976, in Chryse Planitia, while Viking 2 (Shorthill et al. 1976) touched down on September 3 in Utopia Planitia, 6500 km away. These missions produced over 50,000 images from orbit, with resolutions ranging between 10 and 150 meters, and conducted chemical experiments on Martian soil with the primary goal of detecting organic molecules or signs of life.

More recently, China's Tianwen-1 mission marked a major milestone in Mars exploration by success-

fully deploying the Zhurong rover (Xiao et al. 2023) on the Martian surface in 2021. Zhurong landed in Utopia Planitia, within the Vastitas Borealis Formation, and has since provided valuable in situ evidence supporting the past presence of liquid water. Its observations of sedimentary structures and surface mineralogy suggest that this region may once have been shaped by marine processes, offering direct support for the hypothesis of an ancient ocean in Mars' northern lowlands.

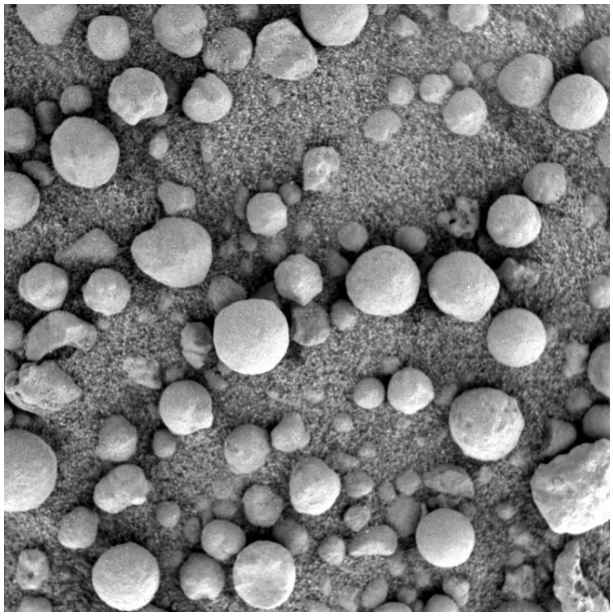

Figure 1.5: Phenomenon known as "blueberries", taken by the opportunity rover. Credits: NASA

The geological record gathered by orbiters and landers on Mars has revealed that the planet's atmosphere was once warm and dense enough to support the presence of stable, flowing liquid water at the surface. The widespread networks of channels etched into ancient, heavily cratered terrains strongly suggest that running water once carved the landscape. Mineralogical analyses conducted both from orbit and in situ, particularly by the Spirit and Opportunity rovers (Morris et al. 2004) (Squyres et al. 2006), point to the presence of a thick atmosphere during at least the Noachian period, the earliest of Mars' three major geologic periods (from 4.6 to 3.5 Gy ago), followed by the Hesperian (from 3.5 to 2.5 Gy ago) and Amazonian (from 2.5 Gy to the present) (Sánchez-Lavega 2011). Opportunity's observations further uncovered small hematite-rich spherules, informally known as "blueberries" (seen in 1.5) (Squyres et al. 2006), whose formation is strongly tied to water-based processes. Additional support for a wetter, more dynamic early Mars comes from the study of SNC meteorites, martian rocks identified by their composition and traced to the red planet (Sánchez-Lavega 2011). Together, this body of evidence supports the idea that early Mars may have resembled the young Earth in important ways, possibly hosting lakes or even an ocean in the Northern Hemisphere (Sánchez-Lavega 2011). Still, the geological record remains complex and at times contradictory, as several regions appear to have escaped exposure to these warmer, wetter conditions, leaving open questions about the extent and duration of early Mars' habitability.

1.2 Key Open Questions

The ancient, dry landscapes of Mars still hold untold stories about the planet's dynamic past. Advancing our understanding of the mineralogical and geological evidence on Mars may allow us to rewrite the history of water in the inner Solar System, revealing not only the conditions that once made Mars a

potentially habitable world, but also shedding light on the broader evolutionary pathways that may lead planets toward environments capable of sustaining life. In doing so, Mars becomes more than just a frozen desert, it becomes a crucial chapter in the narrative of planetary habitability - and perhaps the search for life beyond Earth.

1.2.1 The dichotomy problem

The striking division between the heavily cratered southern highlands and the relatively smooth, low-lying plains of the northern hemisphere defines the planet's surface on a global scale. The southern hemisphere, with its dense distribution of ancient impact craters, appears to have preserved the record of Mars' earliest geologic activity, while the northern plains, comparatively young and sparsely cratered, suggest extensive resurfacing events that have obscured much of their early history (Watters et al. 2007). This hemispheric dichotomy is not only a topographic divide but it also marks a major difference in crustal thickness, geological composition, and thermal evolution (Watters et al. 2007) (Marinova et al. 2008).

Despite its planetary-scale prominence, the origin of the Martian dichotomy remains an open question. Internal models propose mantle-driven processes such as degree-1 convection or early planetary overturn, while external hypotheses point to the possibility of one or more giant impacts (Marinova et al. 2008). Though the single-impact scenario has gained traction in recent years, it remains a complex and somewhat speculative solution, especially given the absence of unambiguous impact signatures (Watters et al. 2007). An increasingly compelling alternative, supported by geomorphological and mineralogical evidence, is the hypothesis that the northern lowlands once hosted a vast body of water, an ancient ocean known as Oceanus Borealis (Sánchez-Lavega 2011) (Xiao et al. 2023). The flatness, elevation, and sedimentary features of the northern plains, combined with shoreline-like structures and the presence of hydrated minerals (Xiao et al. 2023), point toward a standing body of water that may have persisted for extended periods during Mars' early history (Xiao et al. 2023).

This oceanic model not only helps to explain the apparent youth and smoothness of the northern hemisphere, but also integrates naturally with observations of outflow channels and deltaic formations that appear to terminate at a common elevation (Xiao et al. 2023) (Barlow 2008). Moreover, such a water body could have played a significant role in the thermal and geochemical evolution of the Martian crust, reshaping the surface through sedimentation and possibly influencing the dichotomy itself. The antiquity of the boundary, indicated by crater statistics and buried impact basins revealed through radar sounding, suggests that both the dichotomy and any associated ocean would have formed early, possibly during the Noachian eon (Xiao et al. 2023).

1.2.2 The big impactor hypothesis

As previously mentioned, one of the most prominent and enigmatic features of Mars is its hemispheric dichotomy, a stark contrast in elevation, crustal thickness, and crater density between the southern highlands and northern lowlands. While endogenic models invoking mantle convection or lithospheric overturn provide partial explanations (Wenzel et al. 2004), they often fall short by failing to account for observed crustal asymmetries. In this context, the exogenic hypothesis of a single massive impactor has gained traction as a plausible alternative (Marinova et al. 2008). Recent three-dimensional hydrodynamic simulations demonstrate that an oblique collision involving an impactor with a diameter between 1600 and 2700 kilometers could have produced the observed crustal thinning and elliptical boundary of the northern lowlands (Marinova et al. 2008). Under conditions of relatively low velocity (6–10 km/s) and

impact angles between 30°and 60°(Marinova et al. 2008), the energy released, on the order of 3 to 6 $\times 10^{29}$ joules, would have been sufficient to strip away vast portions of the crust without wholly melting the lithosphere, thereby preserving key structural features that are still observable today.

This scenario aligns well with the current understanding of Mars' internal structure, particularly its thinner crust in the north and the concentration of ancient, heavily magnetized crust in the southern hemisphere (Marinova et al. 2008). It also helps explain the widespread resurfacing in the northern plains, which exhibit far fewer craters compared to the southern highlands, an observation often interpreted as the result of later volcanic and sedimentary activity, potentially covering the original impact basin. The timing of such an event appears consistent with the Noachian period, during which the planet was subject to intense bombardment (Marinova et al. 2008) (Encrenaz et al. 2003). If a mega-impact did occur early in Mars' evolution, it would have had far-reaching implications not only for the planet's thermal and tectonic history but also for its potential to develop regional magnetic fields, support crustal recycling, and influence subsequent volcanic construction, such as that of the Tharsis Ridge (Wenzel et al. 2004).

1.2.3 The Oceanus Borealis hypothesis

The Martian hemispheric dichotomy, the stark contrast between the ancient, elevated southern highlands and the low-lying northern plains, has not only inspired models rooted in internal or impact-driven dynamics (Marinova et al. 2008), but has also led to an enduring hypothesis: the existence of a primordial ocean in the northern hemisphere (Xiao et al. 2023) (Baker 2023) (Wang et al. 2024). This concept, known as Oceanus Borealis, gained initial traction following the identification of putative paleoshorelines (see Figure 1.6) in Viking Orbiter imagery (Corliss 1974) (Mutch et al. 1976) (Shorthill et al. 1976). While later analyses raised doubts due to the irregular elevation of these contacts and the possible volcanic origin of some features, attention shifted to sedimentary evidence preserved within the Vastitas Borealis Formation (VBF), a widespread unit covering nearly half of the northern lowlands (Salvatore et al. 2014).

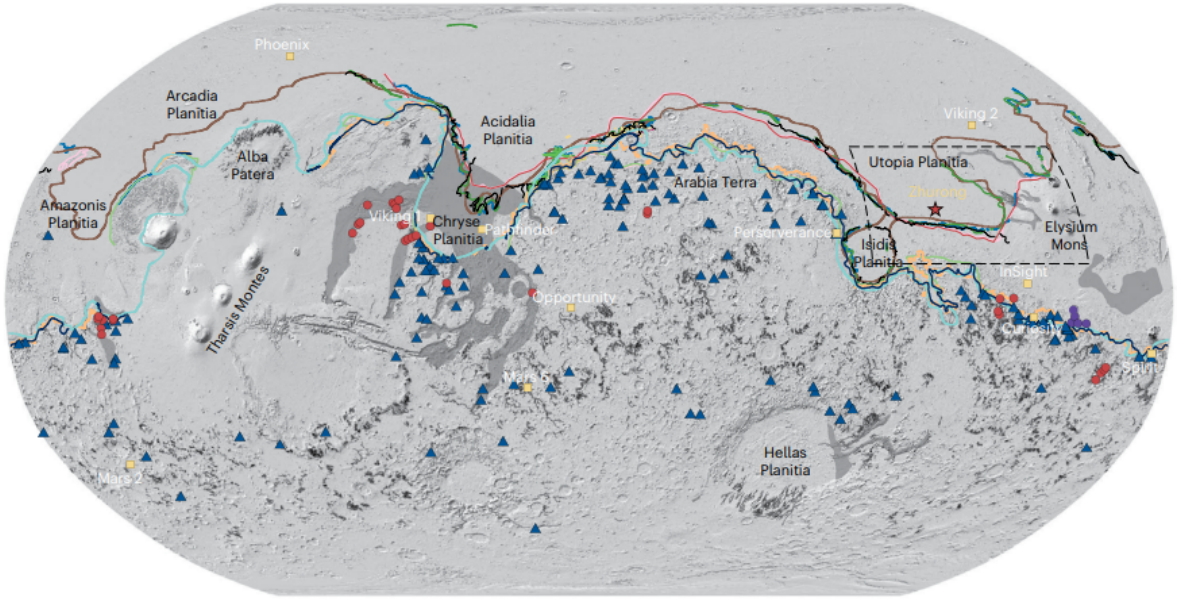

Figure 1.6: Global map of the putative paleoshorelines of Mars. The colored curved lines along the dichotomy represent potential shorelines already theorized (Wang et al. 2024). The dark gray areas represent the outflow channels, the blue triangles global deltas, the red dots knickpoints in channels and the purple dots, deltas at the Aeolis Mons region. The black lines represent the valley networks. The red star indicates the landing site of the Zhurong rover. The yellow squares are the landing sites of Mars rovers or landers.

The VBF, dated to the late Hesperian–early Amazonian, is stratigraphically contemporaneous with the formation of the planet's outflow channels (Tanaka et al. 1987) (Kreslavsky et al. 2002), suggesting a genetic link between catastrophic flooding and widespread sedimentation. The boulder-sized clasts encountered by the Zhurong rover in Utopia Planitia (Xiao et al. 2023) have been interpreted as products of marine-like deposition, with analogues in Earth's shallow seas. Their textures and bedding characteristics, such as sorting, rounding, and matrix-supported structures, parallel terrestrial marine sediments deposited under high-energy conditions. These observations support a scenario in which the VBF represents ancient seafloor material, possibly shaped by turbidite flows or hyperpycnal plumes generated by sediment-rich megaflooding events (Baker 2023).

Further reinforcing the marine hypothesis, terrestrial analogues have been documented in several morphological features on the Martian surface. These include teardrop-shaped islands downstream of major outflow channels, interpreted as erosional remnants similar to those in submarine environments on Earth (Moscardelli et al. 2011), as well as large-scale polygonal terrains resembling deep-water polygonal fault systems (Cooke et al. 2011) (Brož et al. 2020). High-albedo mounds in Acidalia Planitia have also been likened to submarine mud volcanoes (Rodriguez et al. 2012), indicating possible sediment mobilization and degassing under marine conditions. Most recently, comparisons between boulder fields in the VBF and seismically imaged slope-failure deposits in terrestrial deep-water settings (Alves et al. 2010) (Moscardelli et al. 2012) offer additional sedimentological parallels that strengthen the plausibility of a marine origin.

Despite these converging lines of evidence, the interpretation of the VBF remains debated, with alternative origins ranging from glacial to volcanic. Nonetheless, the ocean hypothesis continues to function as a productive working model, directing investigation toward the stratigraphy, composition, and spatial distribution of northern plains deposits. Rather than relying solely on climate modeling, which often struggles to reconcile ancient surface water with Mars' present low pressure and temperature, the geological record itself provides a basis for reconstructing early hydrospheric activity. In this context, Oceanus Borealis is not merely a speculative addendum to the Martian dichotomy, but a possible consequence of it: a vast basin formed or deepened by tectonic or impact-driven processes, and subsequently filled, reshaped, and recorded by a short-lived but transformative era of surface water. In this work I intend to further increase the amount of evidence that supports this theory of an ancient ocean on Mars.

1.2.4 Northern Low Lands and Impact craters

The northern lowlands of Mars, which cover nearly one-third of the planet's surface, preserve a critical record of the long-term geological and climatic evolution of the planet (Pan et al. 2017). These lowlands consist of extensive topographic basins filled with volcanic and sedimentary deposits that conceal the nature of the underlying crust (Pan et al. 2017). In short, this region of Mars' surface can be interpreted as a martian "garbage disposal". Every lava flow, every dust storm, every sediment, or every water channel will lead to the northern plains, and deposit all types of sediments, preventing any kind of surface study to accurately analyze the original crustal layers (Pan et al. 2017). Impact craters, by excavating material from depths of up to several kilometers, provide unique access to this buried stratigraphy (Senft et al. 2007) (Senft et al. 2008).

In order to more accurately understand what kind of restructuring occurs when an asteroid impacts the surface of Mars, it is important to know what the surface is predominantly made of. In the context of impact cratering, there are two main types of layers to worry about, weak layers and strong layers (Senft et al. 2007). This nomenclature refers to their attrition coefficient, at the moment of impact, for

example, a porous/fractured/weathered layer would be considered a weak layer, where as a solid basalt, with strong interlocking mineral structure layer, would be considered a strong layer (Senft et al. 2007). As seen in Figure 1.7, when the impactor is relatively big, the underlying layers will tend to restructure themselves, allowing for some of the more deep minerals to become exposed to the surface and becoming prime targets for mineralogical studies.

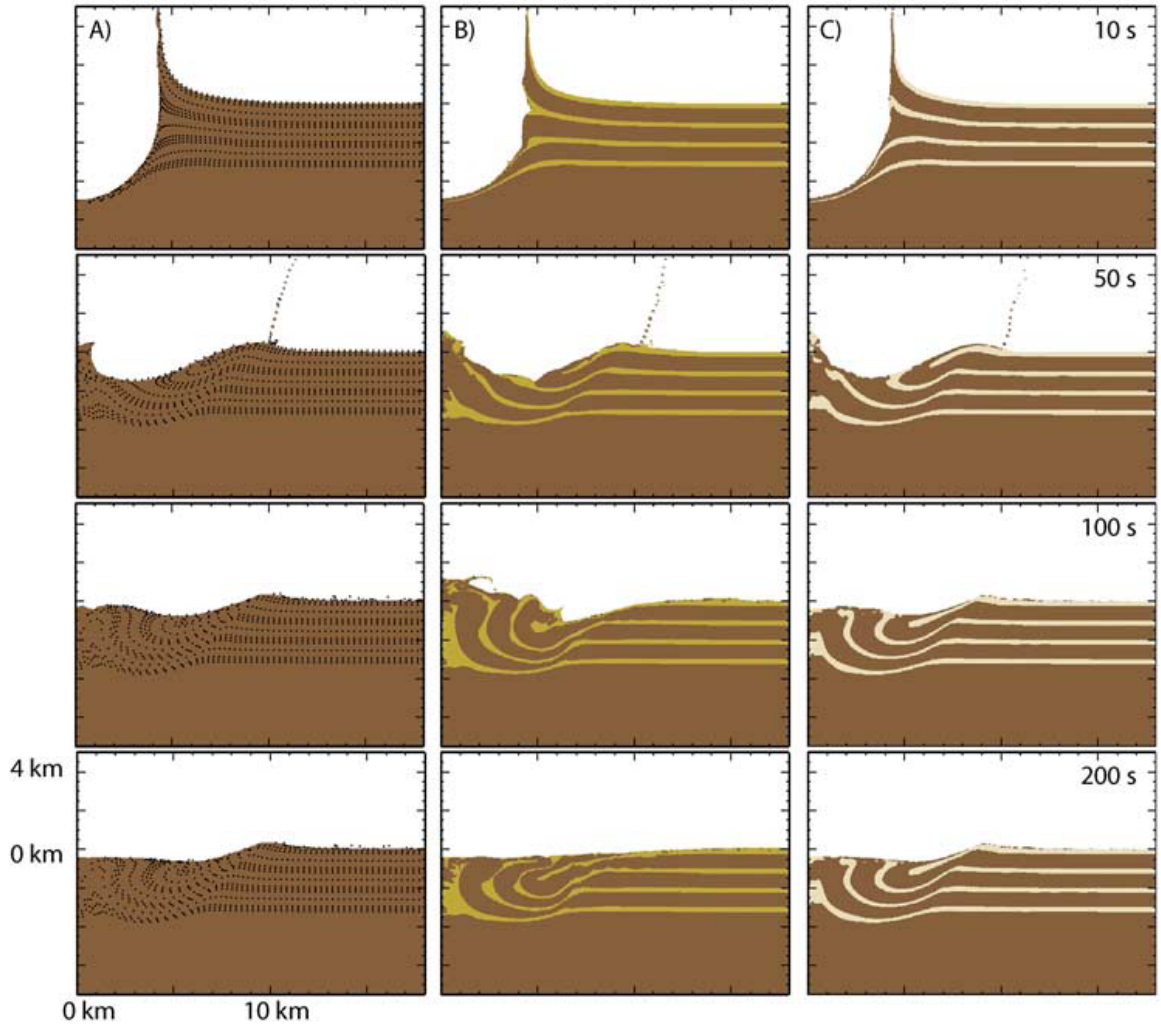

Figure 1.7: Comparison of complex impact craters formed in different layered targets. Homogeneous basalt (a), weak basaltic layers (b) and strong basaltic layers (c). The impactor has 1km in diameter with a vertical velocity of 17km/s, under Earth's gravity. The black dots in (a) are massless Langrangian tracer particles, highlighted only to show structural deformation (Senft et al. 2007).

The study shown in Figure 1.7 (Senft et al. 2007) was modeled with Earth's surface as a reference. However, in our study, the interest is focused on how the martian surface would behave to these same conditions and impacts. In Senft et al. 2008, a very similar approach is taken when studying the surface of Mars and how it behaves to big impactors. The main difference being, in this case, the introduction of ice layers, and how they behave after an impact, as well as the different gravitational field exerted by the smaller planet.

In the models presented in Senft et al. 2008, even relatively small amounts of subsurface ice can exert a significant influence on the formation and morphology of the resulting craters. Late-stage icy extrusion and crater infilling become particularly evident when the subsurface ice fraction reaches about 50% by volume. Nevertheless, even at lower concentrations (around 25%), distinct effects remain noticeable

(Senft et al. 2008), including higher ejecta angles, increased fragmentation of the ejecta blanket, and the collapse of the crater walls. This can be seen in Figure 1.8. However, for this study, our focus is set on bigger craters since the amount of material dug out is more substantial.

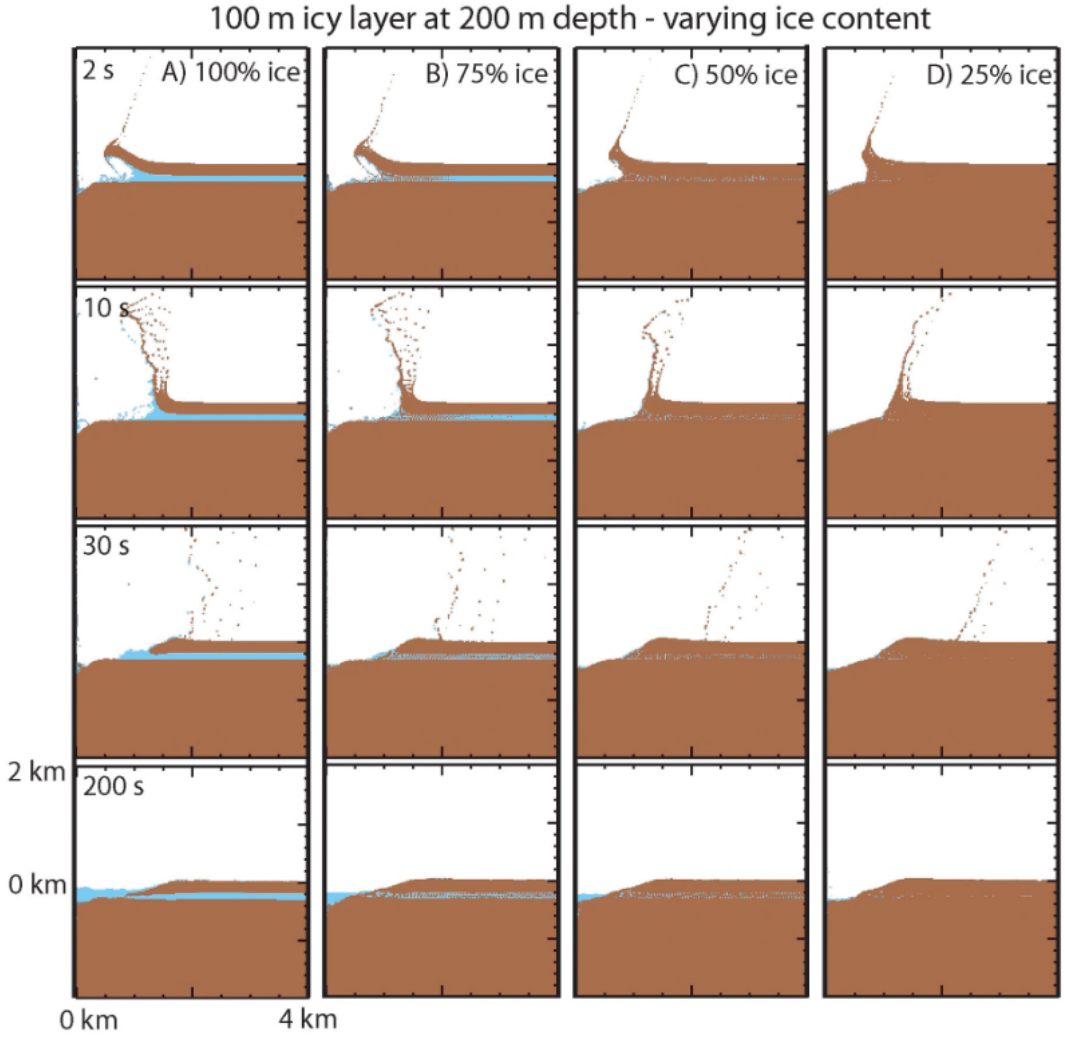

Figure 1.8: Crater formation by a 200m impactor at 10km/s. A 100m icy layer with different concentration is present. The dark color represents basalt, and the light blue color the icy layer (Senft et al. 2008).

For bigger size impactors, the simulations show that a surface ice layer promotes non-ballistic ejecta motion, while a buried layer modifies ejecta trajectories due to wave reflections and can also generate late-stage icy extrusions from the walls into the crater floor, see Figure 1.9 (Senft et al. 2008). The magnitude and type of effects caused by icy layers ultimately depend on multiple interrelated factors, including burial depth, thickness, volumetric ice content, and the surrounding material properties (Senft et al. 2008). Nevertheless, a consistent outcome of the modeling shown in Senft et al. 2008 is that significant modifications to crater structure, such as late-stage icy extrusions, are observed when the icy layer is at least 25% of the diameter of the impacting projectile. The lower threshold for detectability is less well constrained, as thinner layers have not yet been simulated. Observational data, however, suggest that such conditions are realistic for Mars.

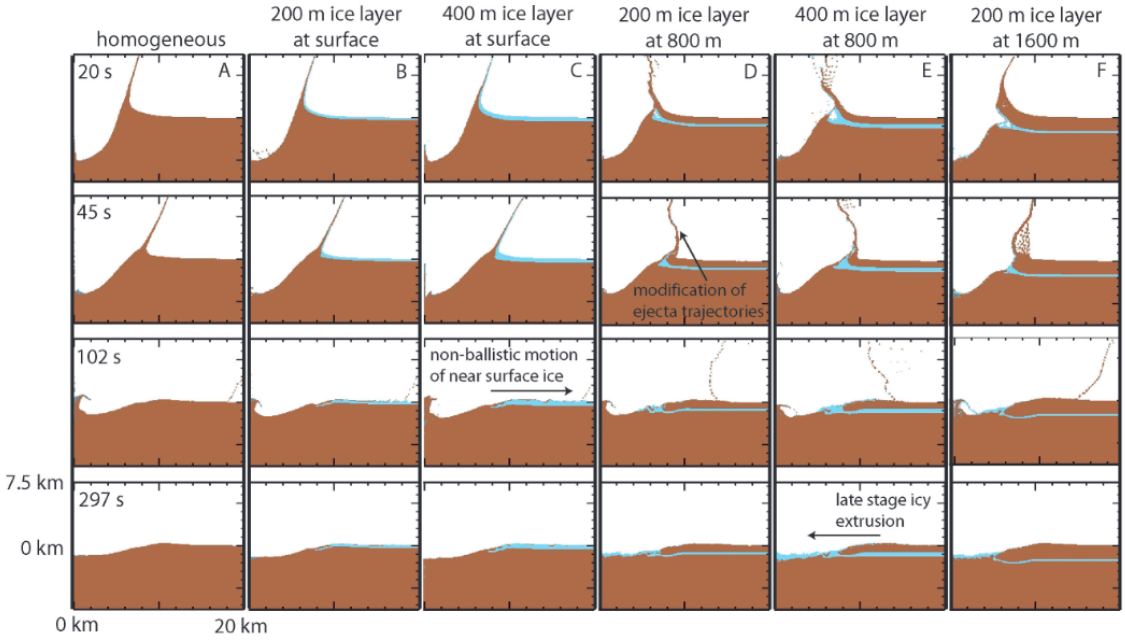

Figure 1.9: Crater formation by a 1600m impactor at 10km/s. Different configurations of a surface with ice layers are shown. The dark color represents basalt, and the light blue color the icy layer (Senft et al. 2008).

1.3 Dissemination of Results

Parts of this work have already been presented in several conferences: at Europlanet Space Congress (EPSC) in 8-13 September 2024; at Encontro Nacional de Astronomia e Astrofísica (ENAA) in 10-12 September 2025; at a workshop hosting Dr. John Carter, principal investigator (PI) of OMEGA and will also be presented at European Astrobiology Network Association (EANA) in 21-24 October 2025.

Chapter 2

Observational Data

2.1 Instruments

2.1.1 Observatoire pour la Mineralogie, l'Eau, les Glaces et l'Activit (OMEGA)

Since Mars' exploration began, in the 1960s (Harvey 1996) (Perminov 1999), missions have increasingly emphasized the importance of orbital platforms in complementing surface landers. While landers and rovers provide direct, high-fidelity data from specific locations, orbiters enable global-scale monitoring, comparative geology, and targeted high-resolution observations from above. This dual approach began with NASA's Viking program (Corliss 1974) (Mutch et al. 1976) (Shorthill et al. 1976), which paired orbiters with landers to investigate the Martian surface and atmosphere in tandem, a paradigm that has since shaped Mars exploration strategies. Orbiters such as Mariner 9 (McCauley et al. 1972) and Mars Express (Chicarro et al. 2004) have been instrumental in transforming our understanding of the planet's surface, revealing a rich geologic history that includes volcanic, fluvial, and possibly even marine processes. In contrast, landers like the Viking modules (Corliss 1974) (Mutch et al. 1976) (Shorthill et al. 1976) or China's more recent Zhurong (Xiao et al. 2023) rover offer granular, localized insights, such as sedimentary textures or mineralogical context. However, the limited range and operational lifespans of surface assets constrain their spatial coverage. Orbital spectrometers, especially instruments like OMEGA on Mars Express (Chicarro et al. 2004) (Bibring et al. 2005), overcome this limitation by systematically mapping the surface with broad spatial reach and moderate resolution.

(a)

(b)

Figure 2.1: Images of both Mars Express (a) and the OMEGA instrument (b). Credits: ESA.

The OMEGA instrument onboard the European Space Agency's Mars Express mission (Figure 2.1) is a visible–near-infrared imaging spectrometer that has played a foundational role in characterizing the

Martian surface and atmosphere. Operating across a spectral range of 0.35 to 5.2 μm (Bibring et al. 2005), OMEGA acquires hyperspectral data with spatial resolutions ranging from 350 meters to 10 kilometers per pixel , depending on orbital geometry (Bibring et al. 2005). This spectral coverage enables the identification and mapping of both primary igneous minerals (e.g., pyroxenes, olivines) and alteration products such as phyllosilicates and sulfates, as well as seasonal CO_2 and H_2O ices (Bibring et al. 2005). OMEGA has also proven critical in observing transient atmospheric phenomena including dust storms, clouds, and haze through its flexible observational modes, including nadir, limb, and spot-tracking geometries.

At the macroscale, OMEGA data has been instrumental in delineating compositional boundaries between key geological provinces, particularly at the interface between ancient, heavily cratered southern highlands and the relatively younger, volcanically resurfaced northern plains. Special attention is given to sedimentary carbonate deposits, long hypothesized to store atmospheric CO_2 and thus potentially record Mars' climatic transition. The instrument's capacity to target high-interest sites near periapsis dramatically increases sensitivity, allowing for the detection of carbonates even at low concentrations through absorption features between 3.4 and 4.0 μm (Bibring et al. 2004).

Since our aim is to collect high resolution spectra and analyze the reflectance of several points of interest, we resorted to observations with spectral cube widths of 16 and 32 pixels (see Figure 2.2)). With this configuration, we focus primarily on the 1.0 to 2.6 μm spectral window, a range particularly sensitive to hydrated silicates and OH-bearing minerals (Pan et al. 2019) (Voigt et al. 2024a) (Ehlmann et al. 2009) (Voigt et al. 2024b). These wavelengths are crucial for detecting phyllosilicates and related alteration phases, especially in geomorphic contexts such as paleolake basins, valley networks, and crater central peaks. Diagnostic absorption bands attributed to Fe/Mg-rich clays, sulfates, and iron oxides allow us to constrain past environmental conditions and trace the extent of aqueous alteration over time.

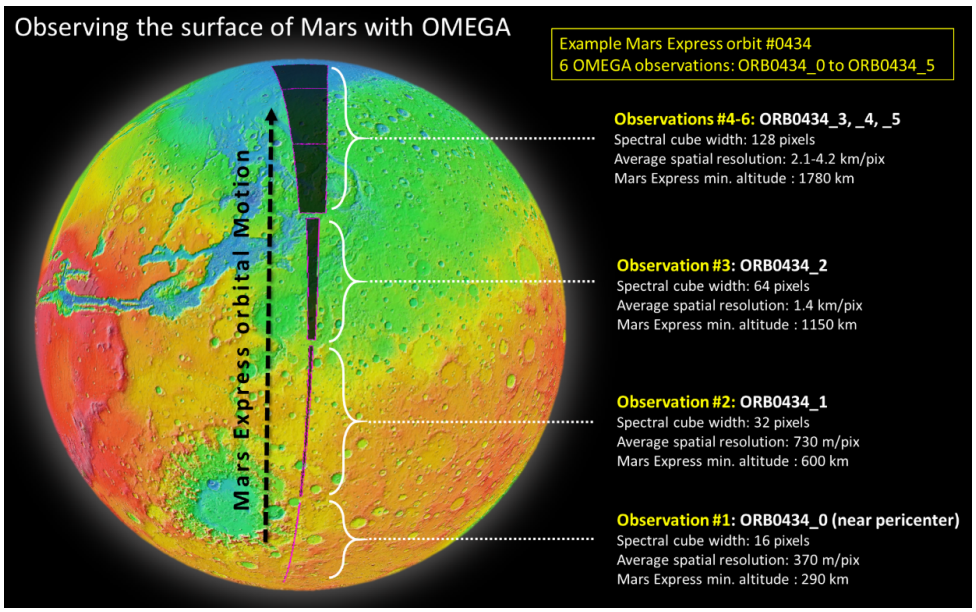

Figure 2.2: Visual representation of the different available observation styles from the OMEGA archives. Ranging from spectral cube widths of 16-128 pix, and a spatial resolution of 370m/pix to 4.2km/pix. Credits: ESA

OMEGA is a pushbroom and whiskbroom imaging spectrometer with two coaligned channels: a VNIR channel (Visible and Near-Infrared) covering 0.38-1.05 μm using a 2D CCD detector in pushbroom mode (where an entire line of the image is captured simultaneously across the field of view as the spacecraft moves forward), and a SWIR channel (Short-Wavelength Infrared) covering 0.93-5.1 μm using two InSb

(Indium Antimonide) linear arrays in whiskbroom mode (where each pixel is scanned individually across-track using a moving mirror), operating at 0.93-2.73 μm and 2.55-5.1 μm respectively (see Figure 2.3). Both channels provide up to 128-pixel-wide swaths with a shared 8.8°field of view. Data is acquired as spectral cubes (x, y, λ), with spacecraft motion providing along-track imaging. The IR arrays are cooled to 70 K via cryocoolers, and the spectrometer body to 190 K by passive radiators. Integration times range from 2.5-5 ms for SWIR and 50-200 ms for VNIR, yielding a signal-to-noise ratio greater than 100 across the entire spectral range (Bibring et al. 2004) (Bibring et al. 2005).

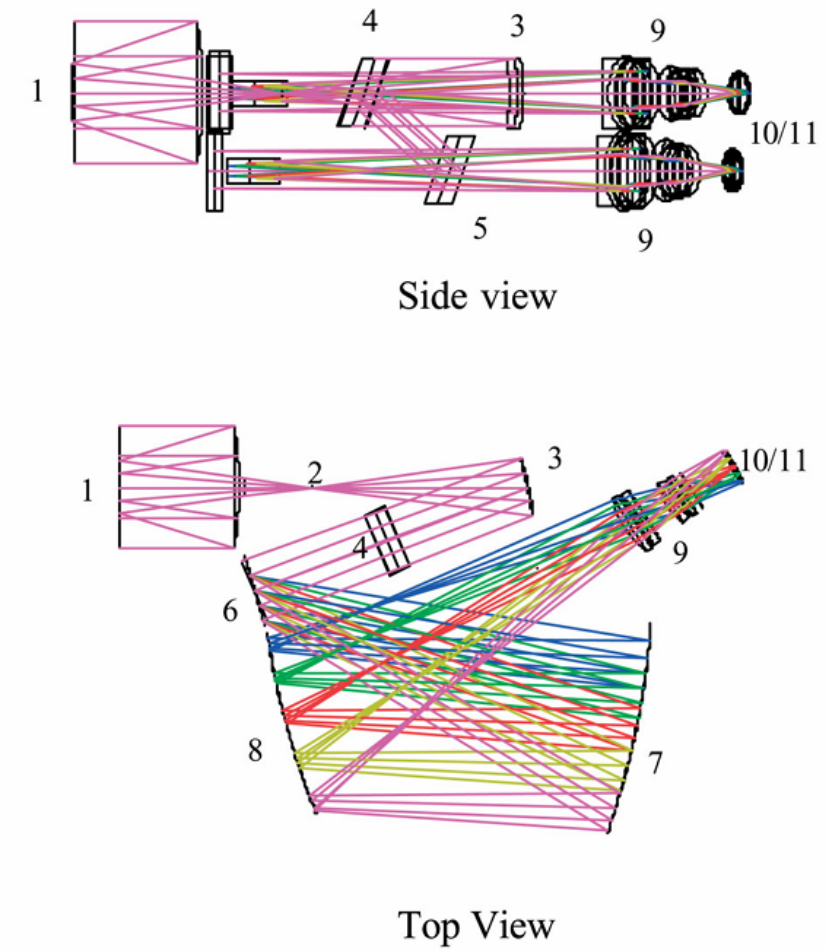

Figure 2.3: Accurate diagram representing the SWIR channel optical layout. 1: Cassegrain telescope of 200mm focal length, f/4 aperture, 4 arcmin IFOV and 15 arcmin free FOV (including the positioning tolerances). 2: Entrance slit 800µm high (spatial dimension). 3: Collimator (off-axis parabolic mirror R=192.85mm, offset 37.14mm) to collimate the beam from the slit to the dichroic and the gratings. 4: dichroic filter, separates the two channels (short wavelength is reflected; long wavelength is transmitted). 5: folding mirror, reflects the short wavelength channel to the grating. 6: blazed flat gratings working in the first order. Short wavelength: groove density 180/mm, incidence angle –6.5°and blazed wavelength 1.7μm; long wavelength: groove density 120/mm, incidence angle –10.6°and blazed wavelength 3.8 μm. 7: spherical collector mirrors (R=378.49mm), re-image the diffracted image of the slit near the field mirrors. 8: spherical field mirrors (R=378.49mm), image the grating inside the objective. 9: objectives, four spherical ZnSe lenses, re-image the diffracted image of the slit. 10: sets of filters in front the detector. 11: InSb detector linear arrays (128 pixels of 90x120μm photosensitive area and pitch of 120μm.) (Bibring et al. 2004).

2.1.2 Compact Reconnaissance Imaging Spectrometer for Mars (CRISM)

The CRISM instrument onboard NASA's Mars Reconnaissance Orbiter (MRO) is a visible to near-infrared imaging spectrometer designed to detect mineralogical signatures associated with aqueous and

hydrothermal processes on the Martian surface (Figure 2.4). Operating over a spectral range of 0.362 to 3.92 μm (Murchie et al. 2007), CRISM collects hyperspectral data at multiple spatial resolutions. In its high-resolution "targeted" mode, it acquires data at 15–38 meters per pixel across 544 spectral channels, while in global survey mode, it captures lower-resolution multispectral images at 100–200 meters per pixel using a subset of 72 selected wavelengths. This configuration allows for both wide-scale mineralogical mapping and the precise identification of localized alteration products, including hydrated sulfates, phyllosilicates, and iron oxides (Pelkey et al. 2007).

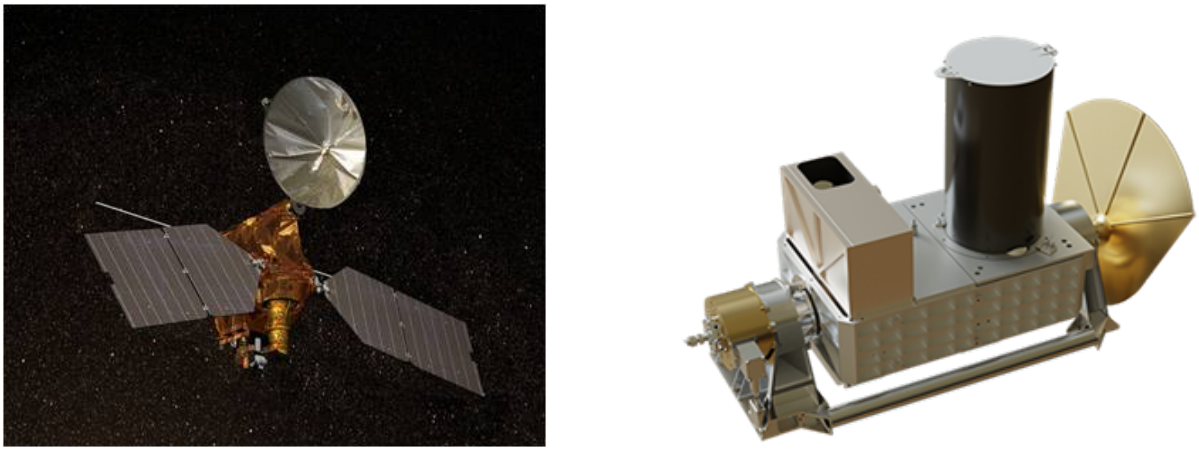

(a) (b)

Figure 2.4: Images of both Mars Reconnaissance Orbiter (a) and the CRISM instrument (b). Credits: NASA.

CRISM's dual observational strategy combines global reconnaissance with targeted follow-ups. The multispectral survey provides near-global coverage for detecting minerals that may be morphologically subtle or spatially confined, such as phyllosilicate-bearing outcrops along crater rims or talus slopes. These observations also support one of MRO's secondary objectives: the identification of new scientifically compelling sites for future exploration. In targeted mode, CRISM produces detailed mineralogical maps of candidate sedimentary basins, volcanic terrains, and crustal sections, regions critical for understanding Mars' aqueous and climatic evolution (Murchie et al. 2007).

To capture high-resolution reflectance spectra of key sites, we rely on targeted observations with full spatial and spectral resolution (15-38 m/pixel, 544 channels). These focus on the 1.0 to 2.6 μm window, which is particularly sensitive to hydroxyl- and water-bearing minerals (see Figure 2.5). In this range, diagnostic absorptions from Fe/Mg-phyllosilicates, hydrated sulfates, and iron oxides help constrain past aqueous environments and identify alteration sequences in ancient terrains such as Nili Fossae, Mawrth Vallis, and Jezero Crater (Ehlmann et al. 2009) (Mustard et al. 2005) (Voigt et al. 2024a). CRISM's increased resolution over OMEGA enables the detection of alteration phases at sub-kilometric scales that were previously undetectable from orbit (Pelkey et al. 2007).

CRISM is a pushbroom imaging spectrometer comprising two coaligned spectral channels. Light from a 100 mm aperture, 441 mm focal length Ritchey–Chrétien telescope passes through a narrow entrance slit and is split by a dichroic beamsplitter into VNIR (0.362-1.05 mum) and IR (1.0-3.92 mum) paths. Each is routed to a modified Offner spectrometer and focal plane assembly (Murchie et al. 2007), where the light is dispersed via custom dual-zone gratings and projected onto two detectors: a CCD for VNIR and a cryogenically cooled HgCdTe array for IR wavelengths. Spectral cubes are recorded in (x, y, λ) format as the spacecraft moves forward, with each detector optimized for high signal-to-noise performance across its range (Murchie et al. 2007).

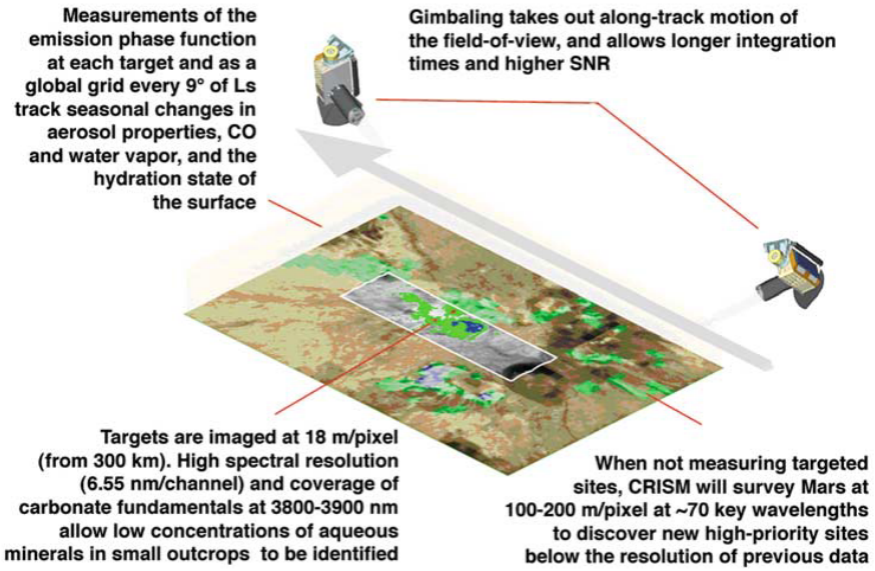

Figure 2.5: Schematic diagram of CRISM's data aquisition strategies (Murchie et al. 2007)

The instrument structure is built from aluminum to maintain focus stability under thermal fluctuations, and the optical bench doubles as a Mars-facing radiator to reduce thermal background. The IR detectors are passively cooled via the bench and radiator assembly, enabling sensitive acquisition even in the longer wavelengths. Spectral integration times and readout modes are optimized for each channel, and extensive internal baffling and order-sorting filters minimize stray light and suppress higher-order contamination. These design features allow CRISM to maintain strong spectral fidelity across both survey and targeted operational modes (Figure 2.6) (Murchie et al. 2007).

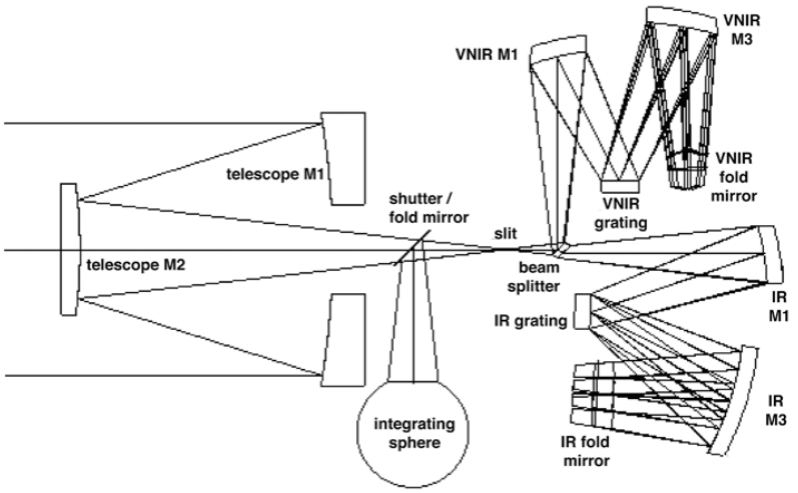

Figure 2.6: Optical design of CRISM's telescope and spectrometers (Murchie et al. 2007)

2.2 The Data: 10 sets of spectroscopic images from both OMEGA and CRISM

The first step in acquiring the data is to select suitable candidates for study. A total of ten areas were analyzed. Our starting point, as previously mentioned, was the work of Xiao et al. 2023 and the landing zone of the Zhurong rover. From there, we looked for potential water channels, or even craters that could have harbored paleo lakes. In the surrounding regions of Tianwen-1, four points of interest were chosen, two craters and two other features potentially formed under the influence of flowing water. One of the goals of this work was to follow the putative shorelines seen in Figure 1.6, and accordingly, three more areas of interest were chosen. The remaining two regions studied were big impact craters in the northern hemisphere, further away from the shorelines in Wang et al. 2024. Although this choice may seem counter intuitive, these sites were of particular interest due to their location within the northern lowlands and the geological implications of large impacts on surface and subsurface sedimentary structures as seen in section 1.2.4 (all regions described can be see in Figure 2.7). One last region will be shown, the Terby crater, a previously studied and analyzed area. This will serve as a starting point, and as a calibration mechanism for this study by doing comparative analysis with the results gotten from our methods with the results in literature.

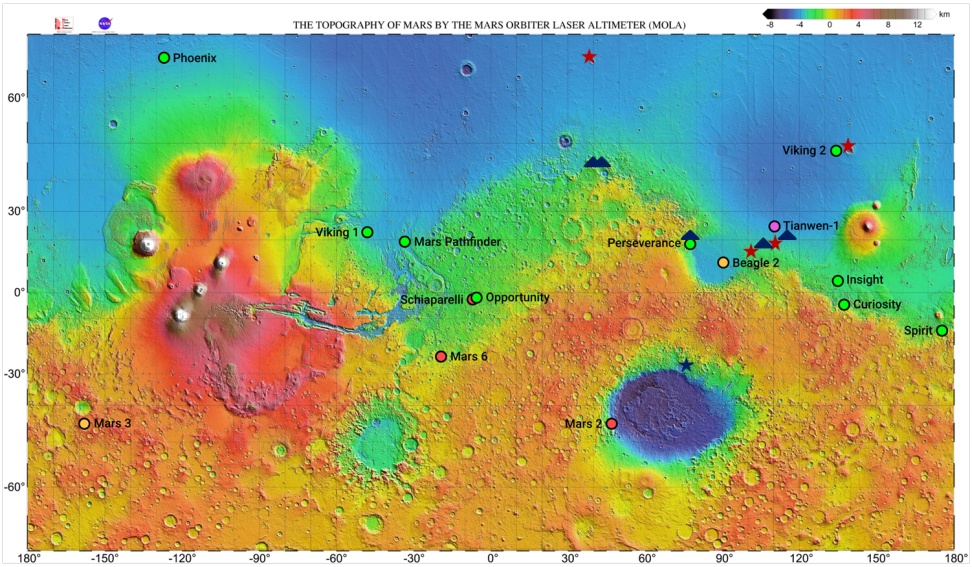

Figure 2.7: Martian topographic map by MOLA. In this map, the different rover landing spots are highlighted as colored circles. The regions studied in the context of this work are seen as red stars, for the craters, and the blue triangles, for possible water channels.

All spectral data were retrieved from the MARSSI database. For OMEGA, we prioritized the highest available spatial resolution (16-pixel-wide cubes) whenever possible. However, not all selected regions were fully covered at this resolution, forcing us to use of some 32-pixel-wide observations as well (see Table 2.1). For CRISM, we exclusively used TARGETED LONG observations, as they provide the spectral range required for this study (see Table 2.2). It is also worth noting that several of the selected regions were extensive enough to warrant the analysis of multiple images to adequately capture all relevant features.

Table 2.1: OMEGA observations of the different points of interest studied in the context of this work. The first column represents the names of the orbits, the second represents the resolution of the images, either 32px or 16px spectral cube width. The third column the date the images was taken, and the final two, the respective coordinates. The last, highlited row, represents Terby's crater image used. The images, as well as the date/resolution was taken from the MARSSI database.

Image	Type	Date	Lat (N)	Lon (E)
ORB7475_0	16px	October 31 2009	45.1547°	39.9247°
ORB3073_5	32px	June 2 2002	45.1593°	38.1881°
ORB2977_5	32px	May 6 2006	18.1372°	113.2285°
ORB3003_5	32px	May 13 2006	17.2831°	77.3999°
ORB0907_5	32px	October 3 2004	20.2609°	115.4006°
ORB0022_3	32px	January 15 2004	16.1129°	100.9849°
ORB7228_0	16px	August 21 2009	20.4809°	109.4832°
ORB5237_2	32px	January 30 2001	48.1477°	139.5587°
ORB1578_0	32px	April 9 2005	66.3250°	39.8062°
ORB4199_3	16px	April 13 2007	-27.5220°	74.2799°

Table 2.2: CRISM observations of the different points of interest studied in the context of this work. The first column represents the names of the images, the second represents the date the images was taken, and the final two, the respective coordinates. The last, highlited row, represents Terby's crater image used. The images were taken from the MARSSI database.

Image	Date	Lat (N)	Lon (E)
FRS0002EFEE_01	April 4 2014	45.1547°	39.9247°
FRT00017688_07	March 23 2010	45.1593°	38.1881°
HRL000166AD_07	February 10 2009	18.1372°	113.2285°
FRS00038CD4_01	October 28 2015	17.2831°	77.3999°
FRT00009E1A_07	February 11 2008	20.2609°	115.4006°
FRT0000A4AF_07	March 7 2008	16.1129°	100.9849°
FRT0000876A_07	October 27 2007	20.4809°	109.4832°
FRT0000B116_07	June 13 2008	48.1477°	139.5587°
HRL0000B1FA_07	June 17 2008	66.3250°	39.8062°
FRT000059DF_07	April 25 2007	-27.5220°	74.2799°

2.3 Observational data reduction: OMEGA-PY, CAT and EN-MAPBOX

2.3.1 The OMEGA-PY python module

The correction of OMEGA spectral data begins with the removal of atmospheric gas absorption features, following the methodology outlined by Jouglet et al. 2007, Langevin et al. 2005 and Stcherbinine et al. 2021. This process involves dividing each observed spectrum by a reference transmission spectrum derived from observations taken at both the summit and base of Olympus Mons (the equivalent of more than 20 km of atmosphere removal). This reference spectrum accounts for the absorption effects of the Martian atmosphere and is scaled to the appropriate atmospheric column height using the 2 μm CO_2 absorption band as a calibration feature.

To facilitate this process, OMEGA data are processed using the Python module OMEGA-Py, which re-implements the latest version of the official OMEGA reduction pipeline (SOFT10) and extends its functionality (Stcherbinine et al. 2021). This open-source tool includes built-in routines for atmospheric and thermal emission corrections, along with a suite of utilities for data visualization and composite map generation. The ability to perform all essential pre-processing steps, ranging from radiometric calibration

to the application of spectral corrections, within a single, user-friendly framework that greatly streamlines the analysis of OMEGA data products and supports reproducible science (Stcherbinine et al. 2021).

In addition to its robust correction routines, OMEGA-Py offers tools for detailed spectral analysis at the pixel level. We can easily extract individual spectra from selected pixels across a scene, enabling localized and composite investigations. The module also provides interactive visualization features that allow us to browse through OMEGA images, select specific regions of interest, and directly analyze the associated spectra (see Figure 2.8).

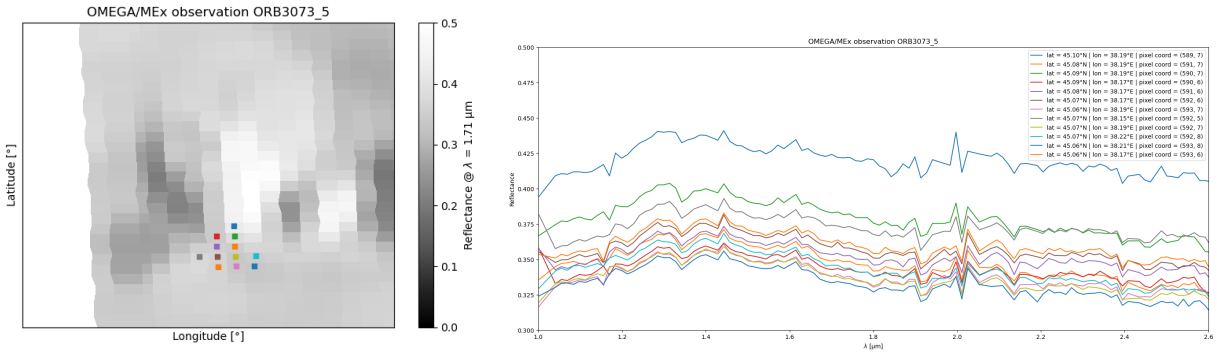

(a) (b)

Figure 2.8: Example of one of the studied OMEGA observations (ORB3073_5). The left image shows the region of interest zoomed in, as well as the pixels from which the spectra were taken (a); on the right hand side, the respective spectra and their coordinates (b). This very well highlights the capabilities and simplicity of the OMEGA-PY software.

2.3.2 CRISM Analysis Tool (CAT) and EN-MAPBOX

The correction of CRISM spectral data begins with the application of the MTRDR (Map-projected Targeted Reduced Data Record) processing pipeline, which systematically corrects the raw radiance data collected by the instrument. This includes a Lambertian photometric correction, a refined atmospheric removal based on the "volcano scan" method (Langevin et al. 2005) (Viviano et al. 2014) and empirical adjustments to mitigate instrumental artifacts such as spectral smile and shifts in wavelength calibration due to changing observation geometry (Murchie et al. 2007) (Viviano et al. 2014). A key step in the correction process involves aligning data from the VNIR (0.4-1.0 μm) and IR (1.0-3.9 μm) detectors to create a continuous spectral cube, which in our case, only the IR portion is relevant. This is achieved through nearest-neighbor resampling, avoiding spectral averaging and ensuring accurate geospatial registration between the detectors.

These corrections are typically performed using the CRISM Analysis Tool (CAT), an IDL-based software package developed to support targeted hyperspectral data processing. CAT provides access to all essential functionalities needed to handle CRISM MTRDR products, including atmospheric and photometric corrections, detector alignment, parameter calculation and advanced spectral analysis. It also supports the generation of mineralogical summary products and the extraction of spectra for comparison with reference libraries (Viviano et al. 2014).

The final step in analyzing CRISM images is to load them into a QGIS plug in called EN-MAPBOX. This software allows the images and their corresponding parameters to be plotted simultaneously, allowing for a more user friendly experience, see Figure 2.10. With both the corrected image and the corresponding parameters, the plug in now allows for different filters to be applied. In alignment with Viviano et al. 2014, we apply the different filters that correspond to the different minerals to better identify where, if at all, they are concentrated in our images. It should also be mentioned, that some CRISM observations

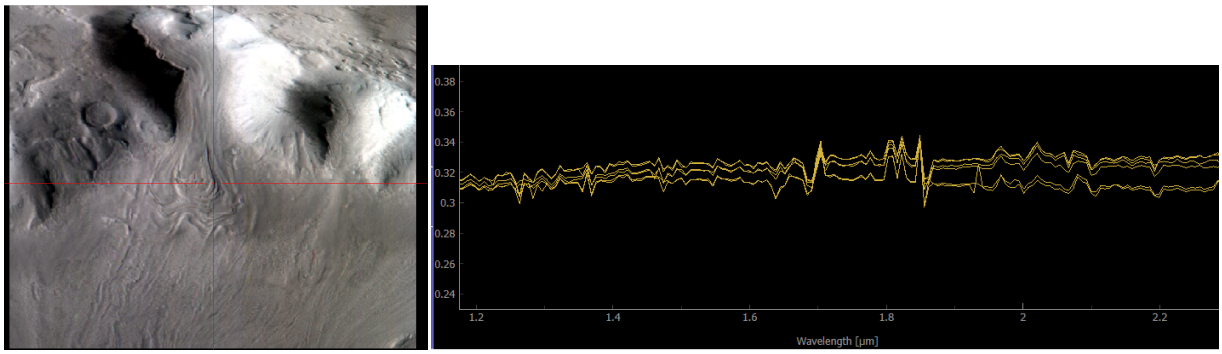

(a) (b)

Figure 2.9: Example of one of the studied CRISM observations (FRT00017688_07). The left image shows the region of interest zoomed in, as well as the region from which the spectra were taken (a); on the right hand side, the respective spectra (b). The image was processed using the EnMap-Box 3 software.

are not as "noise-free" as we would like, and as such, not every filter, for every mineral, will provide an accurate description of the areas in study.

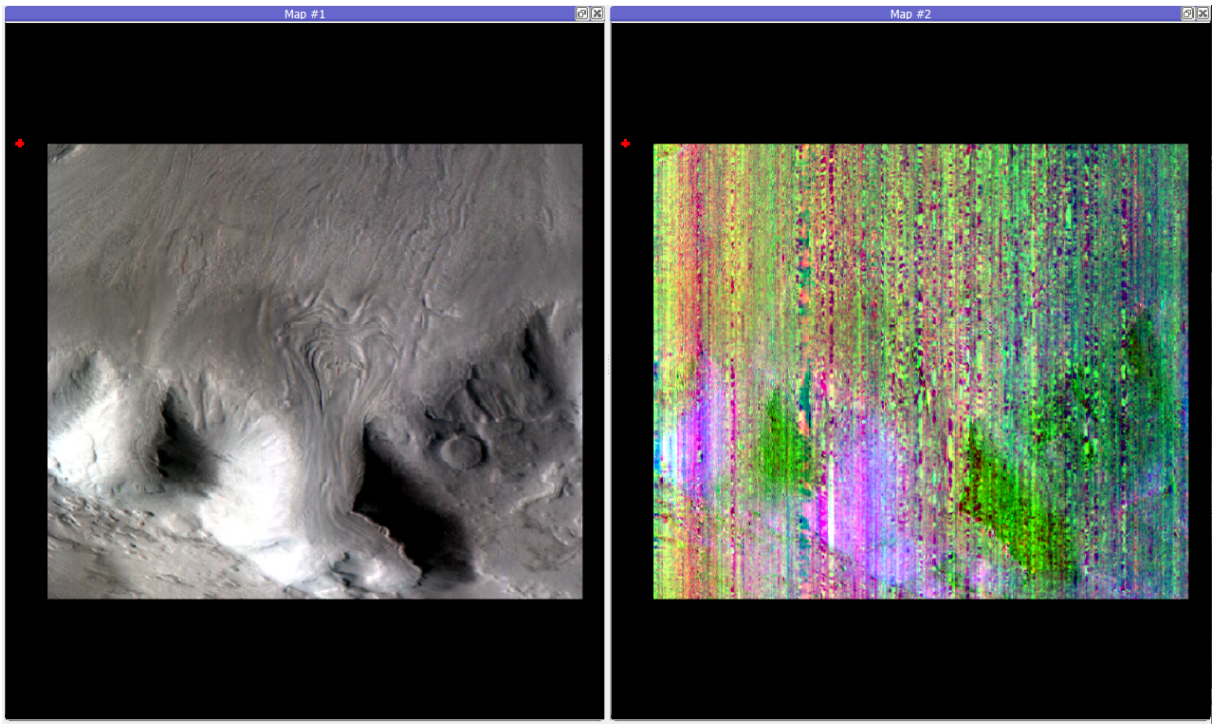

Figure 2.10: Example of one of the studied CRISM observations (FRT00017688_07) plotted into EN-MAPBOX. The left image shows the actual observation of the region of interest, and the right image shows the parameters obtained after the CAT corrections were applied.

Chapter 3

Methods and Tools

3.1 Reflectance

Reflective optical radiation corresponds to electromagnetic energy within the wavelength range of 0.4 to 3 μm (Baumgardner et al. 1986). When such radiation interacts with a surface, several processes may occur: part of the incoming energy can be absorbed by the subsurface material, part can be transmitted through the bulk into another medium, and the remainder is reflected. The ratio between the reflected portion and the total incident radiation is defined as reflectance (Baumgardner et al. 1986). This term represents a measurable property dependent on surface interactions and should be distinguished from reflectivity, which describes an intrinsic material property.

In order to frame the concept of reflectance more precisely, it is necessary to introduce some fundamental radiometric terminology. Irradiance (E) refers to the optical radiative power incident on a unit area, expressed in watts per square meter (W/m^2). When this radiative power is described as a function of wavelength, the term spectral irradiance is employed, with units of watts per square meter per micrometer [W/(m^2 μm)](Baumgardner et al. 1986). In contrast, the quantity most commonly used to describe reflected radiation is radiance (L), which measures the power per unit area per unit solid angle, with units of watts per square meter per steradian [W/(m^2 sr)]. Its wavelength-dependent counterpart is spectral radiance, expressed in watts per square meter per steradian per micrometer [W/(m^2 sr μm)](Baumgardner et al. 1986). The terminology here described can be seen in practice in Figure 3.1. These properties are best described using a parameter called bidirectional reflectance distribution function (BRDF). The BRDF is defined as:

$$f_r(\theta, \phi; \theta', \phi') = \frac{dL(\theta, \phi; \theta', \phi'; E)}{dE(\theta, \phi)} sr^{-1} \tag{3.1}$$

The BDRF has units of sr^{-1} since it represents the ratio of a radiance to an irradiance. If both the numerator and denominator are spectral quantities, a spectra BRDF is defined and can be represented by λ (Baumgardner et al. 1986). Upon careful examination of Figure 3.1, it is visible that it is a ratio of two differential solid angles. This is a mathematical technique commonly used in physical situations where the solid angles are small enough to be approximated to their differential counterpart.

What we now see in Figure 3.2 is a very simplified diagram of what the orbiters on Mars and their respective spectrometers are doing when capturing reflectance data. On our case, the reference target is the minerals studied in laboratory conditions, more specifically, the MICA Library, which will be described in further detail in the next sections. With spectra to use as references, we can now point our spectrographs to the martian soil and perform comparative analyses to identify the different minerals.

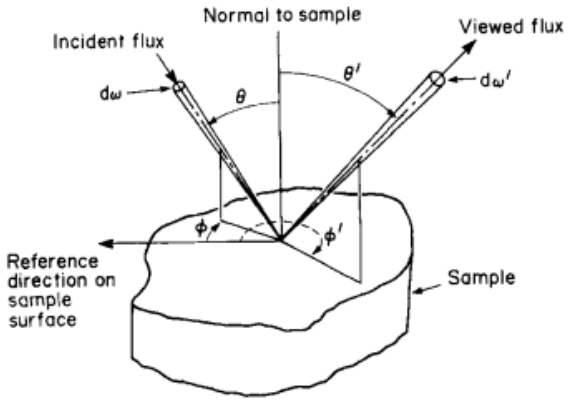

Figure 3.1: Geometric parameters that describe the reflection of a surface. zenith angle: θ, azimuth angle: ϕ and beam solid angle: ω. (Baumgardner et al. 1986).

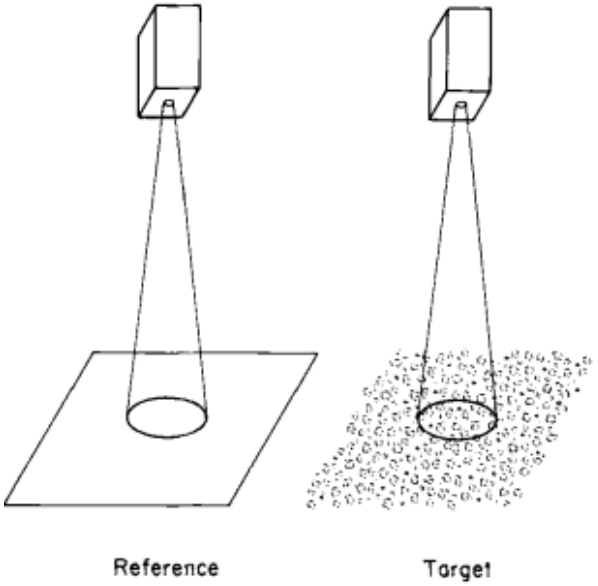

Figure 3.2: Illustration of the procedure for measuring the reflectance factor. A reference measurement is made in predetermined conditions in order to catalog the materials, and only then is the method applied on the target in study (Baumgardner et al. 1986).

3.2 The MICA Library

The MICA (Mars Investigations of Composition and Alteration) spectral library is a curated collection of representative CRISM spectra designed to reflect the full range of mineralogical diversity observed on the Martian surface in the combined CRISM and OMEGA wavelength range. Initially, CRISM summary products were tailored to a limited set of 72-band multispectral data, guided by prior detections from OMEGA (Pelkey et al. 2007) (Viviano et al. 2014). However, as hyperspectral imaging by CRISM and continued OMEGA analysis have revealed increasingly diverse and spatially complex mineral assemblages, the need for a more comprehensive spectral reference became evident.

To address this, the MICA library was developed by selecting type spectra from well-characterized Martian locations that represent key mineral classes identified to date, such as phyllosilicates, sulfates, carbonates, and mafic silicates. These spectra were derived from fully corrected CRISM hyperspectral data, processed to MTRDR level and ratioed to remove atmospheric and photometric effects, and selected for their clarity, distinctiveness, and geological context. Each entry in the library is tied to a specific

CRISM observation and geographic site, providing both spectral and spatial provenance. By offering a standardized set of high-quality reference spectra, the MICA library enables consistent mineral identification across the Martian surface and supports the continued refinement of CRISM's spectral analysis tools and summary products (Viviano et al. 2014).

3.3 Minerals

3.3.1 Ices

Water ice and CO_2 ice on Mars can be distinguished spectrally despite often coexisting within a single observation pixel. Crystalline water ice is characterized by a broad absorption band centered around 1.5 μm, whereas CO_2 ice exhibits a sharp, narrow absorption feature at 1.435 μm, linked to the asymmetric stretching overtone of the CO_2 molecule (Viviano et al. 2014). This CO_2 band is particularly valuable because it remains unsaturated even at path lengths exceeding 20 cm, is not obscured by nearby atmospheric CO_2 absorptions at 2 μm, and is 2.3 times stronger than the next most prominent CO_2 ice band at 2.281 μm. The strength of these absorptions in both ices depends largely on the mean path length of photons through the material, which in turn is influenced by factors such as grain size, internal fractures, and the presence of dust inclusions (Viviano et al. 2014) (see Figure 3.3).

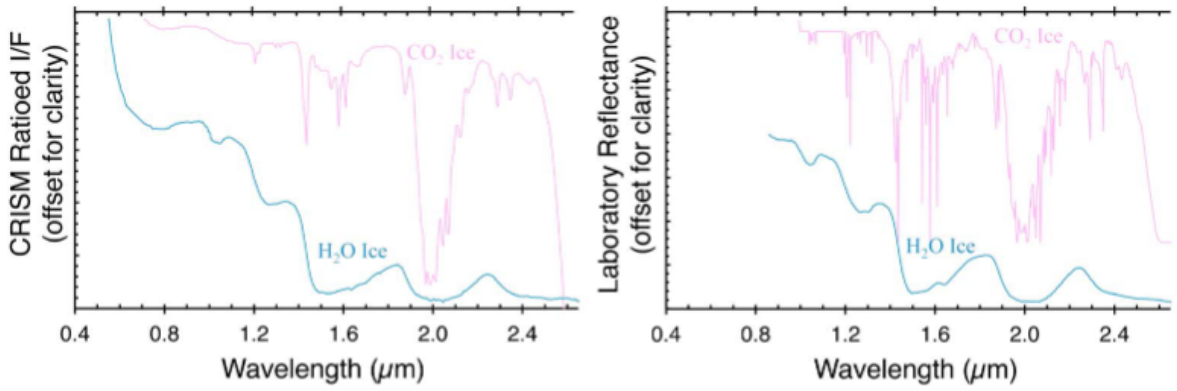

Figure 3.3: MICA type spectra of both H_2O ice and CO_2 ice (left) and their respective analog laboratory materials (right) (Viviano et al. 2014).

3.3.2 Iron Oxides and Primary Mafic Silicates

Variations in mafic silicates and iron oxides are key to reconstructing the igneous and alteration history of the Martian crust. Among iron oxides, hematite, maghemite, jarosite, and nanophase oxides are commonly detected due to their characteristic absorption features in the visible and near-infrared (VNIR) spectrum (Viviano et al. 2014). Hematite, for instance, exhibits a broad absorption near 0.86 μm, while ferric iron causes a sharp absorption edge at 0.53 μm, both useful markers within the spectral range of CRISM and OMEGA instruments. The detection of these ferric phases helps constrain recent weathering processes and dust contributions on Mars (Viviano et al. 2014). Notably, iron oxides are widespread across the planet and can be observed in both soils and dust coatings, underscoring their geochemical importance.

Olivine and pyroxene, two of the most abundant primary mafic silicates, are critical for understanding mantle composition and volcanic history. Olivine shows a broad 1 μm absorption band, which varies in

position and shape with Fe/Mg content and grain size, reflecting compositions ranging from forsterite-rich (Fo_91) to fayalite-rich (Fo_5). Its spectral simplicity beyond 1.5 μm makes it distinguishable from other mafic minerals, and its occurrences span from the ancient Noachian crust to basin ejecta and tectonic features like dikes (Viviano et al. 2014). Pyroxenes, on the other hand, exhibit two prominent absorptions near 1 and 2 μm , with low-calcium pyroxenes (LCP) and high-calcium pyroxenes (HCP) differentiated by band positions at 0.9/1.8 μm and 1.05/2.3 μm respectively (Viviano et al. 2014). Their distribution, especially the restriction of LCP to ancient terrains, suggests a chemically evolving Martian mantle and supports petrologic models involving fractional crystallization (Viviano et al. 2014).

Plagioclase, while spectrally subtle, is the most abundant mineral in the Martian crust (Viviano et al. 2014). Thermal Emission Spectrometer (TES) observations suggest compositions near An_60, and while feldspar is often obscured by stronger mafic signatures in mixed spectra, minor Fe^{2+} substitution can introduce a broad absorption feature around 1.25-1.31 μm, detectable in feldspar-dominated exposures. These have been identified in regions such as northern Hellas, Syrtis Major, and large crater rims, and are frequently associated with hydrated alteration minerals. Together, the identification and mapping of these mafic silicates and iron oxides offer crucial insights into Mars' volcanic, tectonic, and aqueous history (Viviano et al. 2014). All of these minerals' spectral features can be seen in Figure 3.4.

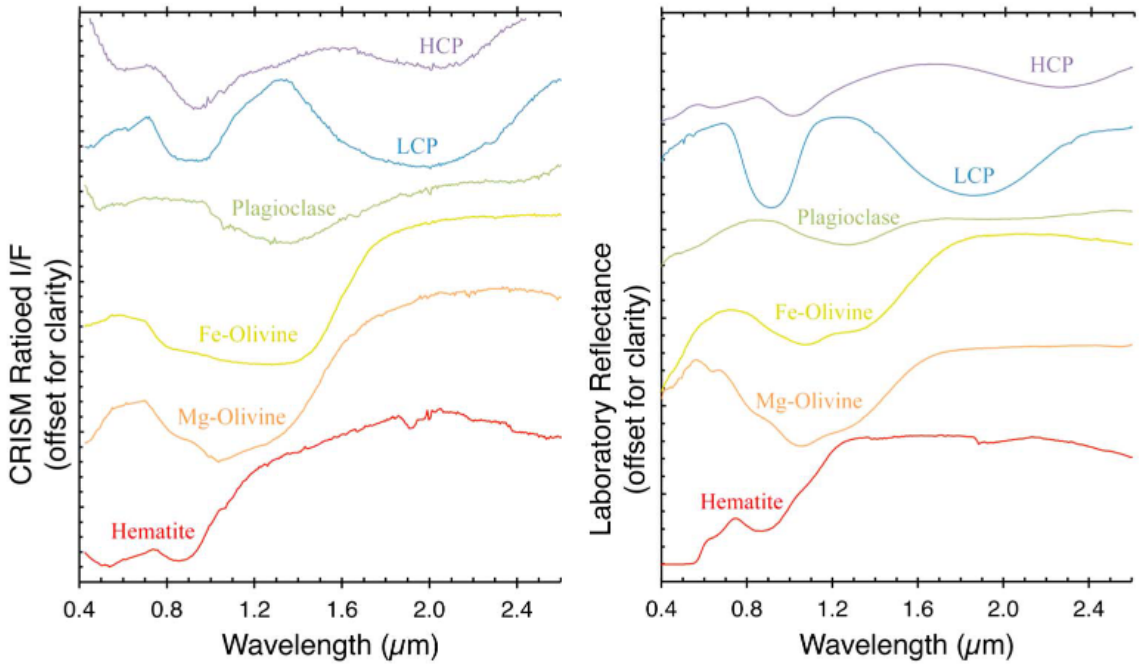

Figure 3.4: MICA type spectra of iron oxides and mafic silicates (left) and their respective analog laboratory materials (right) (Viviano et al. 2014).

3.3.3 Sulfates

Sulfate-bearing deposits on Mars record secondary alteration processes driven by acidic groundwater circulation, acidic precipitation, frost activity, or the evaporation of briny waters. Extensive sulfate signatures are observed in Valles Marineris' interior layered deposits and adjacent chaos terrains, as well as in Meridiani Planum and surrounding Arabia Terra. Gypsum-rich dunes dominate the periphery of the northern polar ice cap, indicating sulfate formation in both equatorial and polar settings. The mineralogy of these deposits reflects varying hydration states: polyhydrated sulfates exhibit a broad

1.9 μm absorption from combined water stretching and bending vibrations, while monohydrated sulfates display a 2.1 μm absorption whose precise position depends on the associated cation (e.g., Mg-kieserite vs. Fe-szomolnokite), visible in Figure 3.5. Both groups also show a feature near 2.4 μm from water combination bands or overtones (Viviano et al. 2014).

Distinctive spectral signatures allow the identification of several sulfates, including kieserite, jarosite, bassanite, gypsum, alunite, and an enigmatic Fe-rich hydroxylated sulfate with no terrestrial analogue. Likely surface-stable polyhydrated sulfates such as epsomite, hexahydrite, amorphous Mg-sulfate, and starkeyite have also been proposed (Viviano et al. 2014). However, polyhydrated sulfates are more challenging to confirm due to spectral overlap with other hydrous minerals.

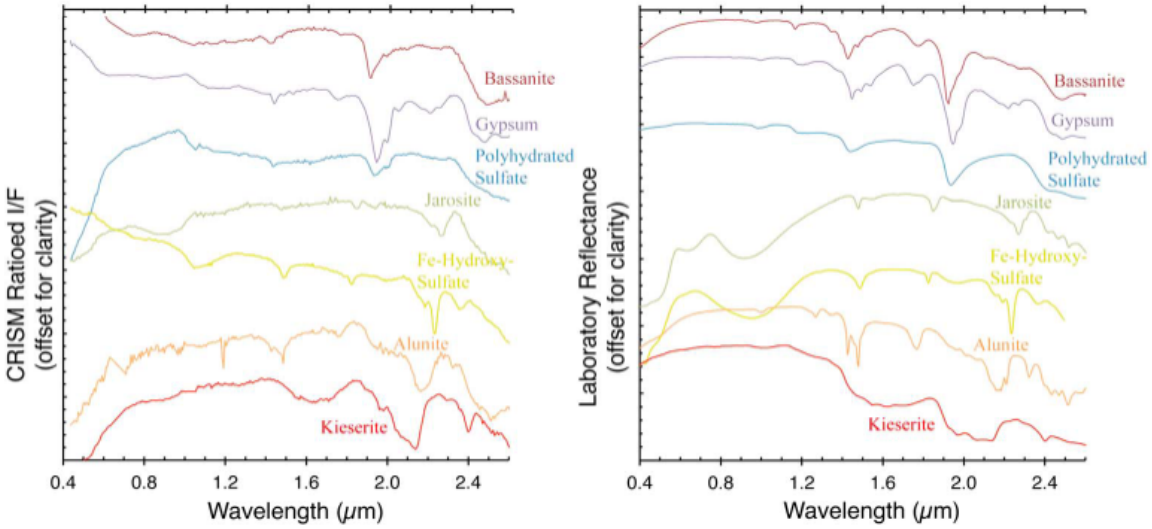

Figure 3.5: MICA type spectra of sulfates (left) and their respective analog laboratory materials (right) (Viviano et al. 2014).

3.3.4 Phyllosilicates

Phyllosilicates on Mars encompass a wide variety of mineral groups, including Al-rich phases (Al-micas, Al-smectites, kaolinite-group minerals) and Fe/Mg-bearing phases (smectites, serpentine, talc, chlorite, prehnite), most abundantly preserved in ancient Noachian crust. Al-smectites such as montmorillonite and beidellite, kaolinite, and Al-micas like illite, muscovite, and margarite are identified through prominent absorptions near 2.2 μm, with micas further distinguished by additional bands at 2.26, 2.35, and/or 2.44 μm. Kaolinite displays a diagnostic 1.4 μm OH vibration and a 2.16–2.21 μm doublet from Al–OH combinations (Viviano et al. 2014). These Al-rich clays are particularly prevalent in Mawrth Vallis and Arabia Terra, often forming stratigraphic sequences with Fe/Mg clays below, indicative of surface weathering. Similar sequences appear in Valles Marineris, Thaumasia Planum, Eridania Basin, Noctis Labyrinthus, Nili Fossae, and Noachis Terra, with Al-micas frequently associated with impact craters, suggesting diagenetic alteration of Al-smectites to illite (Viviano et al. 2014).

Fe/Mg-bearing phyllosilicates are the most common hydrous minerals on Mars and include Fe-smectite (nontronite), Mg-smectite (saponite), serpentine, talc, chlorite, and prehnite. They are recognized by OH and structural H_2O absorptions at 1.4 and 1.9 μm, along with a 2.28–2.32 μm band that shifts with Mg–Fe substitution (Viviano et al. 2014). Talc shares the 2.31 and 2.39 μm absorptions with Mg-smectite but is distinguished by the absence of interlayer water and specific continuum changes near

2.35 μm. Chlorites display a strong 2.33–2.35 μm Mg–OH absorption that shifts with iron content, as well as weaker bands near 2.25–2.26 μm. Prehnite, stable under specific hydrothermal or low-grade metamorphic conditions, exhibits a 2.35–2.36 μm band with a diagnostic 1.48 μm feature distinguishing it from Fe-rich chlorite. Serpentine is characterized by absorptions at 2.32 and 2.51 μm from Mg–OH or metal–OH combinations, a weaker but diagnostic 2.1 μm band, and OH overtones at 1.39 μm (Viviano et al. 2014), all of these absorptions are seen in Figure 3.6.

Geologically, Fe/Mg-phyllosilicates are distributed in stratified deposits such as those in Mawrth Vallis, in crustal exposures revealed by impact craters (e.g., Tyrrhena Terra), within ancient outcrops, and more rarely in alluvial fans or deltaic deposits. Chlorites often occur in crater settings, consistent with diagenetic transformation of Mg-smectite. Prehnite's restricted stability range makes its detection a valuable indicator of past hydrothermal systems at 200–350 °C and pressures below ~3 kbar. Serpentine occurrences are sparse but confirmed in Nili Fossae, Claritas Rise, and in several southern highland craters, representing key markers of past ultramafic rock alteration under aqueous conditions.

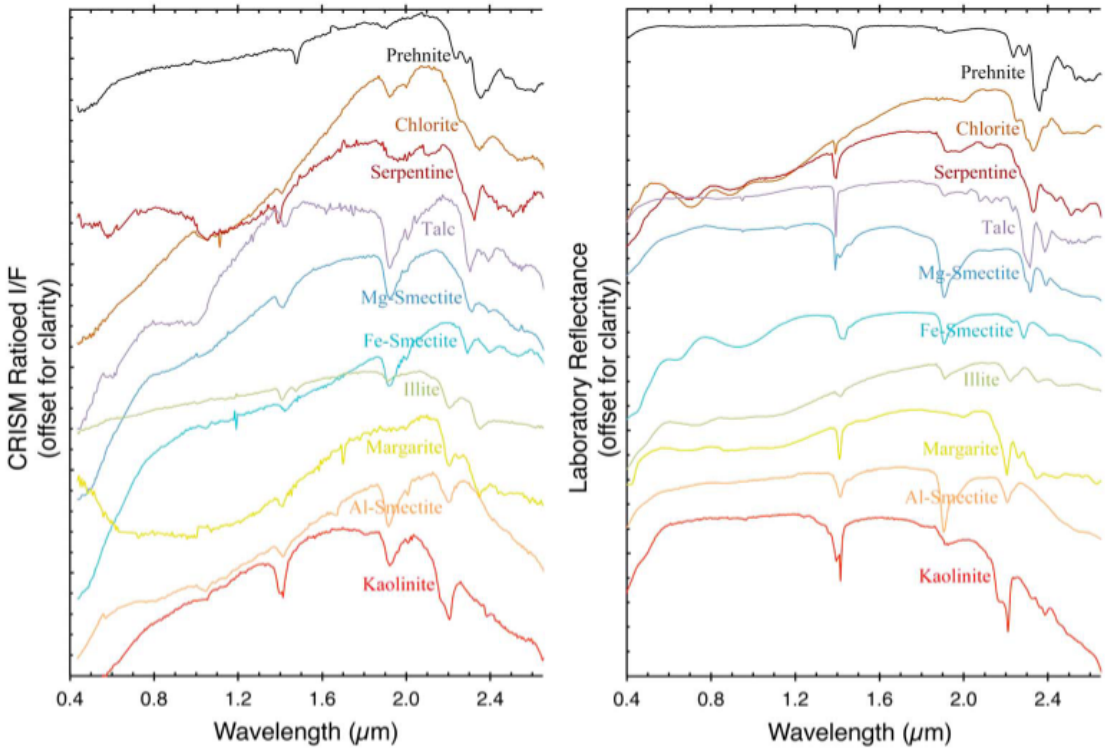

Figure 3.6: MICA type spectra of phyllosilicates (left) and their respective analog laboratory materials (right) (Viviano et al. 2014).

3.3.5 Carbonates

Carbonate deposits on Mars, expected from water–basalt interaction in a CO_2-rich atmosphere, represent a potential sink for ancient atmospheric CO_2 and form only under neutral-to-alkaline conditions. They are identified by paired absorptions near 2.3 and 2.5 μm from C–O bond overtones, with Fe/Ca carbonates centered at 2.33 and 2.53 μm and Mg-rich varieties shifted to 2.30 and 2.51 μm. Since these features can overlap with phyllosilicates and zeolites, both absorptions must be present for confirmation, and additional weaker bands at 3.45 and 3.9 μm, despite lower CRISM signal-to-noise and instrument artifacts, can strengthen identification (Viviano et al. 2014). Orbital detections have revealed carbonates

in Nili Fossae, as well as in Tyrrhena Terra, south of Isidis Basin, and Syrtis Major, providing key evidence for past neutral-to-alkaline aqueous environments on Mars.

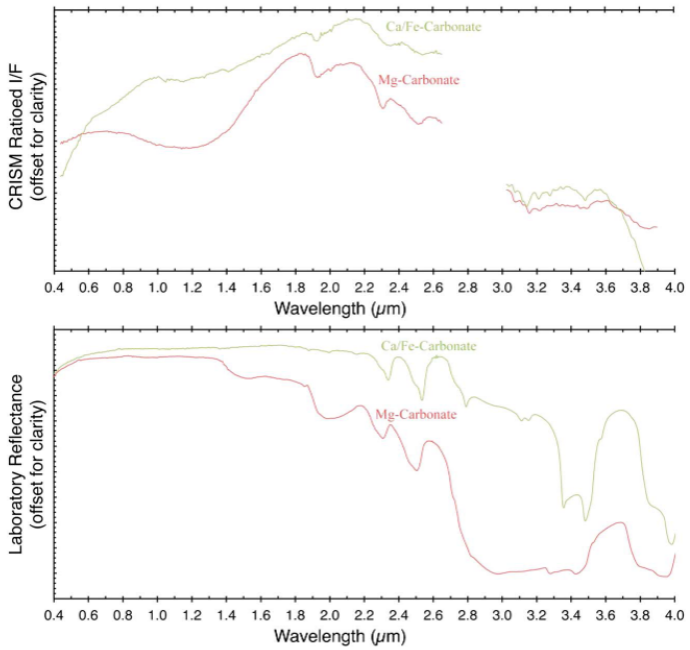

Figure 3.7: MICA type spectra of carbonates (left) and their respective analog laboratory materials (right) (Viviano et al. 2014).

3.3.6 Halides and Other Hydrated Silicates

Hydrated silica on Mars can form through multiple abiotic processes and is the primary mineral of interest in this study due to its significance as a marker of past aqueous activity. It may precipitate from solution, producing either opal-A (amorphous /noncrystalline) in chemical weathering environments or chalcedony (micro/cryptocrystalline) in hydrothermal systems. It can also arise through diagenetic alteration, where opal-A transforms into paracrystalline opal-CT, or by replacing other minerals, with opal-A or opal-CT precipitating as nodules in limestones or dolostones. Spectrally, hydrated silica is recognized by absorption bands at 2.21–2.22 μm from Si–OH combination tones, 2.26 μm from hydrogen-bound Si–OH, 1.91 μm from structural water, and 1.4 μm from both structural water and OH. As crystallinity increases, the 1.4 μm band center shifts from 1.38 to 1.42 μm, see Figure 3.8, and the depth ratio of the 1.91/1.96 μm bands becomes greater, providing clues about formation history (Viviano et al. 2014).

On Mars, hydrated silica has been found in diverse geological contexts, including layered plains around Valles Marineris, aeolian dunes near Antoniadi and Isidis basins, Toro crater at the edge of Syrtis Major, the Nili Patera caldera, Terra Sirenum intercrater plains, the upper Al/Si-rich unit in Mawrth Vallis, and Noctis Labyrinthus. These deposits show varying crystallinity, from noncrystalline hydrated glass to weakly crystalline opal and fully crystalline quartz, indicating they formed under different environmental conditions and alteration processes (Viviano et al. 2014).

Prehnite-bearing assemblages on Mars indicate that most metamorphic conditions did not exceed the sub-greenschist facies, suggesting relatively low-grade metamorphism. However, spectral analyses have also identified epidote in Hesperia Planum and near olivine–serpentine occurrences in Nili Fossae, pointing to localized higher-grade metamorphism. Epidote is characterized by major absorption bands

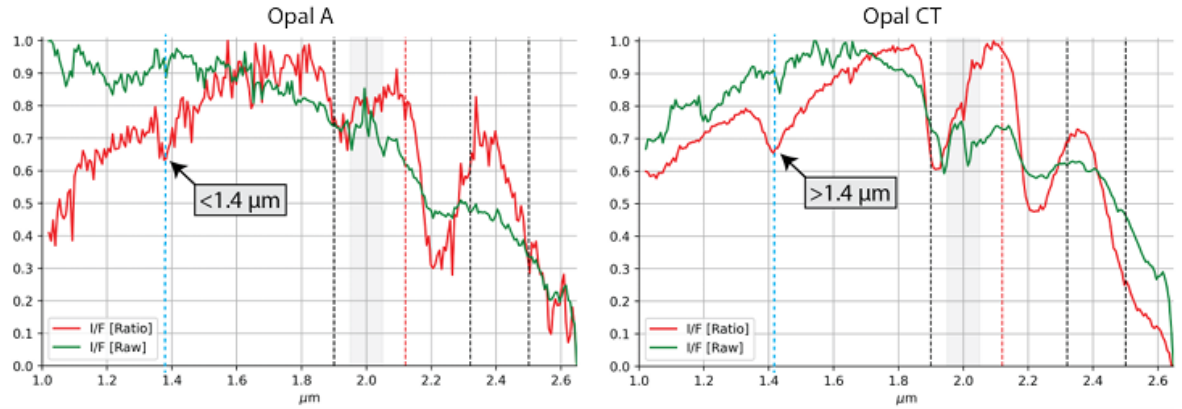

Figure 3.8: Spectral examples fo both Opal-A and Opal-CT, on the left, and right side, respectively. As explained above, the absorption shifts to smaller wavelength values if the mineral is amorhpous, and to bigger wavelength values if the mineral is crystalline (Voigt et al. 2024a).

at 2.34 and 2.25 μm, which can resemble mixtures containing calcite, chlorite, and illite, making clear identification challenging. The detection of a weaker but distinctive 1.55 μm band present in laboratory spectra of epidote supports its identification, though CRISM data quality renders this feature faint and somewhat uncertain. If confirmed, epidote-bearing assemblages would imply the presence of rock types on Mars typically associated with convergent plate margins on Earth, challenging the prevailing single-plate, stagnant-lid tectonic model for Mars and opening the possibility of limited or early-stage plate tectonic activity in the planet's history (Viviano et al. 2014).

Zeolites on Mars are thought to form in diverse environments, including alkaline waters, as alteration products of volcanic glass, and within low-temperature hydrothermal systems. While most zeolites are spectrally similar to polyhydrated sulfates, both showing strong absorptions near 2.4 μm, 1.9 μm, and 1.4 μm due to bound water, the zeolite analcime is notably distinct, with a characteristic strong 2.5 μm absorption and a weaker 1.79 μm band identifiable in CRISM data. Other spectrally unique zeolites, such as natrolite, have not yet been observed on Mars. TES data suggest zeolites may be a significant component of Martian dust, though their precise composition remains debated. Analcime has been definitively detected in several craters near Antoniadi Basin in west and central Nili Fossae, as well as in a crater in southeast Cimmeria Terra, pointing to localized conditions favorable for zeolite formation and preservation (Viviano et al. 2014).

Chloride deposits on Mars typically form through the evaporation of surface waters, such as saline lake waters, or from hydrothermal brines below the surface, and can also originate from volcanic outgassing as fumarolic sublimates. These chlorides are commonly found in flat intercrater plains and crater floors, often occurring alongside phyllosilicate-bearing minerals. Spectrally, chlorides stand out due to their unusually high apparent emissivity in the thermal infrared and a distinctive downward slope toward lower wavenumbers. Unlike many other surface materials, chlorides lack strong diagnostic absorption features in the visible and near-infrared but can be identified by a unique combination of a bluer slope in the VNIR, a redder slope in the infrared, and a notably weaker 3 μm water absorption feature, reflecting their anhydrous nature. These spectral characteristics enable differentiation of chlorides from other minerals using CRISM data. All of the minerals described above can be seen in Figure 3.9.

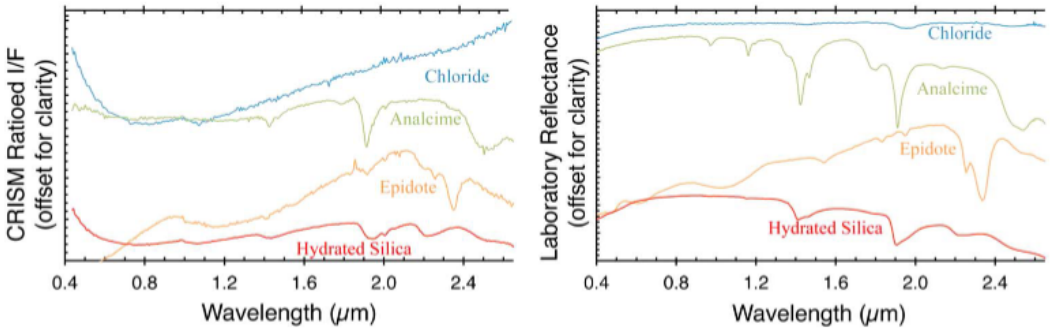

Figure 3.9: MICA type spectra of halides and other hydrated silicates (left) and their respective analog laboratory materials (right) (Viviano et al. 2014).

Chapter 4

Results and analysis

Our goal in this work has been to provide satellite based support to the new findings of Xiao et al. 2023 as well as trying to follow the putative ancient shorelines in Wang et al. 2024. Our data is taken from both OMEGA, as a first, and more broad approach; and from CRISM, as a more detailed and focused secondary analysis. The results are obtained in the form of averaged and normalized spectra, and will be compared to laboratory analogs for mineral identification (Viviano et al. 2014).

For all points of interest shown in 2.2, an OMEGA analysis will be shown first, and only then, the more detailed version of the area, with CRISM. For geological context a CTX image of the area will also be presented. For OMEGA, the orbit used will be plotted with the exact pixels used for spectral analysis, and next to it the corresponding spectra. Then, the averaged and normalized spectra is plotted and compared with the MICA Files shown in Viviano et al. 2014 to identify absorption lines and relate them to the different minerals. For CRISM, the same will be done, with the addition of the filters applied for mineral identification, and subsequently, the resulting spectra obtained. Once again it will be compared with the MICA Files for line identification.

4.1 Terby Crater

Serving as a starting point and as calibration to our analysis, a very well known region, Terby Crater (Yen et al. 2019), will first be presented using our method. It is known to be bearing hydrated minerals and has also remnants of past flowing, liquid water (Yen et al. 2019). Despite its location, in the southern hemisphere, inside Hellas Planitia, not being relevant, specifically to our goal, it is still important and will function as a calibration mechanism, and a way to guarantee that our analysis is on par with the other methods described in the literature.

Figure 4.1 shows a CTX image of Terby crater to provide geological and geographic context to the area. It contains several carved out valleys, and what could be interpreted as a sedimentary deposit. After having a general context of the area, the OMEGA analysis techniques are applied as a first approach. ORB4199_3 is the image used for this analysis. The pixels chosen, and the corresponding spectra are visible in Figure 4.2.

In our OMEGA analysis (Figure 4.3) we already have absorption lines indicating the presence of Fe/Mg clays and other phyllosilicates. The main absorptions to look for are the 1.9 and the 2.3/2.4/2.5 μm. The 1.4 μm absorption would make us tend to hydrated silica. The fact that it is slightly shifted towards larger wavelengths, means it is most likely crystalline opal. Now what is left to do is to run a CRISM analysis in order to confirm this first detection.

Figure 4.1: CTX Image of Terby Crater; Coordinates: -27.5220°N: 74.2799°E. Credits: NASA/MRO.

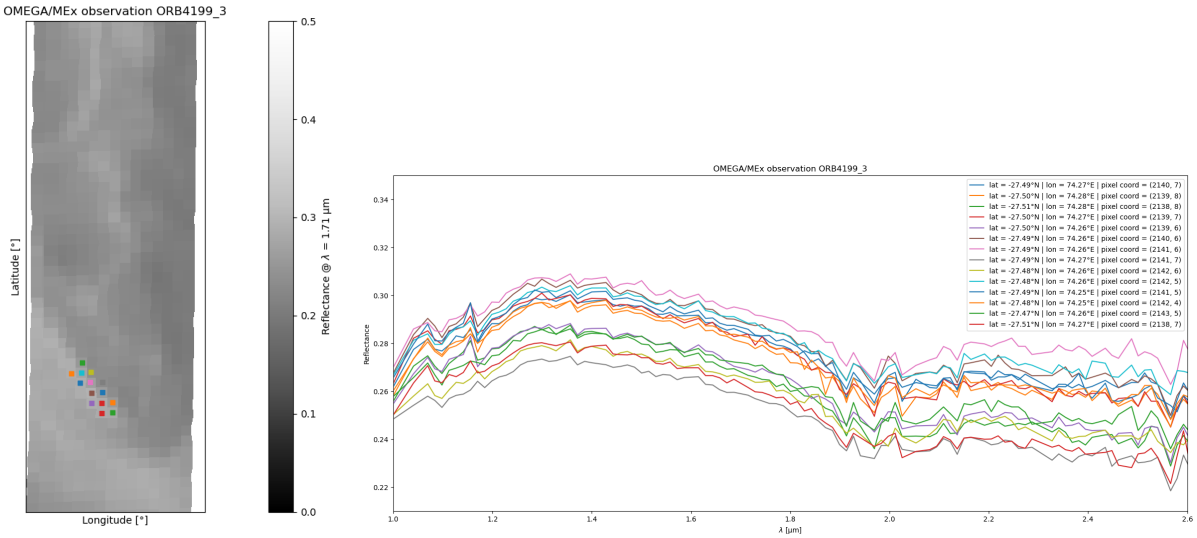

(a) (b)

Figure 4.2: OMEGA observation of the Terby Crater (ORB4199_3). On the left hand side (a), a zoom in of the region is visible, as well as the pixels from which the spectra were taken. On the right hand side (b), the corresponding spectra are visible. For clarity and relevance, the wavelength is limited between 1 and 2.6 μm.

In Figure 4.5, we clearly see the same absorption lines as in the OMEGA analysis. This gives us confidence that our detections are accurate, and also, that they match the literature (Yen et al. 2019).

4.2 First region - inside Isidis Planitia

The first region studied is an area near Isidis Planitia, containing some features possibly created by the presence of flowing water. We once again present a CTX image for geological context (Figure 4.6), then our OMEGA analysis (Figures 4.7) and 4.8) and finally the CRISM analysis (4.10).

The main minerals we were able to detect were water ice, hydrated silica (amorphous) and, possibly, serpentine as well. The CRISM spectra also agree with the OMEGA findings, giving us a robust result.

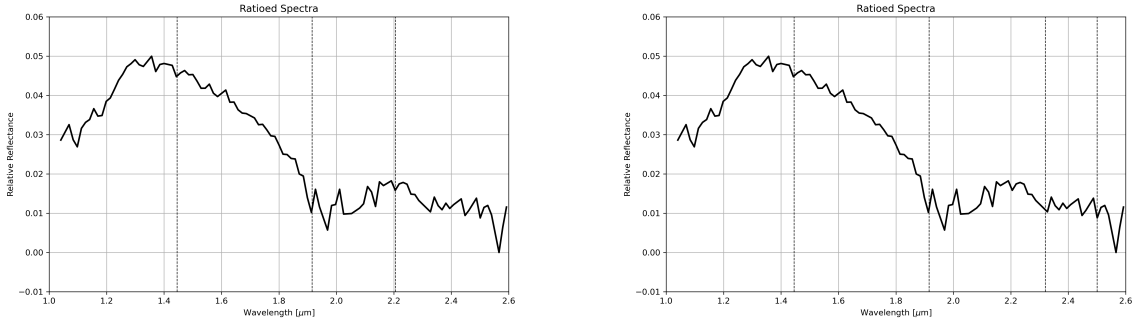

(a) (b)

Figure 4.3: Resulting spectra from the Pixels shown previously. For spectrum (a), the absorption lines of hydrated silica are highlighted by dashed black lines. For spectrum (b), the absorption lines for any non-specific phyllosilicates. For clarity and relevance, the wavelength is limited between 1 and 2.6 μm.

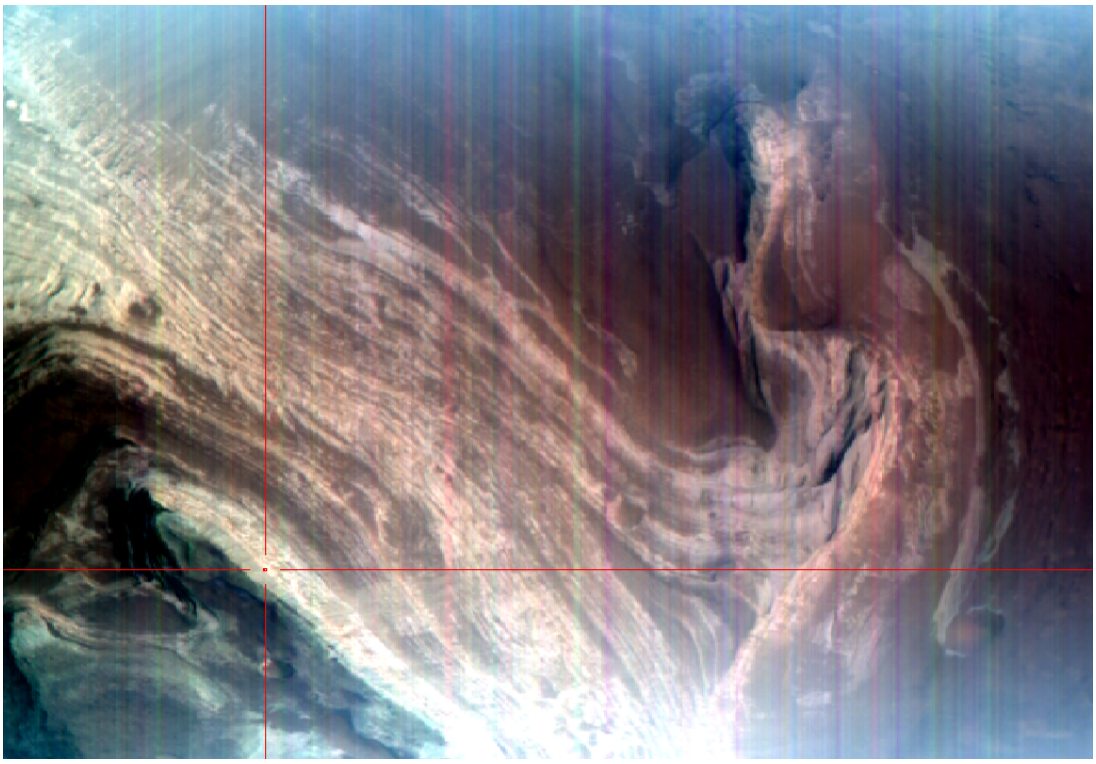

Figure 4.4: CRISM observation of Terby crater used for analysis (FRT000059DF_07) and a red cross pointer showcasing the region from which the spectra was taken from.

4.3 Mie Crater

The second region studied is the Mie Crater, containing some features possibly created by the presence of flowing water. From OMEGA, see the presence of water ice, along side a small detection of hydrated silica (amorphous) and what could potentially be considered serpentine (see Figure 4.13).

From CRISM analysis, the main minerals we were able to detect were water ice, hydrated silica (crystalline) and, possibly, serpentine as well (Figure 4.15). The CRISM spectra also agrees with the OMEGA findings. However, the quality of the CRISM image used is not the best, and the poor signal to noise ratio makes the spectra very difficult to analyze, and very prone to misreadings. Despite this being the case, we are still confident that this region is bearing some clays and phyillosilicates.

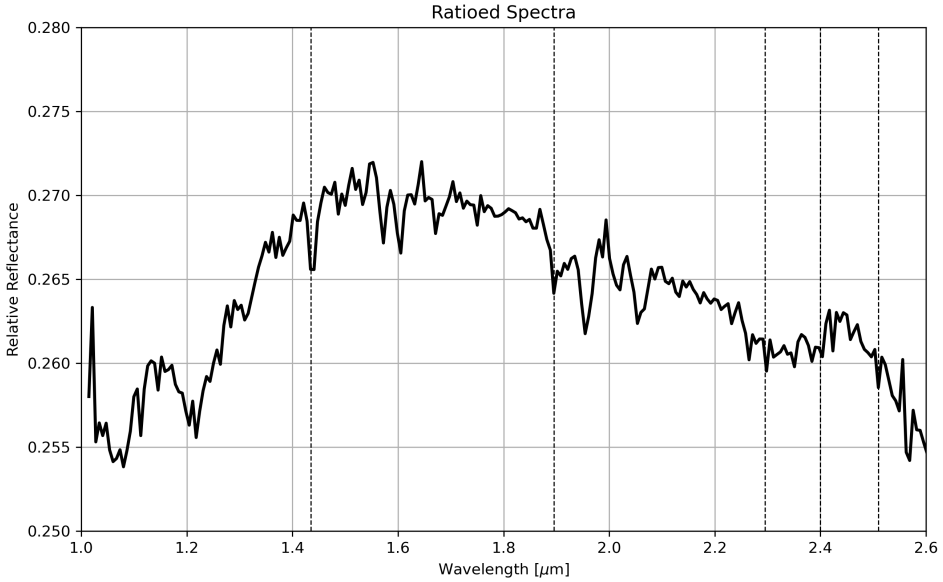

Figure 4.5: CRISM spectra from the region shown of Terby Crater. We can see highlighted, the absorption lines of what can be identified as a phyllosilicate, potentially serpentine.

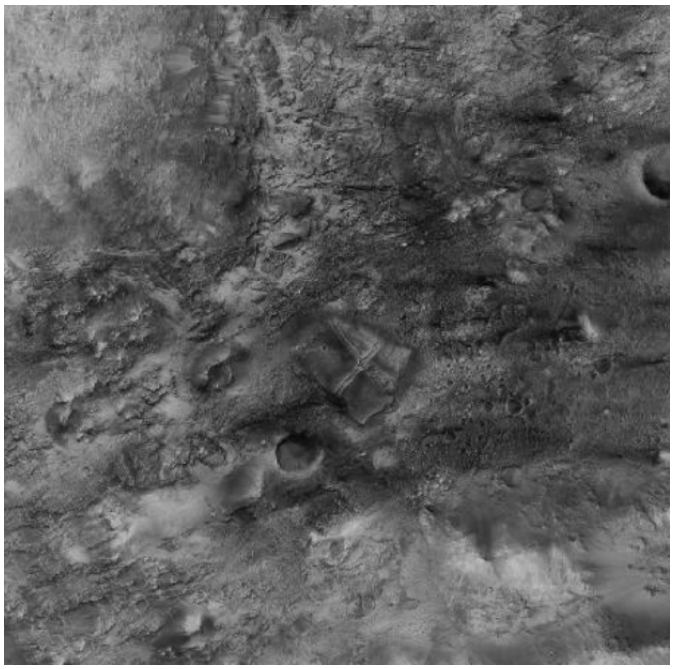

Figure 4.6: CTX Image of a region located near Isidis Planitia, alongside what could be a putative ancient shoreline. Coordinates: 17.2831°N: 77.3999°E. Credits: NASA/MRO.

4.4 Coastal region feature - south of Hephaestus Rupes

The third area studied was a region to the south of Hephaestus Rupes. In both the OMEGA and CRISM spectra (Figure 4.18 and 4.20, respectively) we see the presence of water ice, alongside a small amorphous hydrated silica absorption, and the more detailed images provided by CRISM also detect what could be some serpentine as well.

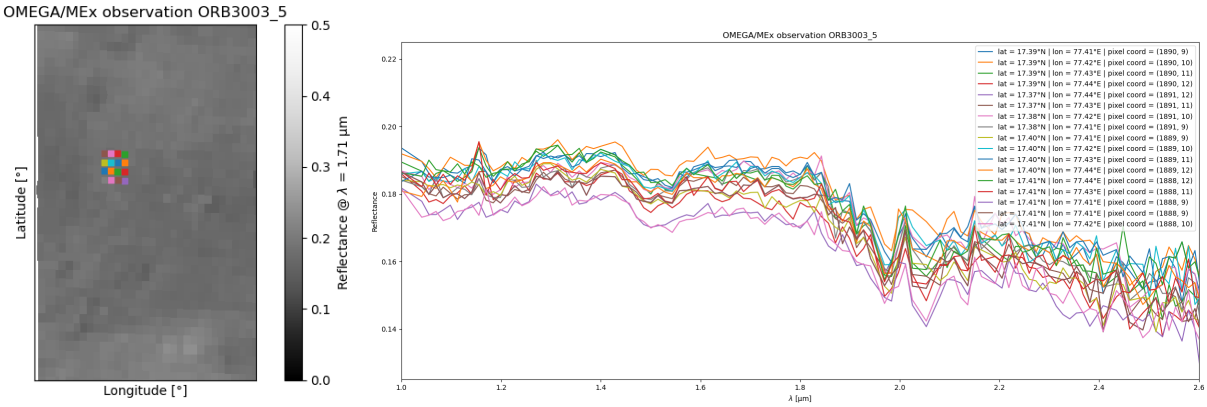

(a) (b)

Figure 4.7: OMEGA observation of the are in question (ORB3003_5). On the left hand side (a), a zoom in of the region is visible, as well as the pixels from which the spectra were taken. On the right hand side (b), the corresponding spectra are visible. For clarity and relevance, the wavelength is limited between 1 and 2.6 μm.

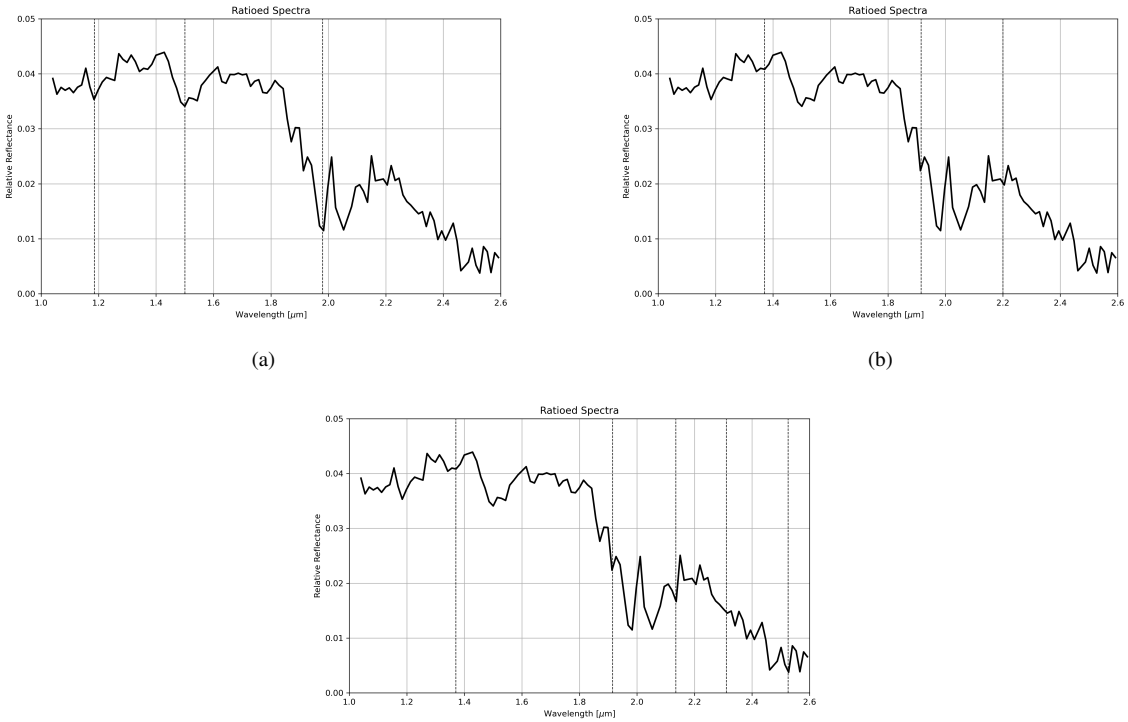

(a) (b)

(c)

Figure 4.8: Resulting spectra from the Pixels shown previously. For spectrum (a), the absorption lines of H_2O ice are highlighted by dashed black lines. For spectrum (b), the absorption lines for hydrated silica are highlighted by dashed black lines. For spectrum (c), the absorption lines for serpentine are highlighted by dashed black lines. For clarity and relevance, the wavelength is limited between 1 and 2.6 μm.

4.5 Two water flow channels - north of Ismeniae fossae

The fourth region studied was a region north of Ismeniae fossae, which seems like it was formed due to flowing water. It also resides along what could be called a putative ancient shore line. The first thing I want to mention about this region is that, on the OMEGA observation, we see clear indication of serpentine, as well as hydrated silica. The square shape that the 1.9 μm absorption line takes (in conjunction with all the other lines), makes it almost undeniable that there is serpentine in this area. With

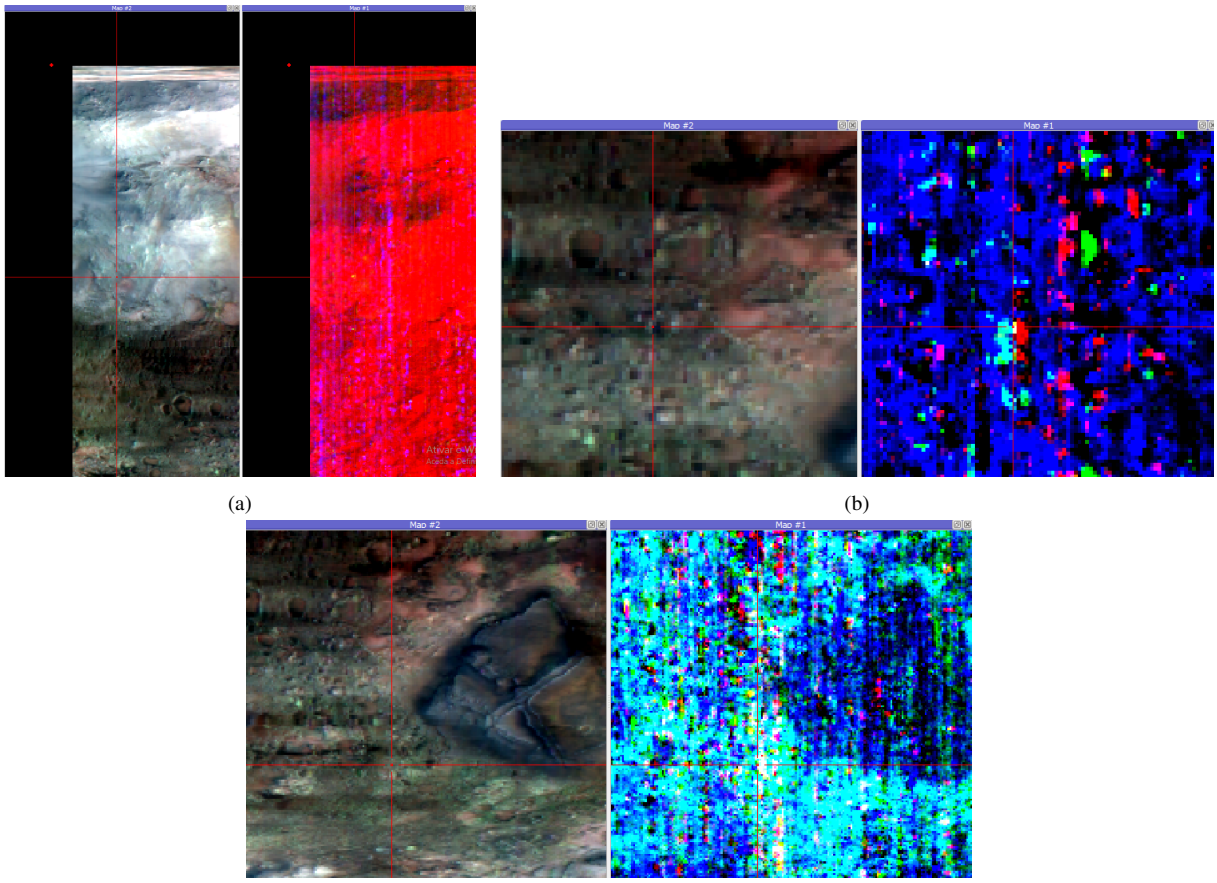

(a) (b)

(c)

Figure 4.9: CRISM image of the area in question (FRS00038CD4_01). This figure shows the three different areas from which the spectra were taken. The images are set up in this way: on the left hand side the unfiltered image is seen with a red cross pointing to where the spectra were taken from, on the right hand side, the filter applied over the original image, with a mirrored version of the red cross pointing to the pixels chosen. In (a), the filter applied highlights in light green any H_2O ice signatures, and red for all iceless minerals. In (b), the filter applied highlights in white/light yellow any hydrated silica signatures. In (c), the filter applied highlights in white/light yellow any serpentine signatures.

this in mind, when applying the filters to our CRISM images, we jumped straight to the serpentine filter. We also found some residual water ice on the other filter, and that is why we have two different spectra from the same region; spectra (a) and (b) from Figure 4.25 corresponding to the water ice filter ((b) from Figure 4.24) and (c) from Figure 4.25 corresponding to the serpentine filter ((a) from Figure 4.24).

The OMEGA analysis (Figure 4.28) points to, once again, some water ice, crystalline hydrated silica, and possibly some serpentine as well. The CRISM analysis (Figure 4.30) also confirms the same minerals.

4.6 Linpu Crater - north of Nepenthes Planum

The sixth region studied was a crater along the putative ancient shorelines, the Linpu Crater. It stands to the north of Nepenthes Planum, and contains some features that could be interpreted as being a result of past flowing water. From our OMEGA analysis we detect some hydrated silica (crystalline), and some water ice (see Figure 4.33). After running the CRISM analysis, the results lead to the same conclusion, and we have another detection of both water ice and crystalline opal (see Figure 4.35).

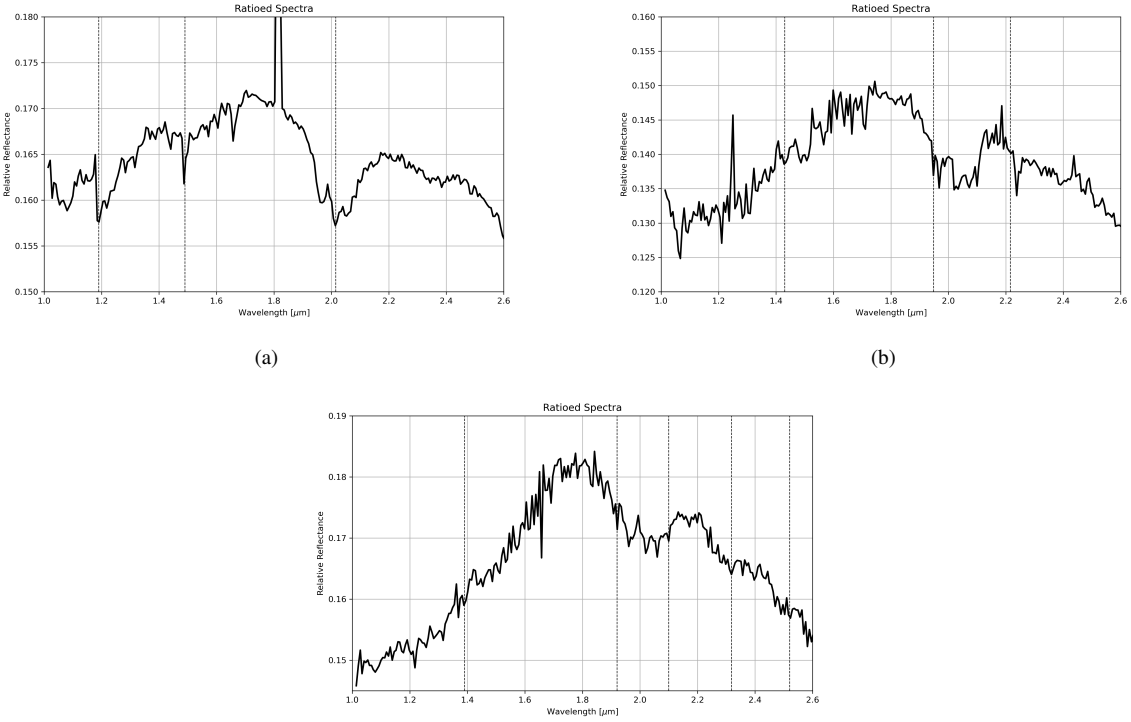

Figure 4.10: Resulting spectra from the Images shown previously. For spectrum (a), the absorption lines of H_2O ice are highlighted by dashed black lines. For spectrum (b), the absorption lines for hydrated silica are highlighted by dashed black lines. For spectrum (c), the absorption lines for serpentine are highlighted by dashed black lines. For clarity and relevance, the wavelength is limited between 1 and 2.6 μm.

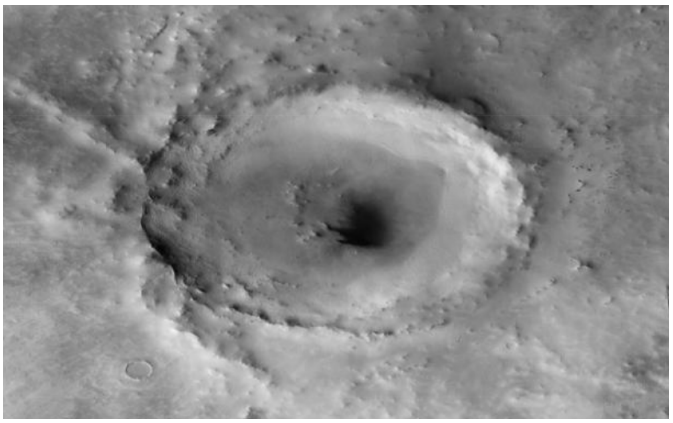

Figure 4.11: CTX Image of Mie Crater, to the east of Utopia Planitia. Coordinates: 48.1477°N: 139.5587°E. Credits: NASA/MRO.

4.7 Crater - east of Isidis Planitia

On our seventh area analyzed, the OMEGA analysis gave us a pretty good detection of hydrated silica, most likely crystalline, and some water ice (see Figure 4.38). However, the CRISM analysis did not confirm these detections entirely (see Figure 4.40). There were definitely some clays present in the area, indicating the presence of liquid water at some point, however, the absorptions were very small, and not very conclusive. From the CRISM spectra we can only consider the possibility of it being serpentine due to to the square shape of the 1.9μm absorption, but not clear enough.

4. RESULTS AND ANALYSIS

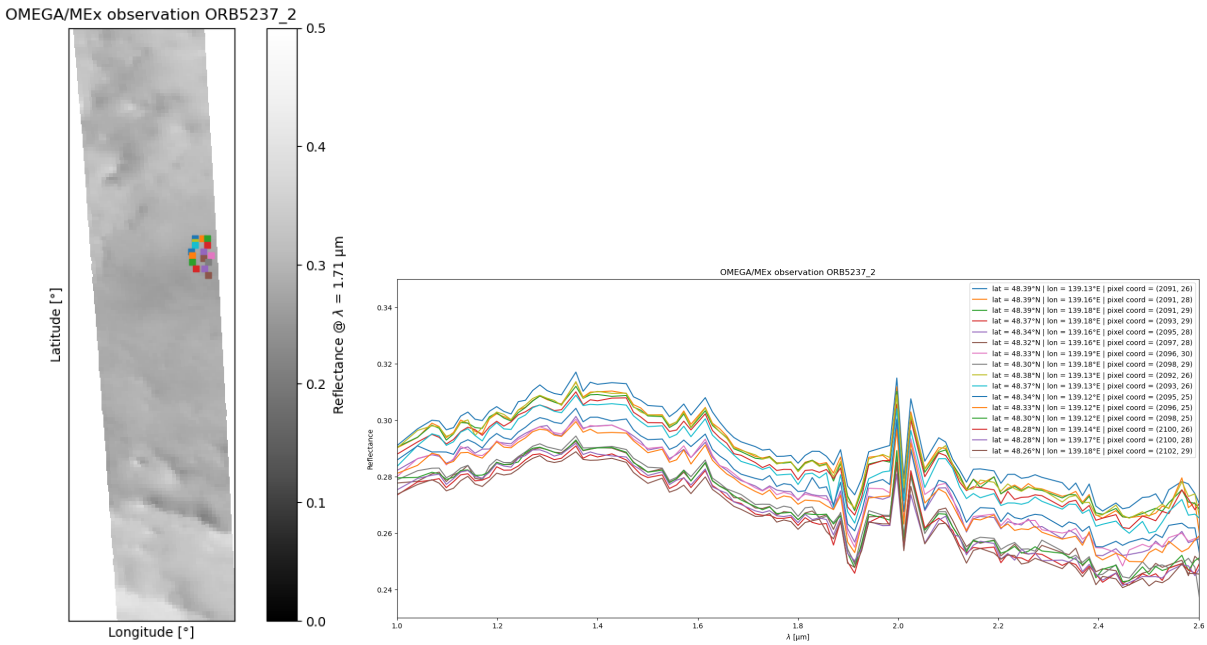

(a) (b)

Figure 4.12: OMEGA observation of the Mie Crater (ORB5237_2). On the left hand side (a), a zoom in of the region is visible, as well as the pixels from which the spectra were taken. On the right hand side (b), the corresponding spectra are visible. For clarity and relevance, the wavelength is limited between 1 and 2.6 μm.

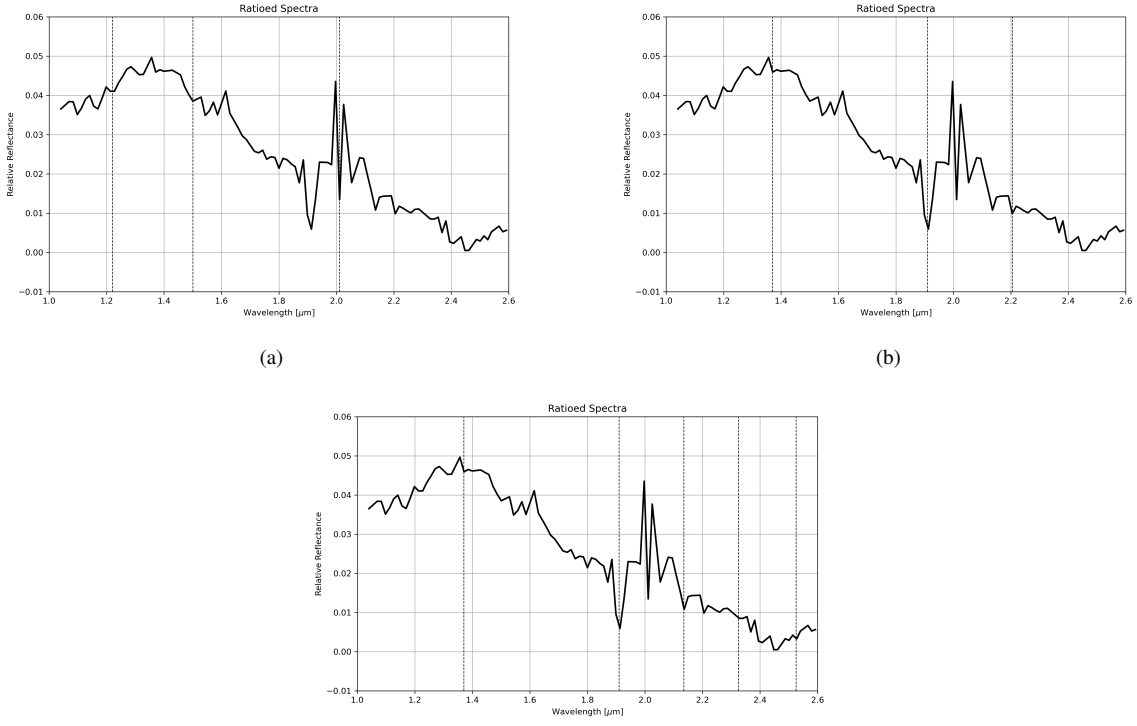

(a) (b)

(c)

Figure 4.13: Resulting spectra from the Pixels shown previously. For spectrum (a), the absorption lines of H_2O ice are highlighted by dashed black lines. For spectrum (b), the absorption lines for hydrated silica are highlighted by dashed black lines. For spectrum (c), the absorption lines for serpentine are highlighted by dashed black lines. For clarity and relevance, the wavelength is limited between 1 and 2.6 μm.

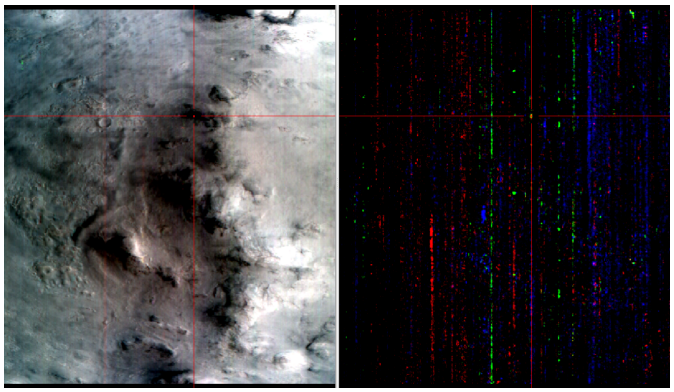

Figure 4.14: CRISM image of the area in question (FRT0000B116_07). This figure shows the area from which the spectra were taken. On the left hand side the unfiltered image is seen with a red cross pointing to where the spectra were taken from, on the right hand side, the filter applied over the original image, with a mirrored version of the red cross pointing to the pixels chosen.

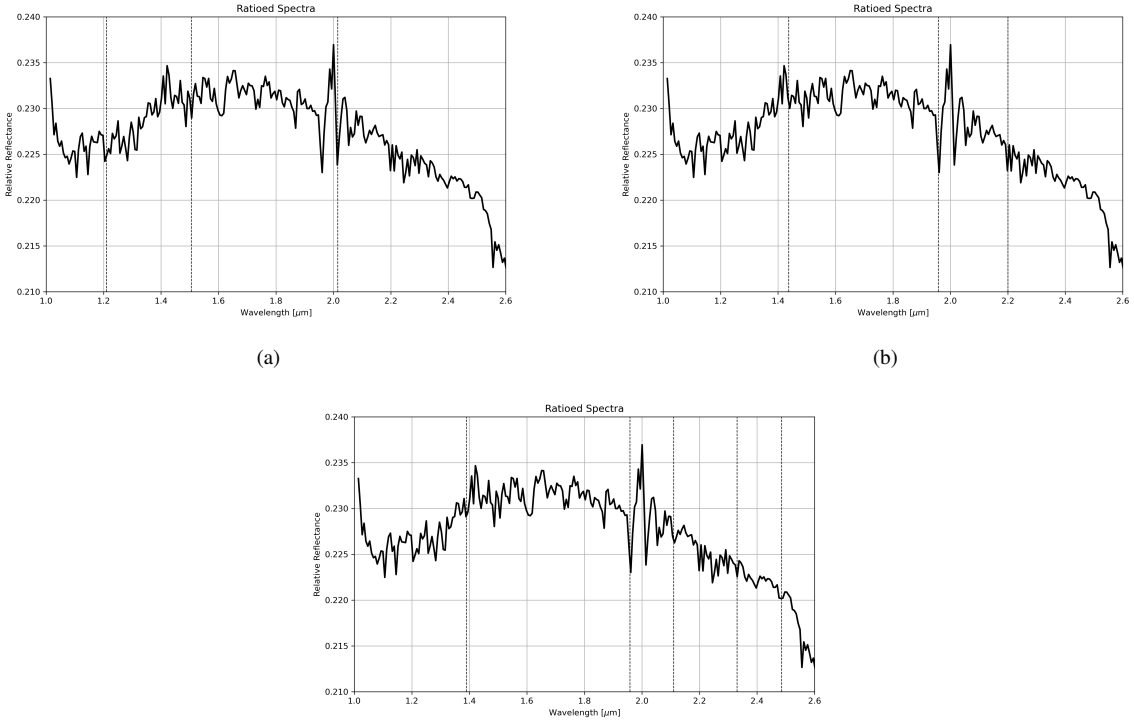

Figure 4.15: Resulting spectra from the Images shown previously. For spectrum (a), the absorption lines of H_2O ice are highlighted by dashed black lines. For spectrum (b), the absorption lines for hydrated silica are highlighted by dashed black lines. For spectrum (c), the absorption lines for serpentine are highlighted by dashed black lines. For clarity and relevance, the wavelength is limited between 1 and 2.6 μm.

4.8 Coastal region - west of Hephaestus Rupes

The eighth region we chose to study is located near the Hephaestus Rupes, and looks like its geological formation involved some amount of flowing liquid water. From the OMEGA analysis (Figure 4.43), we clearly see water ice absorptions, as well as some amorphous hydrated silica. We also see what could be interpreted as serpentine due to the "squarish" shape of the 1.9μm absorption. We also see that there are a lot of Fe/Mg rich phyllosilicates by the deep absorptions in the 2.2-2.5μm range. Our CRISM analysis (Figure 4.45)also confirms some of the detections, however, the 1.9μm line is very shallow and that could

4. RESULTS AND ANALYSIS

Figure 4.16: CTX Image of the third region analyzed, to the south of Hephaestus Rupes. Coordinates: 20.2609°N: 115.4006°E. Credits: NASA/MRO.

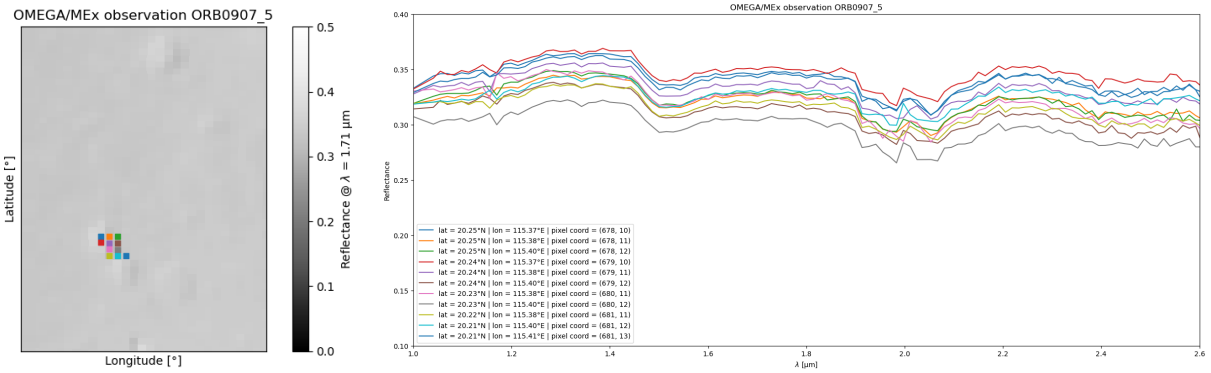

(a) (b)

Figure 4.17: OMEGA observation of the region south of the Hephaestus Rupes (ORB0907_5). On the left hand side (a), a zoom in of the region is visible, as well as the pixels from which the spectra were taken. On the right hand side (b), the corresponding spectra are visible. For clarity and relevance, the wavelength is limited between 1 and 2.6 μm.

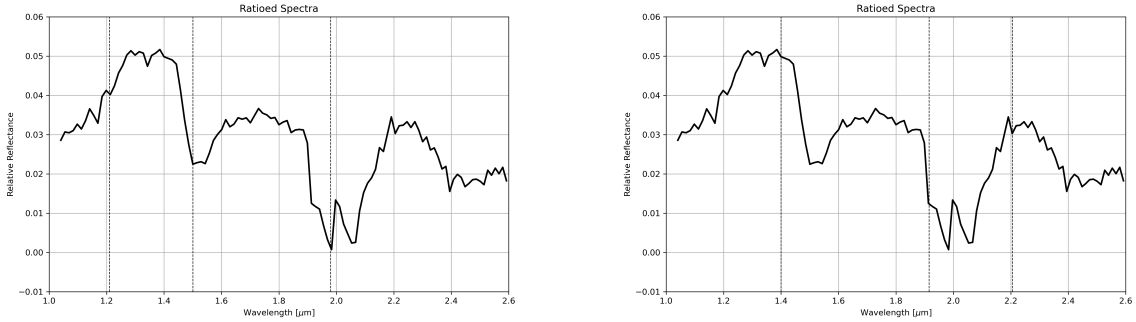

(a) (b)

Figure 4.18: Resulting spectra from the Pixels shown previously. For spectrum (a), the absorption lines of H_2O ice are highlighted by dashed black lines. For spectrum (b), the absorption lines for hydrated silica are highlighted by dashed black lines. For clarity and relevance, the wavelength is limited between 1 and 2.6 μm.

possibly mean that there is little to no phyllosilicates there. Despite this being said, the quality of the our CRISM image is very poor, as seen in Figure 4.44, so in this case, we need to rely more on OMEGA instead.

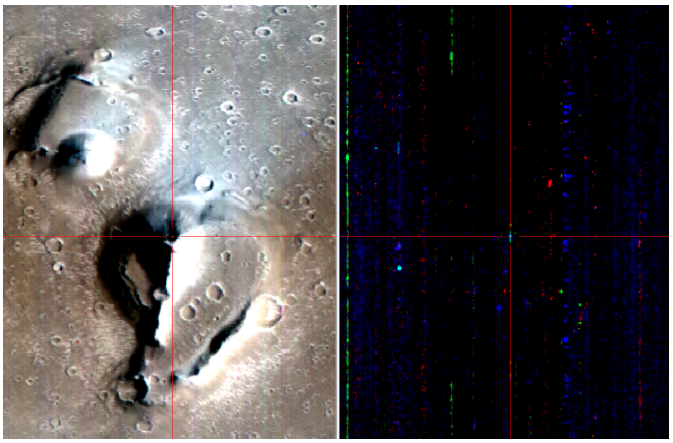

Figure 4.19: CRISM image of the area in question (FRT00009E1A_07). This figure shows the area from which the spectra were taken. On the left hand side the unfiltered image is seen with a red cross pointing to where the spectra were taken from, on the right hand side, the filter applied over the original image, with a mirrored version of the red cross pointing to the pixels chosen.

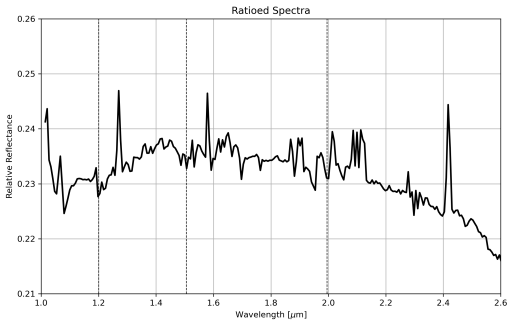

(a)

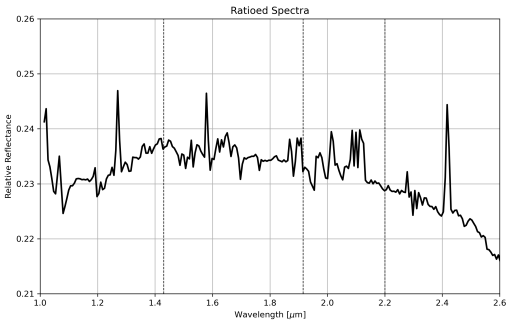

(b)

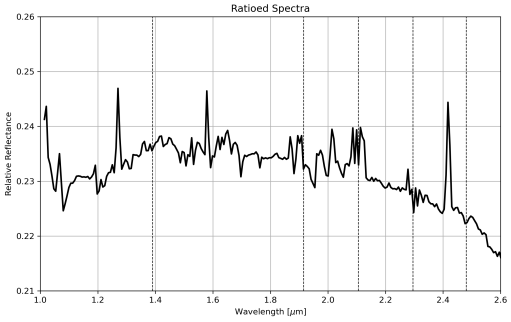

(c)

Figure 4.20: Resulting spectra from the Images shown previously. For spectrum (a), the absorption lines of H_2O ice are highlighted by dashed black lines. For spectrum (b), the absorption lines for hydrated silica are highlighted by dashed black lines. For spectrum (c), the absorption lines for serpentine are highlighted by dashed black lines. For clarity and relevance, the wavelength is limited between 1 and 2.6 μm.

4.9 Crater - north of Cecropia

The ninth and final region analyzed was a big impact crater to the north of Cecropia. From our OMEGA analysis we detected some water ice along side hydrated silica (crystalline) and some other phyllosilicates, possibly serpentine (Figure 4.47b). The CRISM image was quite noisy, however, some of the same minerals could also be identified. Despite having shallow absorptions, we still detected some water ice, hydrated silica and other Fe/Mg rich phyllosilicates, possibly serpentine.

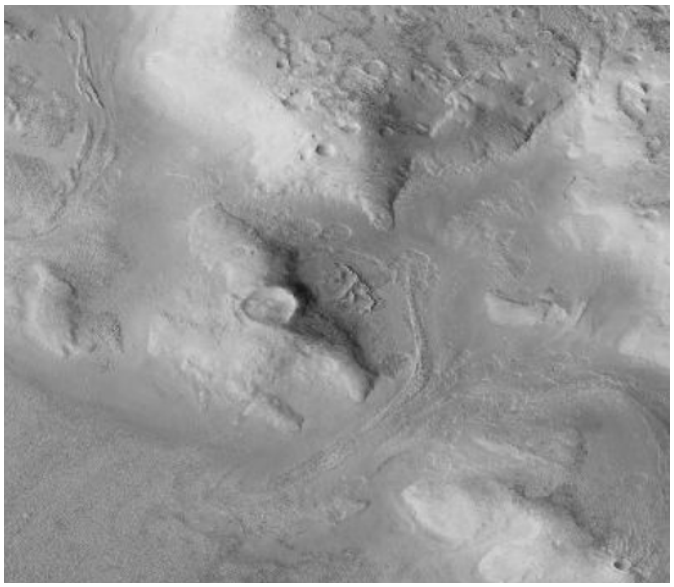

Figure 4.21: CTX Image of the fourth region analyzed, to the north of Ismeniae fossae. Coordinates: 45.1547°N: 39.9247°E. Credits: NASA/MRO.

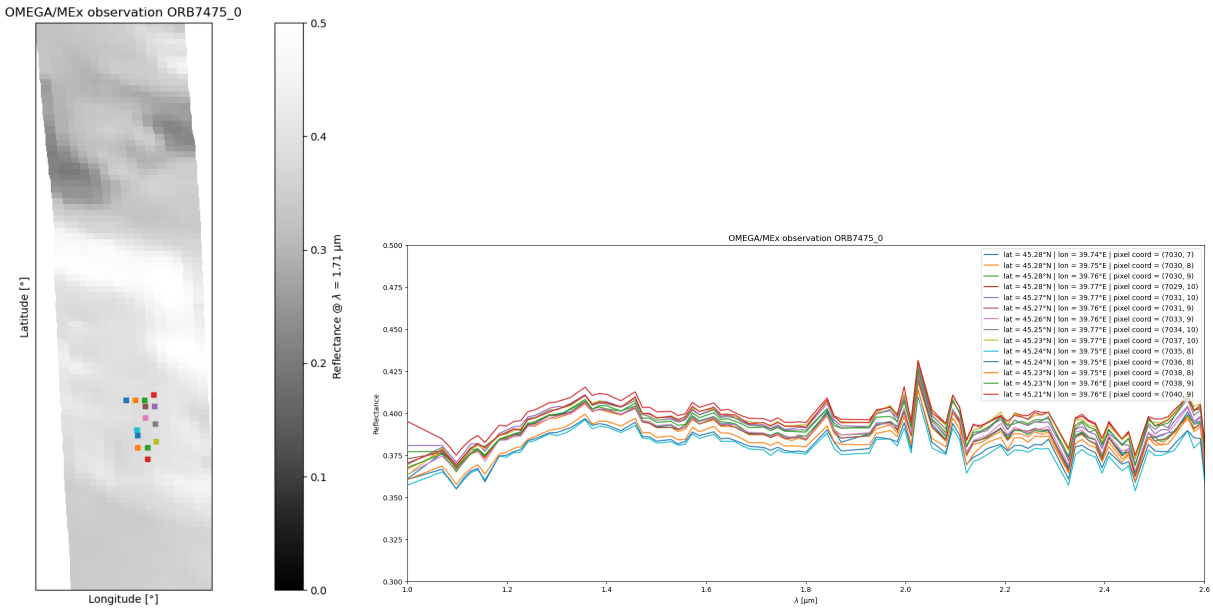

(a) (b)

Figure 4.22: OMEGA observation of the region north of Ismeniae fossae (ORB7475_0). On the left hand side (a), a zoom in of the region is visible, as well as the pixels from which the spectra were taken. On the right hand side (b), the corresponding spectra are visible. For clarity and relevance, the wavelength is limited between 1 and 2.6 μm.

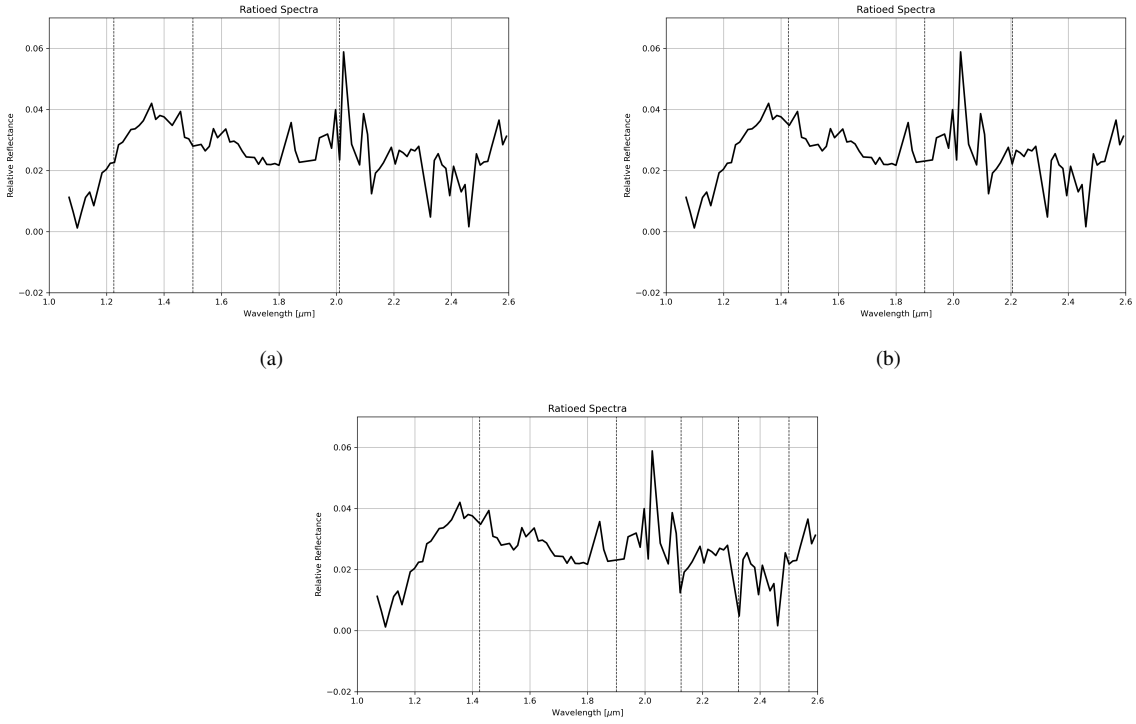

(a) (b)

(c)

Figure 4.23: Resulting spectra from the Pixels shown previously. For spectrum (a), the absorption lines of H_2O ice are highlighted by dashed black lines. For spectrum (b), the absorption lines for hydrated silica are highlighted by dashed black lines. For spectrum (c), the absorption lines for serpentine are highlighted by dashed black lines. For clarity and relevance, the wavelength is limited between 1 and 2.6 μm.

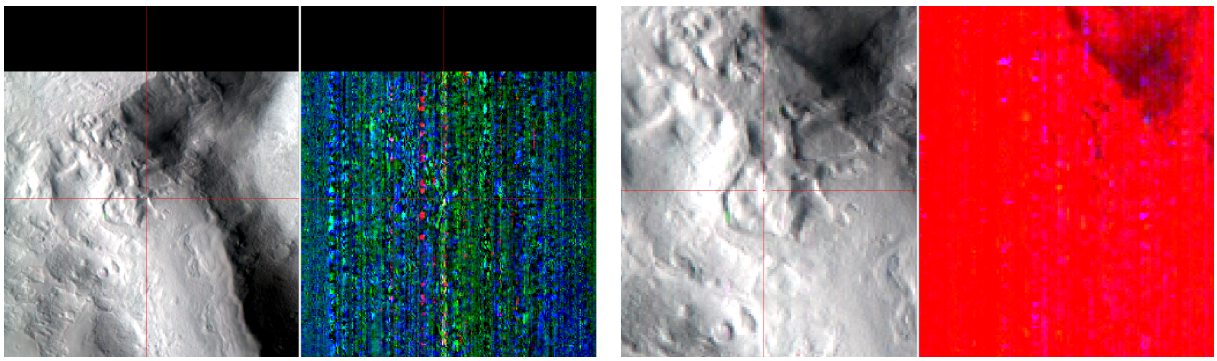

(a) (b)

Figure 4.24: CRISM image of the area in question (FRS0002EFEE_01). This figure shows the area from which the spectra were taken. On the left hand side the unfiltered image is seen with a red cross pointing to where the spectra were taken from, on the right hand side, the filter applied over the original image, with a mirrored version of the red cross pointing to the pixels chosen. On image (a), it shows the first filter applied (serpentine), and image (b) shows the water ice filter.

4. RESULTS AND ANALYSIS

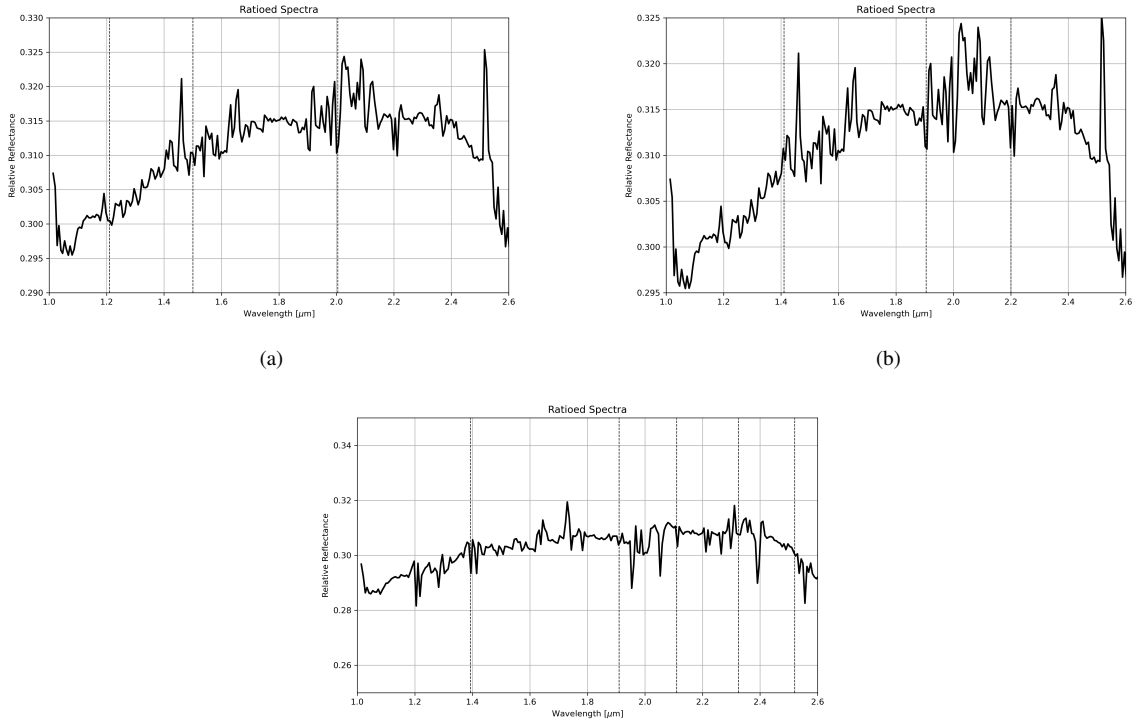

Figure 4.25: Resulting spectra from the Images shown previously. For spectrum (a), the absorption lines of H_2O ice are highlighted by dashed black lines. For spectrum (b), the absorption lines for hydrated silica are highlighted by dashed black lines. For spectrum (c), the absorption lines for serpentine are highlighted by dashed black lines. For clarity and relevance, the wavelength is limited between 1 and 2.6 μm.

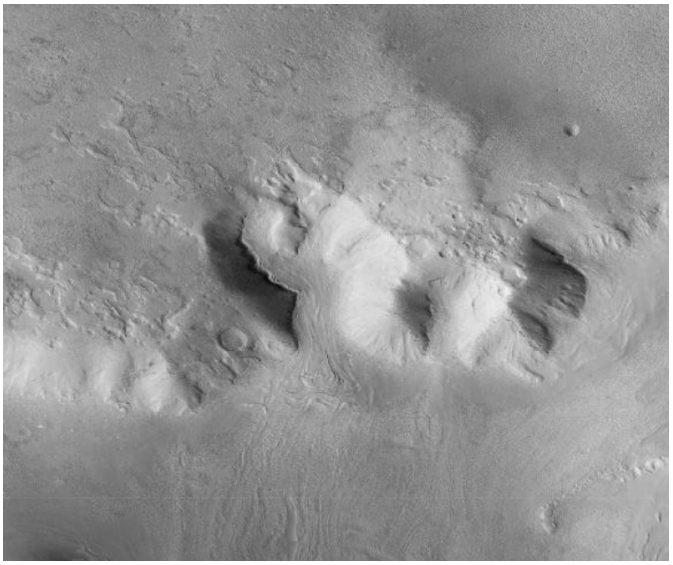

Figure 4.26: CTX Image of the fifth region analyzed, to the north of Ismeniae fossae. Coordinates: 45.1593°N: 38.1881°E. Credits: NASA/MRO.

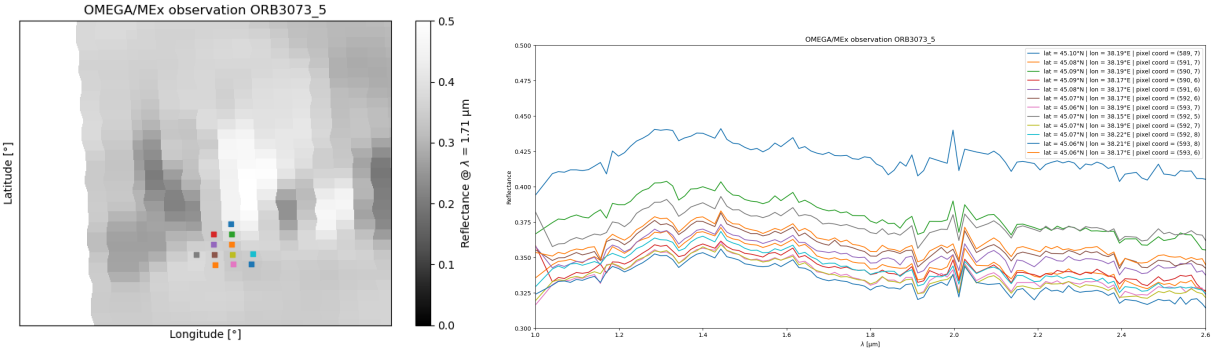

(a) (b)

Figure 4.27: OMEGA observation of the region in question (ORB3073_5). On the left hand side (a), a zoom in of the region is visible, as well as the pixels from which the spectra were taken. On the right hand side (b), the corresponding spectra are visible. For clarity and relevance, the wavelength is limited between 1 and 2.6 μm.

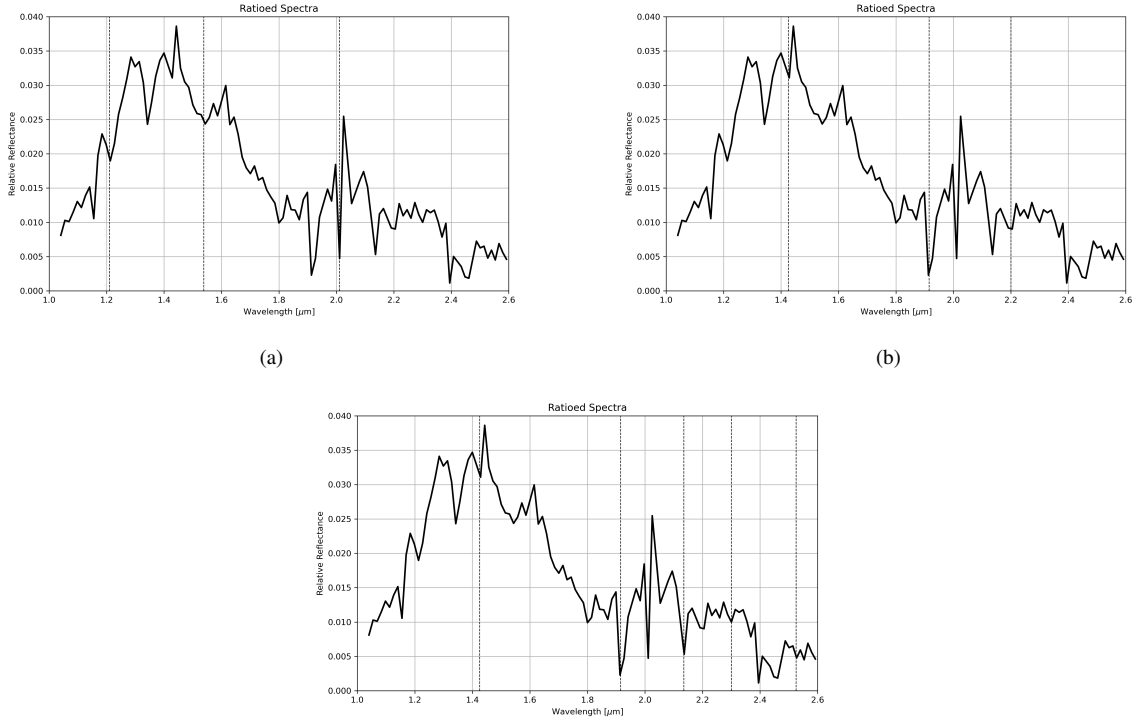

(a) (b)

(c)

Figure 4.28: Resulting spectra from the Pixels shown previously. For spectrum (a), the absorption lines of H_2O ice are highlighted by dashed black lines. For spectrum (b), the absorption lines for hydrated silica are highlighted by dashed black lines. For spectrum (c), the absorption lines for serpentine are highlighted by dashed black lines. For clarity and relevance, the wavelength is limited between 1 and 2.6 μm.

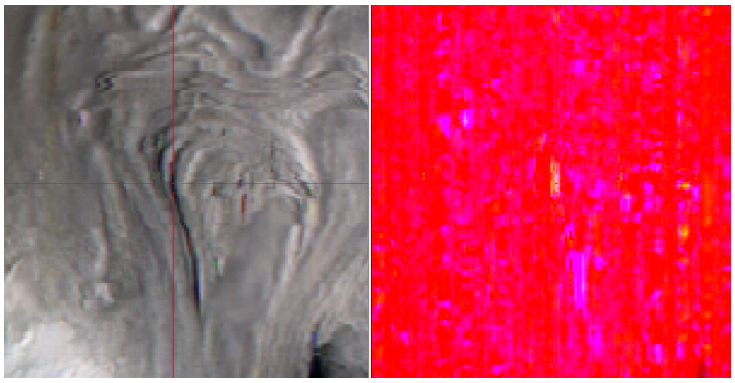

Figure 4.29: CRISM image of the area in question (FRT00017688_07). This figure shows the area from which the spectra were taken. On the left hand side the unfiltered image is seen with a red cross pointing to where the spectra were taken from, on the right hand side, the filter applied over the original image, with a mirrored version of the red cross pointing to the pixels chosen.

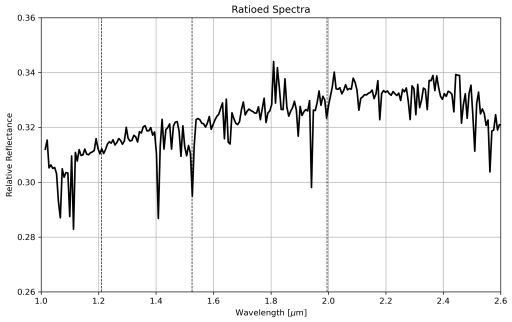

(a)

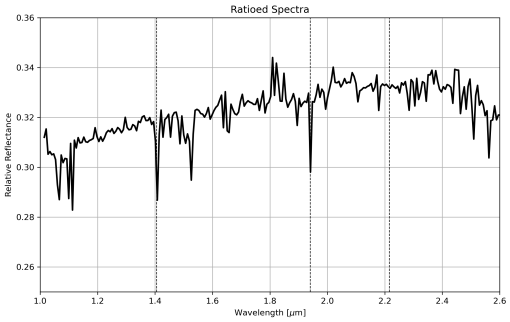

(b)

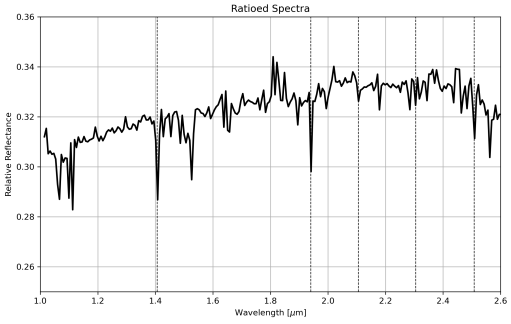

(c)

Figure 4.30: Resulting spectra from the Images shown previously. For spectrum (a), the absorption lines of H_2O ice are highlighted by dashed black lines. For spectrum (b), the absorption lines for hydrated silica are highlighted by dashed black lines. For spectrum (c), the absorption lines for serpentine are highlighted by dashed black lines. For clarity and relevance, the wavelength is limited between 1 and 2.6 μm.

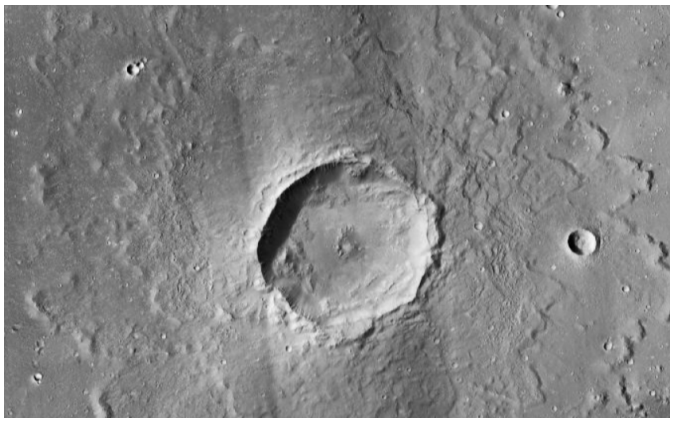

Figure 4.31: CTX Image of the sixth region analyzed, Linpu Crater, to the north of Nepenthes Planum. Coordinates: 18.1372°N: 113.2285°E. Credits: NASA/MRO.

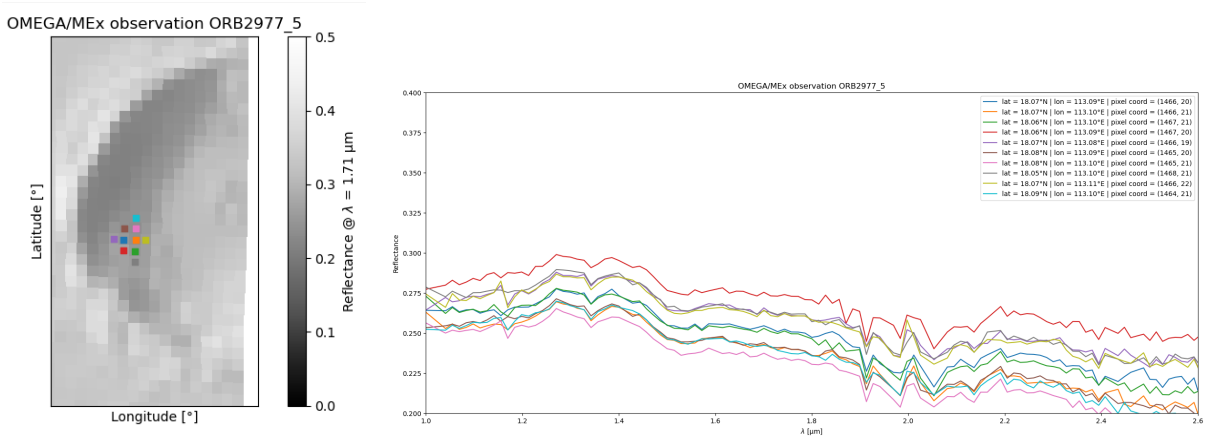

(a) (b)

Figure 4.32: OMEGA observation of the Linpu Crater, to the north of Nepenthes Planum (ORB2977_5). On the left hand side (a), a zoom in of the region is visible, as well as the pixels from which the spectra were taken. On the right hand side (b), the corresponding spectra are visible. For clarity and relevance, the wavelength is limited between 1 and 2.6 μm.

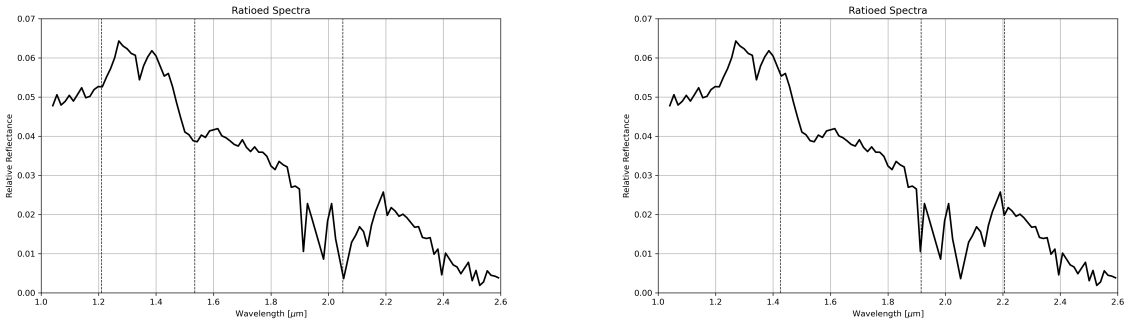

(a) (b)

Figure 4.33: Resulting spectra from the Pixels shown previously. For spectrum (a), the absorption lines of H_2O ice are highlighted by dashed black lines. For spectrum (b), the absorption lines for hydrated silica are highlighted by dashed black lines. For clarity and relevance, the wavelength is limited between 1 and 2.6 μm.

4. RESULTS AND ANALYSIS

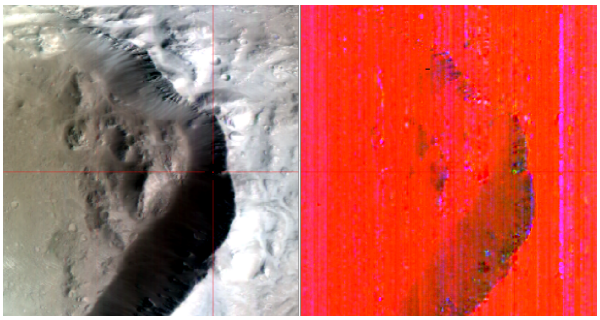

Figure 4.34: CRISM image of the area in question (HRL000166AD_07). This figure shows the area from which the spectra were taken. On the left hand side the unfiltered image is seen with a red cross pointing to where the spectra were taken from, on the right hand side, the filter applied over the original image, with a mirrored version of the red cross pointing to the pixels chosen.

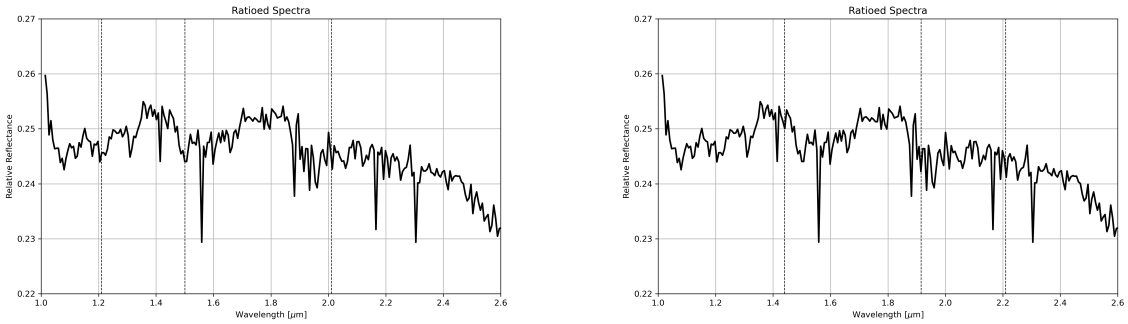

(a) (b)

Figure 4.35: Resulting spectra from the Images shown previously. For spectrum (a), the absorption lines of H_2O ice are highlighted by dashed black lines. For spectrum (b), the absorption lines for hydrated silica are highlighted by dashed black lines. For clarity and relevance, the wavelength is limited between 1 and 2.6 μm.

Figure 4.36: CTX Image of the seventh region analyzed, a crater to the east of Isidis Planitia. Coordinates: 16.1129°N: 100.9849°E. Credits: NASA/MRO.

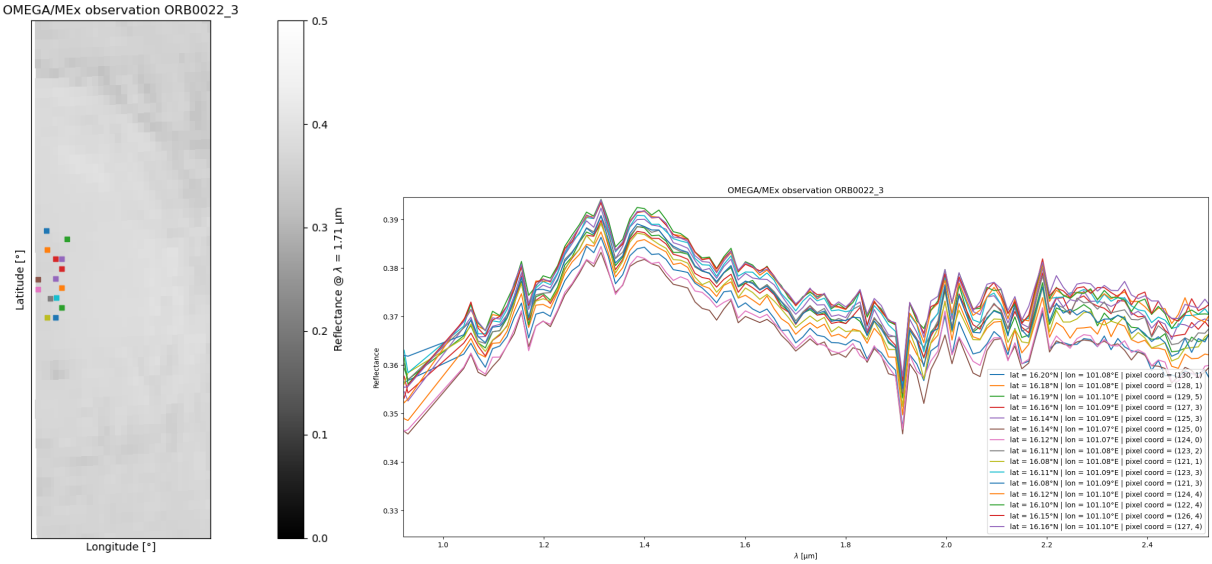

(a) (b)

Figure 4.37: OMEGA observation of the crater to the east of Isidis Planitia. (ORB0022_3). On the left hand side (a), a zoom in of the region is visible, as well as the pixels from which the spectra were taken. On the right hand side (b), the corresponding spectra are visible. For clarity and relevance, the wavelength is limited between 1 and 2.6 μm.

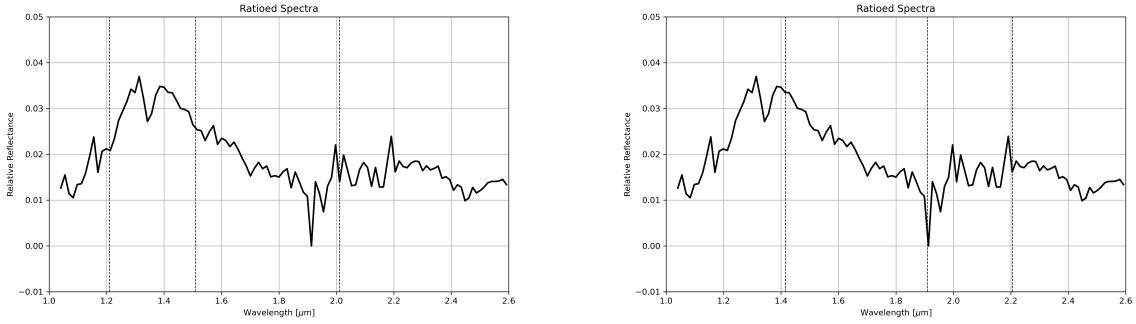

(a) (b)

Figure 4.38: Resulting spectra from the Pixels shown previously. For spectrum (a), the absorption lines of H_2O ice are highlighted by dashed black lines. For spectrum (b), the absorption lines for hydrated silica are highlighted by dashed black lines. For clarity and relevance, the wavelength is limited between 1 and 2.6 μm.

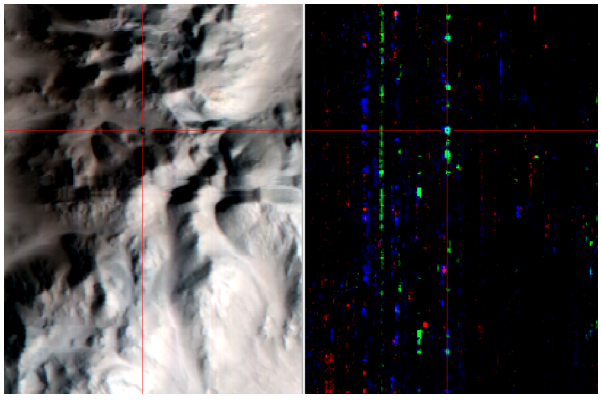

Figure 4.39: CRISM image of the area in question (FRT0000A4AF_07). This figure shows the area from which the spectra were taken. On the left hand side the unfiltered image is seen with a red cross pointing to where the spectra were taken from, on the right hand side, the filter applied over the original image, with a mirrored version of the red cross pointing to the pixels chosen.

4. RESULTS AND ANALYSIS

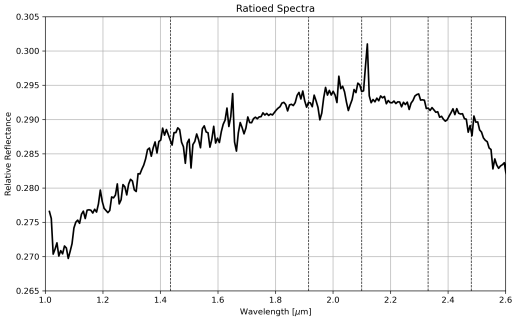

Figure 4.40: Resulting spectrum from the Images shown previously. In this case the generic absorption lines for clays/phyllosilicates are highlighted by dashed black lines. For clarity and relevance, the wavelength is limited between 1 and 2.6 μm.

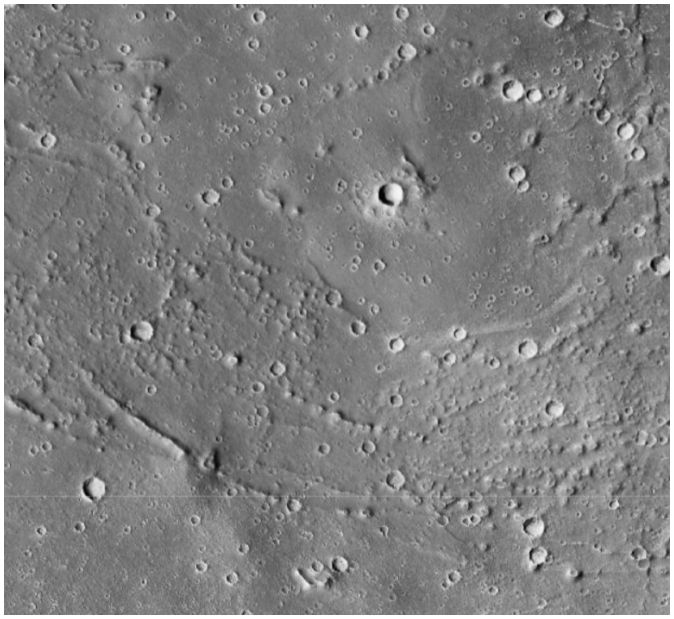

Figure 4.41: CTX Image of the eighth region analyzed, to the west of the Hephaestus Rupes. Coordinates: 20.4809°N: 109.4832°E. Credits: NASA/MRO.

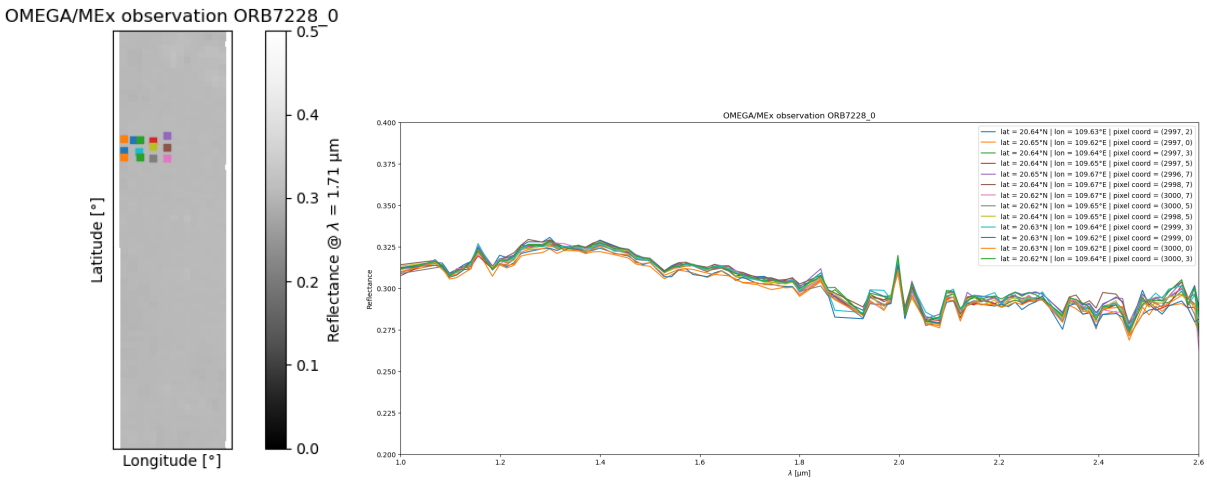

(a) (b)

Figure 4.42: OMEGA observation of the region west of the Hephaestus Rupes (ORB7228_0). On the left hand side (a), a zoom in of the region is visible, as well as the pixels from which the spectra were taken. On the right hand side (b), the corresponding spectra are visible. For clarity and relevance, the wavelength is limited between 1 and 2.6 μm.

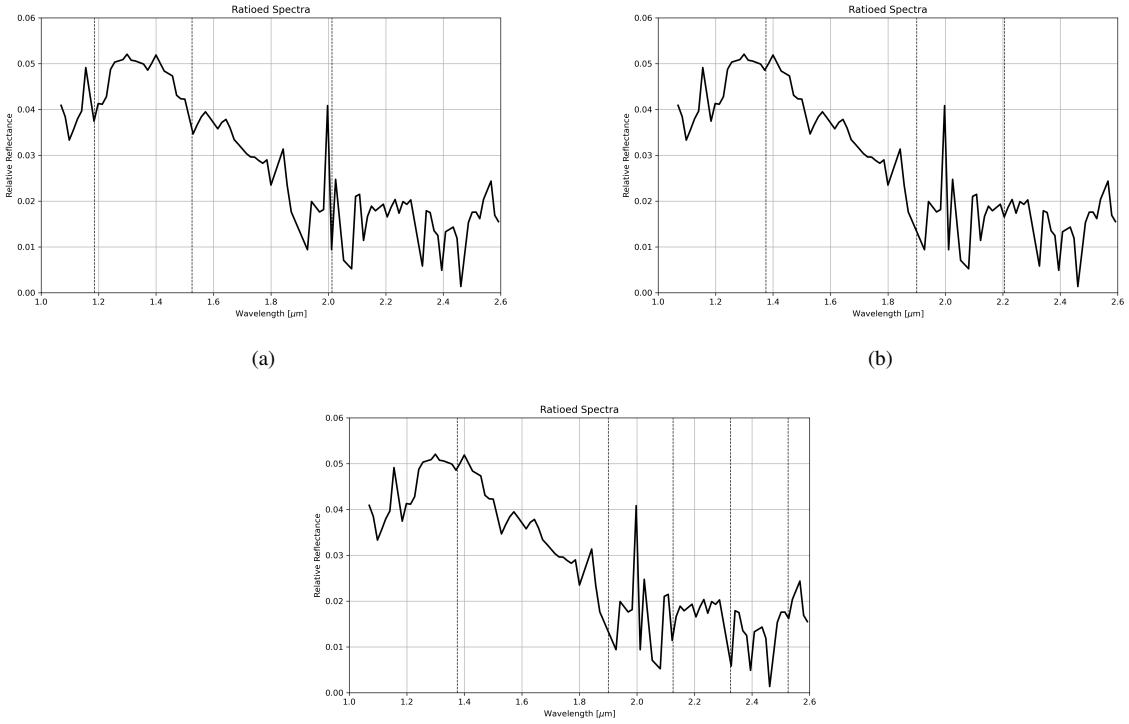

Figure 4.43: Resulting spectra from the Pixels shown previously. For spectrum (a), the absorption lines of H_2O ice are highlighted by dashed black lines. For spectrum (b), the absorption lines for hydrated silica are highlighted by dashed black lines. For spectrum (c), the absorption lines for serpentine are highlighted by dashed black lines. For clarity and relevance, the wavelength is limited between 1 and 2.6 μm.

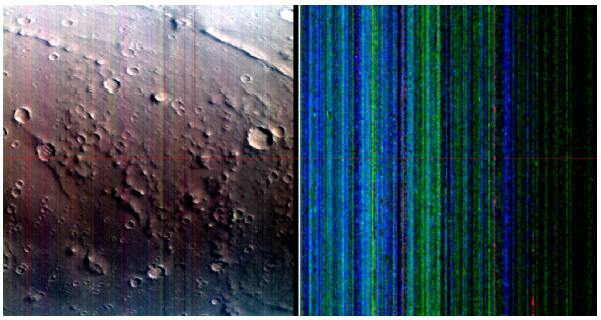

Figure 4.44: CRISM image of the area in question (FRT0000876A_07). This figure shows the area from which the spectra were taken. On the left hand side the unfiltered image is seen with a red cross pointing to where the spectra were taken from, on the right hand side, the filter applied over the original image, with a mirrored version of the red cross pointing to the pixels chosen.

4. RESULTS AND ANALYSIS

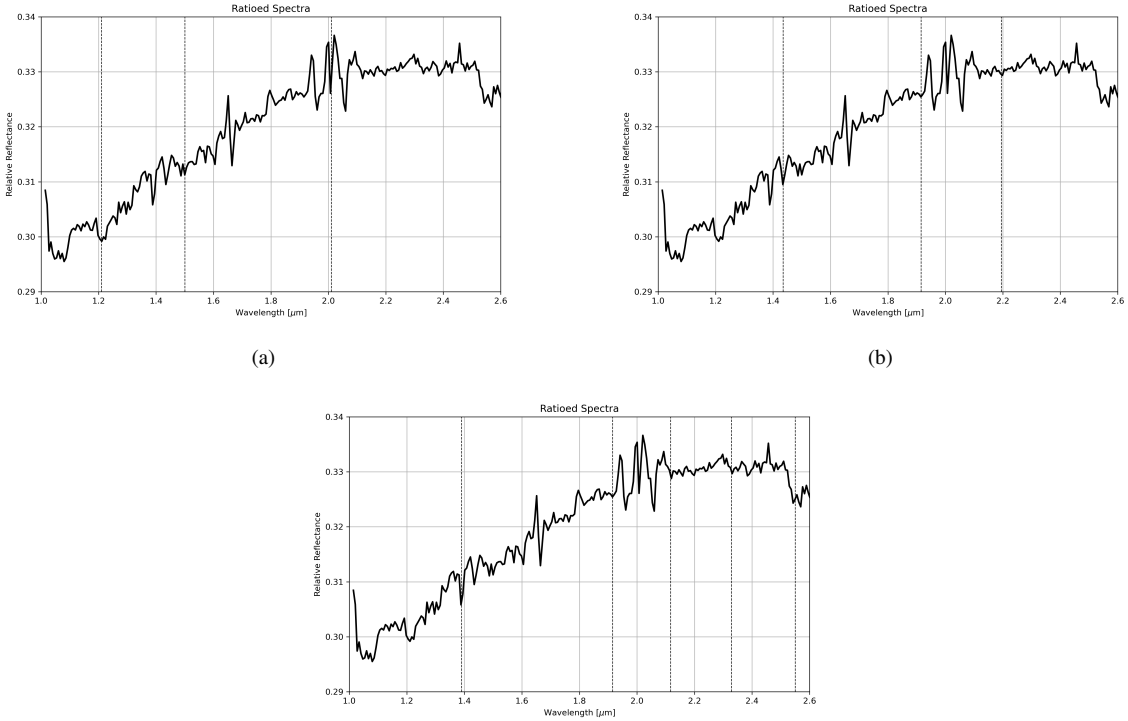

(a) (b)

(c)

Figure 4.45: Resulting spectra from the Images shown previously. For spectrum (a), the absorption lines of H_2O ice are highlighted by dashed black lines. For spectrum (b), the absorption lines for hydrated silica are highlighted by dashed black lines. For spectrum (c), the absorption lines for serpentine are highlighted by dashed black lines. For clarity and relevance, the wavelength is limited between 1 and 2.6 μm.

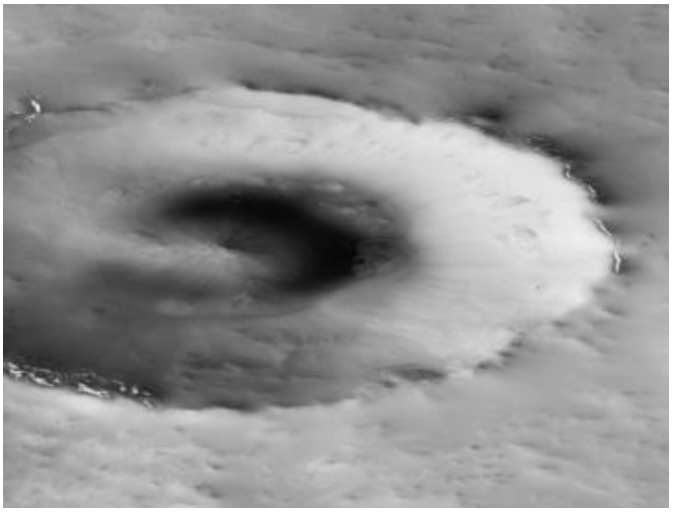

Figure 4.46: CTX Image of the ninth and final region analyzed, to the north of Cecropia. Coordinates: 66.3250°N: 39.8062°E. Credits: NASA/MRO.

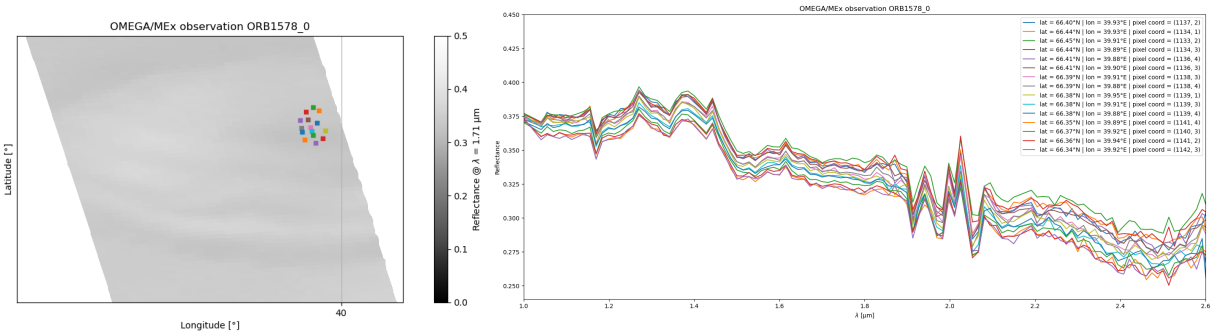

(a) (b)

Figure 4.47: OMEGA observation of the region in question (ORB1578_0). On the left hand side (a), a zoom in of the region is visible, as well as the pixels from which the spectra were taken. On the right hand side (b), the corresponding spectra are visible. For clarity and relevance, the wavelength is limited between 1 and 2.6 μm.

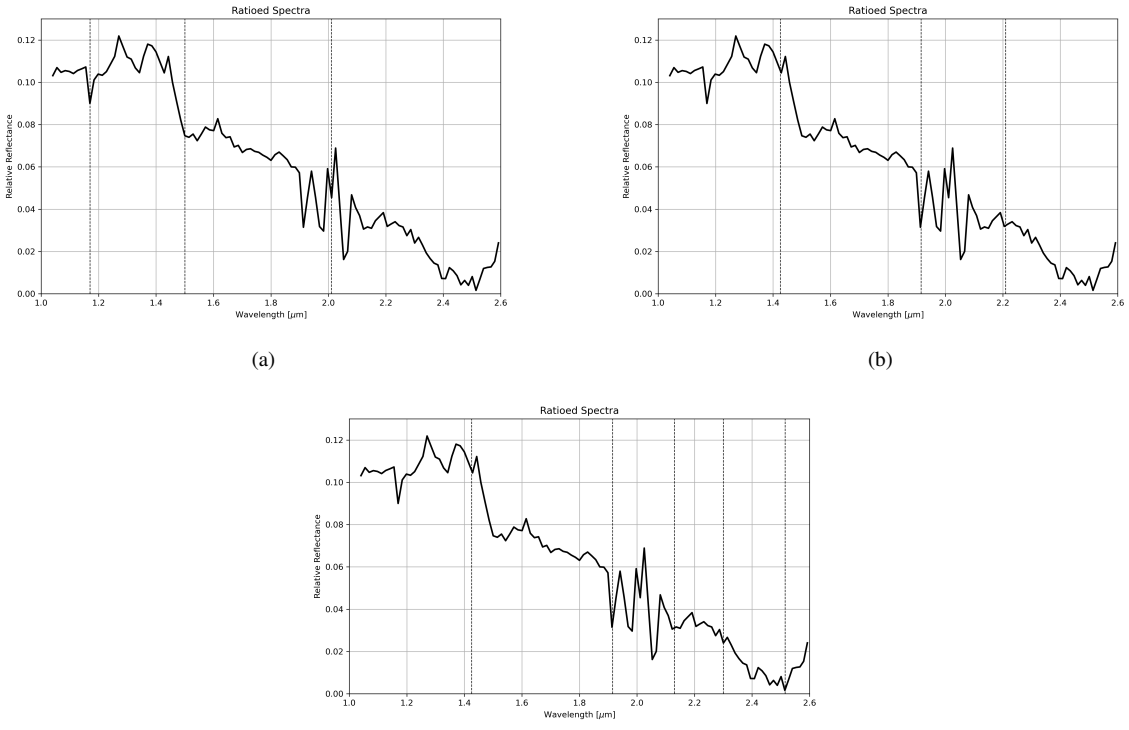

(a) (b)

(c)

Figure 4.48: Resulting spectra from the Pixels shown previously. For spectrum (a), the absorption lines of H_2O ice are highlighted by dashed black lines. For spectrum (b), the absorption lines for hydrated silica are highlighted by dashed black lines. For spectrum (c), the absorption lines for serpentine are highlighted by dashed black lines. For clarity and relevance, the wavelength is limited between 1 and 2.6 μm.

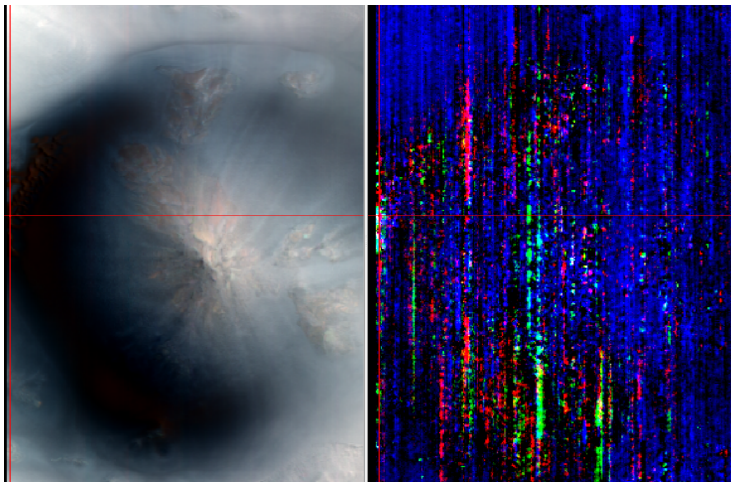

Figure 4.49: CRISM image of the area in question (FRT0000B1FA_07). This figure shows the area from which the spectra were taken. On the left hand side the unfiltered image is seen with a red cross pointing to where the spectra were taken from, on the right hand side, the filter applied over the original image, with a mirrored version of the red cross pointing to the pixels chosen.

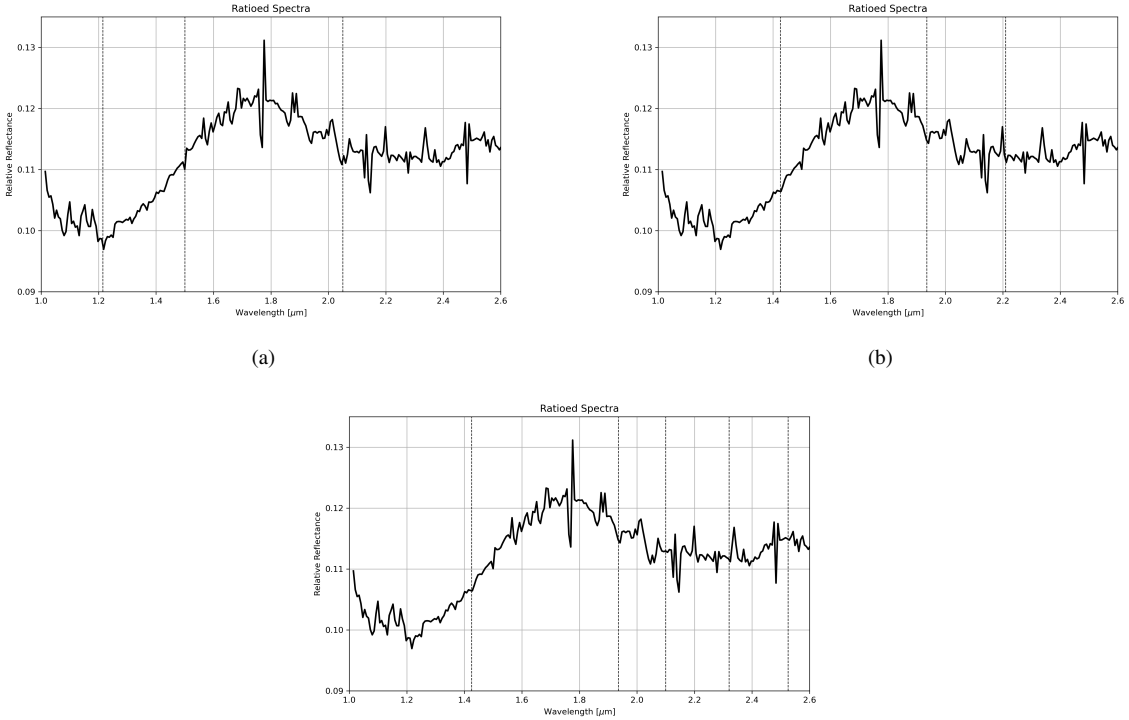

(a) (b)

(c)

Figure 4.50: Resulting spectra from the Images shown previously. For spectrum (a), the absorption lines of H_2O ice are highlighted by dashed black lines. For spectrum (b), the absorption lines for hydrated silica are highlighted by dashed black lines. For spectrum (c), the absorption lines for serpentine are highlighted by dashed black lines. For clarity and relevance, the wavelength is limited between 1 and 2.6 μm.

Chapter 5

Discussion

5.1 Overview and Motivation

Motivated by the findings of Xiao et al. 2023 and their Zhurong rover, we set out to complement their work, but with orbiters instead. This is a very known type of science, and has been used on Mars' surface for a very long time. The introduction of OMEGA from Mars Express and CRISM from Mars Reconnaissance Orbiter, has proven indispensable for surface analysis and mineral identification. The goal of our work however, was focused on studying only the northern hemisphere and following the potential coast lines described in Wang et al. 2024 is search for hydrated minerals. As mentioned in section 4.9, we also studied one other region to use as a calibration mechanism for our method, the Terby crater (Yen et al. 2019).

Our main goal was to add evidence to the current Oceanus Borealis hypothesis. When selecting the areas for analysis, the main focus was to balance quality with quantity. As explained in the earlier sections of this work, impact craters can be true enablers when trying to reach beyond the superficial sedimentary layers, however, if we also want to explore the putative coastlines, we need to look for water flowing formations as well.

5.2 Spatial Distribution of Hydrated minerals

5.2.1 Calibration case - Terby

On this first case, we were not focused on making new detections, instead, we tried reproducing the same results previously found. Both our OMEGA and CRISM detections, when compared to the literature, gave us compelling results. The presence of zeolites and other hydrated minerals (mainly Fe/Mg phyllosilicates) were expected since this region is believed to have been in contact with liquid water in the past (Crown et al. 2004)(Yen et al. 2019).

Terby's geographic context shows what seems to be several outflow channels feeding into a single larger deposit basin, and following the literature, and our own results, we find that there have been detected hydrous minerals all over the region. However, it was mainly shaped by erosion and fluvial processes (Crown et al. 2004), not by an long lasting lake. This is reflected in the type of minerals seen in the spectra. No hydrated silica (in its crystalline form), can be seen, nor serpentine. This means that the sediments were in fact exposed to flowing, liquid water, but for a relatively short period of time.

5.2.2 Coastal regions

Roughly half of the regions chosen for study lie upon the potential ancient coast lines described in Wang et al. 2024 or very near them. This was deliberate since our goal with this work was to look for further evidence of the Oceanus Borealis. To support this hypothesis, these regions would need to be filled with hydrated minerals, and this is exactly what we find. On all of these regions' spectra there are absorptions indicating hydrated silica, on one of the cases, amorphous, the rest all show a crystalline form. The fact that the vast majority of hydrated silica found is of the crystalline form strongly suggests that the presence of water in that region was far more long lasting than previously thought (Viviano et al. 2014), and was not a product of casual global rains (Voigt et al. 2024a).

Another key mineral to look for in our spectra is serpentine, which is also detected in some of these coastal regions. Serpentine has a different formation process than hydrated silica, however, one thing that they have in common is the need for lasting water exposure (Viviano et al. 2014). Thus far, serpentine had only been observed in Nili Fossae, and is also associated with some southern highland impact craters (Viviano et al. 2014).

Hydrated silica usually forms under acidic/neutral aqueous fluids, when silica leeches out of volcanic or basaltic rock by acidic/neutral fluids. The silica stays dissolved in the solution and precipitates as hydrated silica when these conditions change. These alterations are usually linked with either hydrothermal activity or weathering. On the other hand, however, serpentine relies on the alkaline hydration of mafic/ultramafic rocks, rich in iron and magnesium, at relatively low temperatures (Viviano et al. 2014).

Finding both hydrated silica (opal) and serpentine in the same region is not that common since their formation imply such different environments and conditions. However, in some of these coastal regions, we do detect both serpentine and hydrated silica together. This means that those regions were exposed to very active and long lasting aqueous environment.

5.2.3 Impact craters

The remaining regions studied were all impact craters. This was made with the idea explained in section 1.2.4 that these big impactors can carve the surface exposing some underlying layers. The deformation suffered due to the impact can also lead to the resurfacing of deeper layers as well. As previously explained, the northern lowlands work as a martian "dumpster", where all of the sediments, all of the lava flows and all of the dust storms will eventually end up covering these lower altitude regions, with no other area to go. With this in mind, impact craters are invaluable for studying/attempting to study the original surface that could hold clues for the Oceanus Borealis hypothesis.

Our mineralogical analysis of these regions are very similar to the ones in the coastal areas. The vast majority of the craters held these minerals: H_2O ice, hydrated silica (amorphous or crystalline) and possibly some serpentine as well. Both ice and hydrated silica are quiet evident in the spectra, however, some had other Fe/Mg phyllosilicates, possibly indicating the presence of serpentine. Some of the images signla to noise ratio did not allow for a clear distinction, but the presence of the water ice alone and the opals proved enough for some conclusions to be drawn.

In the case of big impact craters, the presence of many hydrated minerals does not immediately mean that we are looking at the surface layers of a buried ancient ocean. As explained by Figure 1.8 and 1.9, there is usually icy layers underneath the martian surface, and with an impactor, this layer can melt and consequently irrigate the crater's interior, forming a temporary lake. Depending on the size of the impactor, its kinetic energy will increase the bigger it is, and this same energy, at the moment of impact, will be transferred into its the surroundings. This stored energy can sustain crater lakes for up to a few

million years, depending on the size of the impactor. This liquid water resulting from the impact itself is most likely what is reacting with the surface rocks and producing these minerals we are seeing in our spectra, not the product of an ocean, necessarily.

However, there are still conclusions to be made. These regions were, nonetheless, in the presence of liquid water for long periods of time. Finding relatively large quantities of hydrated silica inside big impact craters is still relevant to the study of the Oceanus Borealis even if we know that the minerals we are detecting are a product of the impactor's kinetic energy, and not of an ongoing ancient ocean.

Chapter 6

Future Prospects

Ever since the first orbiters and landers sent to Mars, a conjunction of both in situ and orbital data has been used to very accurately detail the composition and geological history of the martian surface. Both OMEGA and CRISM have been crucial in this hunt for the truth, however, in order to better complement the findings of landers such as Tianwen-1 (Xiao et al. 2023), higher resolution imaging would be ideal. One other aspect worth mentioning is the possibility for reanalysis with alternative methods. As a continuation of this work, a research paper is currently being finalized for submission, with the aim of further exploring these alternative methods to our analysis.

It is to note as well that, seen in Figure 2.7, this study, only covered about a quarter of the proposed putative shorelines by Wang et al. 2024. Even then, other interesting features are sure to be present in the region already studied, waiting to be analyzed.

As mentioned above, landers such as Perseverance, Opportunity and many others are the ones that can provide us with some form of ground truth. Our work was more focused on getting orbital confirmation of the findings of Tianwen-1, but running an analysis the other way round would also prove very useful, first orbital detection, and then confirmation from ground/in situ analysis.

We must, once more, recall the true purpose of this work, the Oceanus Borealis theory. The fact that so many different regions along the ancient coastlines in Wang et al. 2024 have detections of many hydrated minerals on both OMEGA and CRISM, means that there is, at least, a reason to do further work and keep studying these areas in hopes of rewriting the history of water on Mars and the potential for habitability. In addition, if the northern hemisphere did, in fact, harbor a large ocean, Mars could have been a life sustaining planet in his early stages. Life as we know it depends on liquid water to exist and evolution traces all of our ancestors back into the first single cellular organisms that appeared in Earth's primitive oceans.

Chapter 7

Conclusion

The goal of our work was to follow the lead of the Tianwen-1 rover deployed near what could be interpreted as a coastal region on the northern hemisphere. Their findings, in Xiao et al. 2023, confirmed the detection of what could be a sedimentary ocean rock. With this in mind, we set out to analyze several regions in the surrounding area of this rover's landing site, in search of further evidence for a substantial presence of liquid water. By integrating the work and the putative ancient shorelines described in Wang et al. 2024, we selected several regions in this context to study.

For the analysis of the regions, we used OMEGA from Mars Express as a first approach. Since this camera has a very wide are coverage, it served as a first step in identifying the mineralogical composition of the areas. We also made use of CRISM, which has higher imaging resolution, but less coverage, perfectly complementing the OMEGA analysis as a second step in mineral identification.

The data analysis techniques used, consisting of the softwares OMEGAPY, CAT and EN-MAPBOX, revealed several hydrous mineral detections in the regions studied. All shoreline features had substantial quantities of phyllosilicates, including hydrated silica, either in amorphous form, or crystalline form (opal). In some cases there were also clear indications of serpentine in the areas, that, when interpreted together with the opal detections, lead to the conclusion that those features were formed in contact with very active and complex underwater environments.

Due to the nature of the martian northern lowlands, the original crust and the first sedimentary layers are all buried under several new coatings and lava flows (Pan et al. 2017). Big impact craters, however, provide a potential solution to this problem by excavating and deforming the deposited layers, and leading to potential resurfacing of the deeper ones (Senft et al. 2007). From our results, we see that in fact, inside these impact craters, there are some interesting hydrated mineral detections. Despite identifying phyllosilicates and other clays inside these basins, there is no guarantee that we are peeking into the original crustal layers, and detecting wet environments from that epoch. Since the martian surface layers are often mixed with some quantities of ice (Senft et al. 2008), the kinetic energy transfered into the surface during an impact is enough to maintain a liquid water environment for several thousands/millions of years, helping the precipitation of, for example, hydrated silica and other phyllosilicates.

Our analyses are pretty straight forward, the shoreline features and the minerals they are harboring provide invaluable insight into what their formation and initial conditions actually were. However, when it comes to the other half of our data set, the impact craters, we cannot conclude, for sure, that the minerals we are observing originate from the resurfaced deep layers. One possible solution to this matter is to, on a future analysis, focus on the morphology of the craters themselves and the accurate position of the mineral deposits. This would allow for an accurate mapping of the minerals and by fitting it on the resurfacing layers, we would be able to conclusively tell, whether these minerals were product of the

impact melting, or previous fluvial-marine environments.

Taken together, our results provide further support to the Oceanus Borealis hypothesis. They have strengthened the idea of a potential ancient shoreline by identifying numerous hydrated minerals near the dichotomy boundary, and have also highlighted promising new targets for future in situ missions.

This master thesis work has allowed new possibilities for the history of water on Mars to be discovered. Through the analysis of orbital spectroscopy data from OMEGA and CRISM, this work has explored the occurrence of hydrated minerals across the northern plains, with a particular focus on the putative shorelines of Oceanus Borealis. The application of our methodology not only contributes to a better understanding of Mars' climatic and geological evolution but also offers a complementary approach to future exploration missions that aim to assess planetary habitability and search for past oceans on Mars.

Bibliography

Alves et al. (Oct. 2010). "The effect of mass-transport deposits on the younger slope morphology, offshore Brazil". In: *Marine and Petroleum Geology* 27, pp. 2027–2036. DOI: 10.1016/j.marpetgeo.2010.05.006.

Baker (Sept. 2023). "The Oceanus Borealis of ancient Mars". In: *National Science Review* 10 (9). ISSN: 2053714X. DOI: 10.1093/nsr/nwad146.

Barlow (2008). *MARS: AN INTRODUCTION TO ITS INTERIOR, SURFACE AND ATMOSPHERE*.

Baumgardner et al. (1986). "Reflectance Properties of Soils". In: Advances in Agronomy 38. Ed. by N.C. Brady, pp. 1–44. ISSN: 0065-2113. DOI: https://doi.org/10.1016/S0065-2113(08)60672-0. URL: https://www.sciencedirect.com/science/article/pii/S0065211308606720.

Bibring et al. (2004). *OMEGA: Observatoire pour la Minéralogie, l'Eau, les Glaces et l'Activité*. Technical Report. Includes contributors from LESIA, IFSI-INAF, IKI, IASF-INAF, University of Lecce, Orsay Terre, Observatoire de Midi-Pyrénées, and other international institutions. Bâtiment 121, F-91405 Orsay Campus, France: Institut d'Astrophysique Spatiale (IAS) and the OMEGA Co-Investigator Team.

— (2005). "Mars Surface Diversity as Revealed by the OMEGA/Mars Express Observations". In: *Science* 307.5715, pp. 1576–1581. DOI: 10.1126/science.1108806. eprint: https://www.science.org/doi/pdf/10.1126/science.1108806. URL: https://www.science.org/doi/abs/10.1126/science.1108806.

Brož et al. (2020). "Mud flow levitation on Mars: Insights from laboratory simulations". In: *Earth and Planetary Science Letters* 545, p. 116406. ISSN: 0012-821X. DOI: https://doi.org/10.1016/j.epsl.2020.116406. URL: https://www.sciencedirect.com/science/article/pii/S0012821X20303502.

Chicarro et al. (2004). *The Mars Express Mission: An Overview*. Tech. rep. European Space Agency. PO Box 299, 2200 AG Noordwijk, The Netherlands: Planetary Missions Division, Research & Scientific Support Department, ESA/ESTEC.

Collins (1971). *Mariner 6 and 7 Pictures of Mars*. NASA Special Publication SP-263. Washington, D.C.: NASA.

Cooke et al. (Sept. 2011). "Basement controls on the scale of giant polygons in Utopia Planitia, Mars". In: *Journal of Geophysical Research* 116. DOI: 10.1029/2011JE003812.

Corliss (1974). *The Viking Mission to Mars*. Vol. 334. Scientific, Technical Information Office, National Aeronautics, and Space . . .

Crown et al. (Feb. 2004). "Geologic Evolution of Eastern Hellas, Mars: Styles and Timing of Volatile-driven Activity". In.

Dauphas et al. (2011). "Hf–W–Th evidence for rapid growth of Mars and its status as a planetary embryo". In: *Nature* 473.7348, pp. 489–492. DOI: 10.1038/nature10077.

Ehlmann et al. (2009). "Identification of hydrated silicate minerals on Mars using MRO-CRISM: Geologic context near Nili Fossae and implications for aqueous alteration". In: *Journal of Geophysical Research: Planets* 114 (10). ISSN: 01480227. DOI: 10.1029/2009JE003339.

Encrenaz et al. (2003). *The Solar System*.

Harvey (1996). *The new Russian space programme from competition to collaboration*.

Jouglet et al. (2007). "Hydration state of the Martian surface as seen by Mars Express OMEGA: 1. Analysis of the 3μm hydration feature". In: *Journal of Geophysical Research: Planets* 112.E8. DOI: https://doi.org/10.1029/2006JE002846. eprint: https://agupubs.onlinelibrary.wiley.com/doi/pdf/10.1029/2006JE002846. URL: https://agupubs.onlinelibrary.wiley.com/doi/abs/10.1029/2006JE002846.

Kreslavsky et al. (2000). "Kilometer-scale roughness of Mars: Results from MOLA data analysis". In: *Journal of Geophysical Research: Planets* 105.E11, pp. 26695–26711. DOI: https://doi.org/10.1029/2000JE001259. eprint: https://agupubs.onlinelibrary.wiley.com/doi/pdf/10.1029/2000JE001259. URL: https://agupubs.onlinelibrary.wiley.com/doi/abs/10.1029/2000JE001259.

— (2002). "Mars: Nature and evolution of young latitude-dependent water-ice-rich mantle". In: *Geophysical Research Letters* 29.15, pp. 14-1-14–4. DOI: https://doi.org/10.1029/2002GL015392. eprint: https://agupubs.onlinelibrary.wiley.com/doi/pdf/10.1029/2002GL015392. URL: https://agupubs.onlinelibrary.wiley.com/doi/abs/10.1029/2002GL015392.

Langevin et al. (2005). "Summer Evolution of the North Polar Cap of Mars as Observed by OMEGA/Mars Express". In: *Science* 307.5715, pp. 1581–1584. DOI: 10.1126/science.1109438. eprint: https://www.science.org/doi/pdf/10.1126/science.1109438. URL: https://www.science.org/doi/abs/10.1126/science.1109438.

Langlais et al. (2004). "Crustal magnetic field of Mars". In: *Journal of Geophysical Research: Planets* 109.E2. DOI: https://doi.org/10.1029/2003JE002048. eprint: https://agupubs.onlinelibrary.wiley.com/doi/pdf/10.1029/2003JE002048. URL: https://agupubs.onlinelibrary.wiley.com/doi/abs/10.1029/2003JE002048.

Marinova et al. (2008). "Mega-impact formation of the Mars hemispheric dichotomy". In: *Nature* 453.4271, pp. 1216–1219. DOI: 10.1038/nature07070. URL: https://doi.org/10.1038/nature07070.

McCauley et al. (1972). "Preliminary mariner 9 report on the geology of Mars". In: *Icarus* 17.2, pp. 289–327. ISSN: 0019-1035. DOI: https://doi.org/10.1016/0019-1035(72)90003-6. URL: https://www.sciencedirect.com/science/article/pii/0019103572900036.

Morris et al. (2004). "Mineralogy at Gusev Crater from the Mössbauer Spectrometer on the Spirit Rover". In: *Science* 305.5685, pp. 833–836. DOI: 10.1126/science.1100020. eprint: https://www.science.org/doi/pdf/10.1126/science.1100020. URL: https://www.science.org/doi/abs/10.1126/science.1100020.

Moscardelli et al. (June 2011). "Deep-water erosional remnants in eastern offshore Trinidad as terrestrial analogs for teardrop-shaped islands on Mars: Implications for outflow channel formation". In: 39, pp. 699–702. DOI: 10.1130/G31949.1.

— (Aug. 2012). "Deep-water polygonal fault systems as terrestrial analogs for large-scale Martian polygonal terrains". In: *GSA Today* 22. DOI: 10.1130/GSATG147A.1.

Murchie et al. (2007). "Compact Reconnaissance Imaging Spectrometer for Mars (CRISM) on Mars Reconnaissance Orbiter (MRO)". In: *Journal of Geophysical Research: Planets* 112.E5. DOI: https://doi.org/10.1029/2006JE002682. eprint: https://agupubs.onlinelibrary.wiley.com/

doi/pdf/10.1029/2006JE002682. URL: https://agupubs.onlinelibrary.wiley.com/doi/abs/10.1029/2006JE002682.

Mustard et al. (2005). "Olivine and Pyroxene Diversity in the Crust of Mars". In: *Science* 307.5715, pp. 1594–1597. DOI: 10.1126/science.1109098. eprint: https://www.science.org/doi/pdf/10.1126/science.1109098. URL: https://www.science.org/doi/abs/10.1126/science.1109098.

Mutch et al. (1976). "The Surface of Mars: There View from the Viking 1 Lander". In: *Science* 193.4255, pp. 791–801. DOI: 10.1126/science.193.4255.791. eprint: https://www.science.org/doi/pdf/10.1126/science.193.4255.791. URL: https://www.science.org/doi/abs/10.1126/science.193.4255.791.

Pan et al. (2017). "The stratigraphy and history of Mars' northern lowlands through mineralogy of impact craters: A comprehensive survey". In: *Journal of Geophysical Research: Planets* 122.9, pp. 1824–1854. DOI: https://doi.org/10.1002/2017JE005276. eprint: https://agupubs.onlinelibrary.wiley.com/doi/pdf/10.1002/2017JE005276. URL: https://agupubs.onlinelibrary.wiley.com/doi/abs/10.1002/2017JE005276.

— (2019). *Hydrated silica in martian alluvial fans and deltas*. URL: https://univ-lyon1.hal.science/hal-02296390v1.

Pelkey et al. (2007). "CRISM multispectral summary products: Parameterizing mineral diversity on Mars from reflectance". In: *Journal of Geophysical Research: Planets* 112.E8. DOI: https://doi.org/10.1029/2006JE002831. eprint: https://agupubs.onlinelibrary.wiley.com/doi/pdf/10.1029/2006JE002831. URL: https://agupubs.onlinelibrary.wiley.com/doi/abs/10.1029/2006JE002831.

Perminov (1999). *The difficult road to Mars - A brief history of Mars exploration in the Soviet Union*.

Reiff (1966). "Mariner IV: Developing the Scientific Experiment". In: *Science* 151.3709, pp. 413–417. DOI: 10.1126/science.151.3709.413. eprint: https://www.science.org/doi/pdf/10.1126/science.151.3709.413. URL: https://www.science.org/doi/abs/10.1126/science.151.3709.413.

Rodriguez et al. (2012). "Infiltration of Martian outflow channel floodwaters into lowland cavernous systems". In: *Geophysical Research Letters* 39.22. DOI: https://doi.org/10.1029/2012GL053225. eprint: https://agupubs.onlinelibrary.wiley.com/doi/pdf/10.1029/2012GL053225. URL: https://agupubs.onlinelibrary.wiley.com/doi/abs/10.1029/2012GL053225.

Salvatore et al. (2014). "On the origin of the Vastitas Borealis Formation in Chryse and Acidalia Planitiae, Mars". In: *Journal of Geophysical Research: Planets* 119.12, pp. 2437–2456. DOI: https://doi.org/10.1002/2014JE004682. eprint: https://agupubs.onlinelibrary.wiley.com/doi/pdf/10.1002/2014JE004682. URL: https://agupubs.onlinelibrary.wiley.com/doi/abs/10.1002/2014JE004682.

Sánchez-Lavega (2011). *An Introduction to Planetary Atmospheres*.

Senft et al. (2007). "Modeling impact cratering in layered surfaces". In: *Journal of Geophysical Research: Planets* 112.E11. DOI: https://doi.org/10.1029/2007JE002894. eprint: https://agupubs.onlinelibrary.wiley.com/doi/pdf/10.1029/2007JE002894. URL: https://agupubs.onlinelibrary.wiley.com/doi/abs/10.1029/2007JE002894.

— (2008). "Impact crater formation in icy layered terrains on Mars". In: *Meteoritics & Planetary Science* 43.12, pp. 1993–2013. DOI: https://doi.org/10.1111/j.1945-5100.2008.tb00657.x. eprint: https://onlinelibrary.wiley.com/doi/pdf/10.1111/j.1945-5100.2008.

tb00657.x. URL: https://onlinelibrary.wiley.com/doi/abs/10.1111/j.1945-5100.2008.tb00657.x.

Shorthill et al. (1976). "The Environs of Viking 2 Lander". In: *Science* 194.4271, pp. 1309–1318. DOI: 10.1126/science.194.4271.1309. eprint: https://www.science.org/doi/pdf/10.1126/science.194.4271.1309. URL: https://www.science.org/doi/abs/10.1126/science.194.4271.1309.

Squyres et al. (2006). "Two Years at Meridiani Planum: Results from the Opportunity Rover". In: *Science* 313.5792, pp. 1403–1407. DOI: 10.1126/science.1130890. eprint: https://www.science.org/doi/pdf/10.1126/science.1130890. URL: https://www.science.org/doi/abs/10.1126/science.1130890.

Stallkamp et al. (1971). *Mariner Mars 1969 Final Project Report, Volume 3 - Scientific Investigations*. Technical Report TR 32-1460. Pasadena, CA: Jet Propulsion Laboratory, California Institute of Technology.

Stcherbinine et al. (2021). "Identification of a new spectral signature at 3μm over martian northern high latitudes: Implications for surface composition". In: *Icarus* 369, p. 114627. ISSN: 0019-1035. DOI: https://doi.org/10.1016/j.icarus.2021.114627.

Tanaka et al. (1987). "Geologic Map of the Polar Regions of Mars". English. In: 1802C. USGS Publications Warehouse. DOI: 10.3133/i1802C. URL: https://pubs.usgs.gov/publication/i1802C.

Viviano et al. (2014). "Revised CRISM spectral parameters and summary products based on the currently detected mineral diversity on Mars". In: *Journal of Geophysical Research: Planets* 119.6, pp. 1403–1431. DOI: https://doi.org/10.1002/2014JE004627. eprint: https://agupubs.onlinelibrary.wiley.com/doi/pdf/10.1002/2014JE004627. URL: https://agupubs.onlinelibrary.wiley.com/doi/abs/10.1002/2014JE004627.

Voigt et al. (July 2024a). *Global Distribution of Hydrated Silica on Mars*. Tech. rep. Abstract #3181. Pasadena, CA. URL: https://www.hou.usra.edu/meetings/tenthmars2024/pdf/3181.pdf.

— (Sept. 2024b). "Investigating Hydrated Silica in Syrtis Major, Mars: Implications for the Longevity of Water–Rock Interaction". In: *Geophysical Research Letters* 51 (18). ISSN: 19448007. DOI: 10.1029/2024GL108610.

Wang et al. (2024). "Hypothesis of an Ancient Northern Ocean on Mars and Insights from the Zhurong Rover". In: *Nature Astronomy* 8, pp. 1220–1229. DOI: 10.1038/s41550-024-02343-3. URL: https://doi.org/10.1038/s41550-024-02343-3.

Watters et al. (2007). "Hemispheres Apart: The Crustal Dichotomy on Mars". In: *Annual Review of Earth and Planetary Sciences* 35.4271, pp. 621–652. URL: https://doi.org/10.1146/annurev.earth.35.031306.140220.

Wenzel et al. (2004). In: *Geophysical Research Letters* 31.4. DOI: https://doi.org/10.1029/2003GL019306. eprint: https://agupubs.onlinelibrary.wiley.com/doi/pdf/10.1029/2003GL019306. URL: https://agupubs.onlinelibrary.wiley.com/doi/abs/10.1029/2003GL019306.

Xiao et al. (Sept. 2023). "Evidence for marine sedimentary rocks in Utopia Planitia: Zhurong rover observations". In: *National Science Review* 10 (9). ISSN: 2053714X. DOI: 10.1093/nsr/nwad137.

Yen et al. (2019). "An Updated Orbital Analysis of Ancient Strata in Terby Crater, Mars: The Thickest Deltaic Sequence on Mars?" In: LPI Contribution No. 2132.

Zurek et al. (2017). "The Atmosphere and Climate of Mars". In: *Cambridge University Press, The Atmosphere and Climate of Mars*. Ed. by Robert M. Haberle et al. DOI: 10.1017/9781139060172.004.